Dissertation
submitted to the
Combined Faculties for the Natural Sciences and for Mathematics
of the Ruperto-Carola University of Heidelberg, Germany
for the degree of
Doctor of Natural Sciences

Put forward by
Diplom-Physiker Georg Robbers
Born in Freiburg im Breisgau, Germany
Oral examination: 03.06.2009

Properties of Quintessence

Referees: **Prof. Dr. Christof Wetterich**
Prof. Dr. Matthias Bartelmann

Eigenschaften der Quintessenz

Wir untersuchen kosmologische Modelle mit Quintessenz, einer im gesamten Universum fast homogen verteilten Energieform, die heute etwa drei Viertel zur gesamten Energiedichte des Universums beiträgt. Wir verwenden Beobachtungsdaten, um Obergrenzen für die Energiedichte der Quintessenz auch zu früheren Zeiten zu bestimmen, und analysieren die Rolle, die diese frühe Quintessenz bei der Interpretation von kosmologischen Beobachtungen spielt. Weiterhin untersuchen wir mögliche Abweichungen von dem Gravitationsgesetz der Allgemeinen Relativitätstheorie auf sehr großen Längenskalen. Schließlich betrachten wir dann Modelle, in denen die Masse der Dunklen Materie oder der Neutrinos von dem Quintessenz-Feld abhängt, und stellen Erweiterungen des Programms CMBEASY vor, die es erlauben, die kosmologischen Vorhersagen dieser Modelle zu berechnen.

Properties of Quintessence

We study cosmological models with quintessence, a form of energy that is distributed almost homogeneously in the Universe, and today makes up about three fourths of its energy density. We use observational data in order to infer upper bounds for the energy density of quintessence also during early times, and analyze the impact of this early quintessence on the interpretation of observational data. Furthermore, we investigate deviations from the law of gravity as described by the theory of General Relativity on very large scales. Finally, we consider models in which the mass of the dark matter or of neutrinos depends on the quintessence field, and present extensions of the software CMBEASY, that allow to compute the cosmological predictions of these models.

Contents

1 Introduction

1.1 Big-Bang Cosmology

The Theory of General Relativity (Einstein 1916) describes gravity as a geometrical effect caused by the curvature of spacetime. It can be applied to our Universe as a whole, and remarkably, even a century after it has been proposed, General Relativity is still the fundamental framework on which modern cosmology is built. However, when the observations of distant supernovae discovered that the expansion of our Universe is accelerating (Riess et al. 1998; Perlmutter et al. 1999), cosmologists had to accept that on large, cosmological scales, gravity might not work as our intuition tells us: all objects should be attracted to each other. But rather than slowing down, the relative velocities of distant galaxies are increasing. This either means that gravity behaves differently than previously thought; or it requires the addition of some mysterious form of energy with exotic gravitational properties, the dark energy, or quintessence, to the cosmic inventory. The properties of this dark energy are the subject of this thesis.

But even before the supernovae observations, there had been hints that the total matter density in the Universe might be well below the 'critical density' required for a geometrically flat universe (e.g. Bahcall et al. 1995). When observations of the Cosmic Microwave Background found that the Universe is indeed geometrically flat (de Bernardis et al. 2000), the combination of these discoveries made a very strong case for some form of dark energy.

In addition to the dark energy, there also is very strong evidence that ordinary matter, the baryons (including electrons etc.), makes up only a fraction of the total matter density. One piece of observational evidence is for example the shape of the rotation curves of galaxies, which shows that the stars revolve around the center of galaxies much faster than they would in the gravitational potential of only the baryonic matter in the galaxy. The rest of the matter content of the Universe must therefore be in the form of 'dark' matter, which gravitationally behaves like ordinary matter, but does not interact (or, at least, very weakly) with the baryons and photons in the standard model of particle physics.

The accelerating Universe requires that the dark energy must be the dominating component in the Universe today; all observations point to a universe with about 70% of its energy density today accounted for by the dark energy and roughly 30% in the form matter, where only 5% is in baryonic matter, and the rest in dark matter. We further know that neutrinos with a certain mass could be responsible for up to a couple of percent of the present-day energy density; however, as we have yet to determine the precise value of the neutrino mass, this number is somewhat model-dependent. The contribution of photons to the

total energy density, in contrast, can be determined very accurately, since it is almost entirely contained in the Cosmic Microwave Background radiation, the CMB. The spectrum of the CMB is well described by a black-body spectrum, with a very precisely measured temperature of $T_{cmb} = 2.725 \pm .001$ K (Fixsen et al. 2009). The contribution of photons to the total energy density of the Universe at the present day then is of the order of only 10^{-5}.

Much of the standard picture of big-bang cosmology can be understood if we accept the notion - and we are going to put this on a mathematically sound footing in the next chapter - that we can describe the expanding universe in a first approximation by a single function of time that parameterizes the expansion of spacetime. In a flat universe, this parameter, the scale factor a, can conveniently be normalized to $a_0 = 1$ today, and was correspondingly smaller in the past. A direct consequence of the cosmological expansion is the redshift z of photons emitted by a distant source and detected by a local observer: the wavelength of these photons will be stretched by a fractional amount $z = 1/a - 1$ by the expansion. In cosmology, the redshift and the scale factor are both often used as a proxy for time.

The expansion also affects the photons of the Cosmic Microwave Background. Therefore, back in time, when the scale factor was smaller, so was the wavelength of the photons; and since the energy of a photon is given by the inverse of this wavelength, the photon energy was larger by a factor of $1/a$. The energy density stored in the photons, the number density times the energy per particle, then scales as a^{-4}, since number density is inversely proportional to volume, and therefore scales as a^{-3}.

Similarly, the energy density of matter, baryonic or dark, should scale as the number density according to a^{-3}, if the rest mass of such particles is constant with time. Going back in time, even if the energy density of photons is miniscule today, at some point radiation was more important than the matter density, if only the scale factor was small enough. Hence, the cosmological evolution is governed by different epochs: today, below a redshift $z \lesssim 0.5$, the dominating component is the dark energy. Earlier, up to a redshift of roughly $z \approx 3000$, matter dominated the overall energy density; this is the period when the structures in the Universe began to form. And even before this, radiation was the dominant component.

Big-Bang cosmology extends back even further. A very important cornerstone of the paradigm is inflation, a very early phase ($t \sim 10^{-35}$ seconds) of exponential expansion. Inflation is responsible for the initial generation of the fluctuations that seeded the present-day structures in the Universe, and explains why the Microwave Background has the same temperature even in directions that never were in causal contact before the photons were emitted. Inflation also naturally suggest that our Universe should be close to spatially flat, and we are going to assume that this holds exactly throughout this work. A full description of Big-Bang cosmology also includes Baryogenesis, the generation of the matter-antimatter asymmetry, and Nucleosynthesis (at 1 second $< t <$ 3 min, $\sim z \approx 10^{10}$), i.e. the production of the first light elements.

In this thesis, however, we will try to trace the evolution of the dark energy

only from the epoch of radiation domination until today. As we will see, for the purposes of this work, the state of the Universe at the end of the very early history can then be encoded in very few parameters, and we will not require a detailed knowledge of the physics that governs that earliest stage of the cosmological evolution.

The simplest form of a dark energy is the cosmological constant, which, when added to Einstein's Equation, can still describe this accelerating Universe in very good agreement with the observations. But in order to explain cosmic acceleration, the cosmological constant has to have a particular numerical value, which is of order 10^{-120} (in units where the Newton constant as well as the speed of light and the reduced Planck constant are all set to unity, $G = c = \hbar = 1$). This is contrary to the usual quantum-theory folklore that the cosmological constant should be of order unity, or - by some symmetry or dynamical mechanism - possibly zero.

Furthermore, if the dark energy is indeed a cosmological constant, then there seems to be no fundamental reason for why the crossover to a dark energy dominated universe happened only recently (in cosmological timescales). From the different scaling behavior of matter and radiation that we have seen above, such a crossover from radiation to matter domination is simply a consequence of the expansion and the age of the universe, but for the cosmological constant, for which the energy density does not change at all in time, there is no such compelling answer to the 'why now?' question, and one is led to accept it as a mere coincidence.

A much more attractive setting than a pure cosmological constant in this regard are cosmological models with light scalar fields (Wetterich 1988b; Ratra & Peebles 1988; Wetterich 1988a; Peebles & Ratra 1988; Frieman et al. 1995). Such a 'quintessence' (Caldwell et al. 1998) or 'cosmon' (Peccei et al. 1987) component, has dynamics, and therefore allows for scenarios in which the dark energy density is evolving with time. Indeed, many quintessence models posses attractor solutions (Wetterich 1995; Zlatev et al. 1999; Copeland et al. 1998), so that over a wide range of initial conditions, the scalar field is driven towards a solution where it tracks the dominant component, and hence its energy density is subdominant compared to radiation or matter, but of a comparable magnitude, and no 'finetuning' of the order of 10^{-120} is needed for the initial conditions in the theory.

Pure tracker models do not answer the 'why now' question, as they need a mechanism that triggers the change from the tracking behavior to the accelerating regime with dark energy domination; such trigger events can be parameterized phenomenologically through specific features in the potential (or the kinetic term) of the scalar field, thereby dodging the question, but also dynamic solutions have been explored. One particular route in this regard are the additional dynamics due to a coupling between the scalar field and other components, which is one specific quintessence property that we will discuss in this work.

1.2 The Properties of Quintessence

More generally, the topics of this thesis are the properties of scalar field dark energy models; we study their cosmological implications, and - where possible - compare their predictions with observational data. As an introduction, Chapter 2 is dedicated to a very brief survey of the homogeneous and isotropic universe, and the mathematical formulation in terms of the Friedmann-Robertson-Walker metric in General Relativity. Chapter 3 then sets the stage for linear perturbations around the homogeneous background, introducing the very basics of cosmological perturbation theory. We also introduce CMBEASY, the computer code that we use throughout this work to numerically compute the predictions of cosmological models.

In Chapter 4, we begin our investigation of quintessence properties by studying its time evolution. Specifically, we consider cosmological models with 'early dark energy'. In these scenarios, the dark energy contributes a substantial fraction to the total energy density even at earlier times, unlike for example a cosmological constant. By comparing the predictions of several early dark energy models with a comprehensive set of observational data, we find upper bounds for the abundance of the dark energy during the time before last scatter and during structure formation (Doran, Robbers, & Wetterich 2007a). At the same time, we compare the values for the standard cosmological parameters in these models to the values that are commonly inferred in the context of the ΛCDM model, and in 'standard' quintessence models, and search for possible differences. In the second part of this chapter (Linder & Robbers 2008), we investigate one particular question in more detail, namely whether early dark energy models have distinct signatures in the power spectra of the Cosmic Microwave Background, i.e. whether a standard quintessence model and one with a certain fraction of early dark energy can have indistinguishable power spectra. We are particularly interested in this as the CMB is used to 'calibrate the standard ruler', that is, to measure the size of the sound-horizon, at the time of last scatter; this same scale can also be observed at a time much closer to today, through measurement of the 'Baryon Acoustic Oscillations' (BAO) in the distribution of matter. These two measurements of the same length scale at two very different times of the cosmological evolution provides very good leverage to constrain the background evolution of the Universe. In order to interpret BAO observations correctly, however, one needs to properly account for the possibility of early dark energy, as we will show.

The boundary region between scalar field dark energy models and modifications to General Relativity is explored in Chapter 5 (Robbers, Afshordi, & Doran 2008). We focus on the Planck Mass, which in General Relativity is the constant that quantifies the strength of the coupling between the energy momentum and the space time metric, and consider the possibility that the value of the Planck Mass might change at the scale of the cosmological horizon. Such a change is a generic feature of certain kinds of early dark energy models, and shows how intimately related the law of gravity is to the properties of quintessence. This connection is even more evident in the 'Cuscuton' models, which can be formulated as a specific limit of scalar field dark energy models of

the k-essence type. In this kind of model, the scalar degree of freedom drops out of the equations, reducing the theory to a constraint system for the evolution of the remaining matter content. The corresponding change of the Planck Mass at the horizon scale can be constrained by observations, and this is the aim of Chapter 5.

Another rather fundamental property of quintessence is studied in Chapter 6, namely a possible coupling between dark matter and dark energy. The formalism for a coupled dark matter - dark energy fluid can be written in a rather general way, and we retain this generality in our numerical implementation in CMBEASY. We then consider a specific example of a coupled dark energy model, and investigate its cosmological properties. The output of our numerical implementation for these specific examples has also been used to perform N-body simulations (Baldi 2009), and we present the combined results of the complete numerical treatment of these models from the background level to the non-linear regime (Baldi, Pettorino, Robbers, & Springel 2008).

Chapter 7 then extends the treatment of quintessence properties to couplings to neutrinos. The 'growing neutrino quintessence' scenario that we investigate provides a possible answer to the 'why now?' question, and here we show that its properties on the level of linear perturbations are quite novel (Mota, Pettorino, Robbers, & Wetterich 2008; Pettorino, Mota, Robbers, & Wetterich 2009).

Finally, Chapter 8 gives a short summary of the results of this work.

2 The Homogeneous and Isotropic Universe

A fundamental assumption in modern cosmology is that our Universe is homogeneous and isotropic, if just the scales under consideration are large enough. Built on this hypothesis is an elaborate theoretical apparatus that is very successful in explaining observational data, and in this chapter we will briefly review the basics of this framework. Although our Universe certainly is not homogeneous on scales of galaxies or even clusters of galaxies, an isotropic and homogeneous description of our Universe is nevertheless immensely useful. Many cosmological observations can be either understood directly in these terms, e.g. distance measurement through the observation of SnIa, or by considering small perturbations around this homogeneous and isotropic background in linear theory, e.g. the Cosmic Microwave Background. In fact, in this thesis, we will only once (in Chapter 6) leave the grounds of linear perturbation theory.

2.1 The Background Equations

General Relativity describes the four-dimensional spacetime of our Universe by a pseudo-Riemannian manifold together with a metric g. Since we assume that our Universe is homogeneous and isotropic on sufficiently large scales, the spacetime therefore must admit a slicing in homogeneous and isotropic 3-spaces on constant time hypersurfaces. Then, there is a preferred geodesic time coordinate t, 'cosmic time', such that the 3-spaces of constant cosmic time are maximally symmetric. In principle, these constant-time hypersurfaces can have either positive, negative or zero curvature. In this thesis, we assume a flat universe, i.e. that the curvature vanishes. Hence, the metric has the Friedmann-Robertson-Walker form,

$$ds^2 \equiv g_{\mu\nu}\mathrm{d}x^\mu \mathrm{d}x^\nu = -dt^2 + a(t)^2 \left(\delta_{ij}\mathrm{d}x^i \mathrm{d}x^j\right), \tag{2.1}$$

with scale factor $a(t)$, Greek indices running from 0 through 3, and Latin indices from 1 through 3. The scale factor can conveniently be normalized to be unity today, so that we can write $a_0 = a(t_0) = 1$, denoting present-day values by a subscript 0. It is useful to define the conformal time τ by $\mathrm{d}\tau \equiv a^{-1}\mathrm{d}t$, so that the metric can be written as

$$ds^2 = a(\tau)^2 \left(-\mathrm{d}\tau^2 + \delta_{ij}\mathrm{d}x^i \mathrm{d}x^j\right). \tag{2.2}$$

The Hubble parameter H is related to the scale factor via

$$H \equiv a^{-1}\frac{\mathrm{d}a}{\mathrm{d}t} \equiv \frac{\dot{a}}{a}, \tag{2.3}$$

where our convention throughout is that a dot denotes derivatives with respect to cosmic time, whereas a prime represents derivatives with respect to conformal time - the comoving Hubble parameter $\mathcal{H}$ then is

$$\mathcal{H} \equiv \frac{a'}{a} = aH. \tag{2.4}$$

The value of the Hubble parameter today is conventionally expressed as $H_0 = 100\,h\,\mathrm{km/sec/Mpc}$, where $h \approx 0.7$ is the Hubble parameter. The energy momentum tensor in a homogeneous and isotropic universe is

$$(T_{\mu\nu}) = \begin{pmatrix} -\rho\, g_{00} & \mathbf{0} \\ \mathbf{0} & p\, g_{ij} \end{pmatrix}, \tag{2.5}$$

where $\rho(t)$ and $p(t)$ are the total energy density and pressure, respectively. The present-day energy density of the flat Universe is called the 'critical density', $\rho_{crit} = 1.88 \times 10^{-29} h^2 \mathrm{gm\ cm^{-3}} = 8.10 \times 10^{-47} h^2 \mathrm{GeV}^4$; the energy density ρ_i of a species i is often expressed as the fraction of the total energy density, $\Omega_i = \rho_i/\rho_{tot}$. The relation between energy density and pressure is parameterized by the equation of state $w(t)$,

$$p(t) = w(t)\rho(t). \tag{2.6}$$

One can also write this equation for the individual contributions to the total energy density and pressure, where e.g. for non-relativistic matter or dust, the pressure vanishes, $w_m = 0$, while for photons and massless neutrinos $w_r = 1/3 =$ const, and a cosmological constant has $w_\Lambda = -1 =$ const.

From the metric, one computes the Ricci Tensor $R_{\mu\nu}$ and the Ricci scalar $\mathcal{R}$ via the Christoffel symbols to get the left hand side of Einstein's Equations, relating the geometry of the Universe to its energy content:

$$G_{\mu\nu} \equiv R_{\mu\nu} - \frac{1}{2} g_{\mu\nu}\mathcal{R} = 8\pi G\, T_{\mu\nu}, \tag{2.7}$$

where G is Newton's constant, and a possible cosmological constant is taken to be part of the energy-momentum tensor. Defining the reduced Planck Mass M_P by $M_\mathrm{P} \equiv (8\pi G)^{-1/2}$, the $0-0$ part of this equation yields the Friedmann Equation,

$$3M_\mathrm{P}^2 H^2 = \rho(\tau), \tag{2.8}$$

and the space-space components give

$$\frac{\ddot{a}}{a} + \frac{1}{2}\left(\frac{\dot{a}}{a}\right)^2 = -\frac{1}{2M_P^2} p. \tag{2.9}$$

These equations can be combined to write

$$\dot{\rho} = -3(\rho + p)\,\frac{\dot{a}}{a}, \tag{2.10}$$

which can also be obtained as a consequence of energy momentum conservation, $T^{\mu\nu}{}_{;\mu} = 0$.

If $w = p/\rho$ is constant, Eq. (2.10) is solved by

$$\rho = \rho_0 \left(\frac{a_0}{a}\right)^{3(1+w)}, \tag{2.11}$$

so that it is easy to see how the energy density of any component with a constant equation of state changes with the scale factor. For example, pressureless matter scales as $\rho_m \propto a^{-3}$, while radiation with $w = 1/3$ scales as $\rho_r \propto a^{-4}$. One can also insert this relation in the Friedmann Equation, Eq. (2.8), to see how the scale factor evolves if the energy is dominated by one particular component with a constant equation of state. One finds that the scale factor evolves as

$$a \propto t^{2/3(1+w)} \qquad \propto \tau^{2/(1+3w)}, \qquad w = \text{const} \quad (\text{but} \neq -1), \tag{2.12}$$

$$a \propto t^{2/3} \qquad \propto \tau^2, \qquad w = 0 \quad (\text{dust matter}), \tag{2.13}$$

$$a \propto t^{1/2} \qquad \propto \tau, \qquad w = 1/3 \quad (\text{radiation}). \tag{2.14}$$

If the equation of state of a particular component varies with time, the energy density involves an integral over its time evolution,

$$\rho_x \propto \exp\left\{-3\int^a \frac{\mathrm{d}a'}{a'}\left[1 + w(a')\right]\right\}. \tag{2.15}$$

It is often very useful to consider energy density and pressure of certain species in terms of their distribution function. For example, the description of perturbations around the homogeneous background in the tightly coupled photon-baryon fluid, responsible for the emergence of the anisotropies in the CMB, is described by following the evolution of the distribution function while keeping track of the Thomson scattering via the collision term in the Boltzmann Equation. Of particular interest to us is the cosmological evolution of neutrinos, since we will study the effects of a coupling of neutrinos to dark energy in Chapter 7. Neutrinos have a Fermi-Dirac distribution,

$$f_0(\epsilon) = \frac{g_s}{h_p^3}\frac{1}{e^{\epsilon/k_b T_0} + 1}, \tag{2.16}$$

where as usual g_s is the number of spin degrees of freedom and h_p is Planck's constant, k_B and Boltzmann's constant (which we set to 1 in our units). With q denoting the comoving momentum, ϵ is given by

$$\epsilon^2 = q^2 + m_\nu^2\, a^2. \tag{2.17}$$

The energy density and pressure in terms of the distribution function are then determined by the phase space integral,

$$\rho_\nu = \frac{1}{a^4}\int q^2 \mathrm{d}q\mathrm{d}\Omega\, \epsilon f_0(q), \text{and} \tag{2.18}$$

$$p_\nu = \frac{1}{3a^4}\int q^2 \mathrm{d}q\mathrm{d}\Omega f_0(q)\frac{q^2}{\epsilon}. \tag{2.19}$$

We have left m_ν as a constant here, but note that in Chapter 7 we will have $m_\nu = m_\nu(\phi)$, which does introduce certain modifications to the equations.

2.2 Distance Measures

In order to infer the geometrical properties of the Universe from observations we need to measure distances in the Universe. We can use the photons emitted by astronomical sources to determine their redshift, assuming we know the wavelength with which they were emitted, for example by considering a specific spectral line. If a photon with wavelength λ is emitted at a time τ, it will reach us today with a wavelength

$$\lambda_{obs} = \frac{\lambda}{a(\tau)} = (1+z)\,\lambda. \tag{2.20}$$

This defines the redshift z,

$$z + 1 = \frac{1}{a}. \tag{2.21}$$

The comoving distance between us and a distant source at a redshift z, or equivalently, a scale factor a is given by

$$\chi(a) = \int_{t(a)}^{t_0} \frac{\mathrm{d}t'}{a(t')} = \int_a^1 \frac{\mathrm{d}a'}{a'^2 H(a')}. \tag{2.22}$$

Another possible measure of distance is the angular diameter distance D_A to an object with a given physical size l, seen at redshift z_1. The angular diameter distance, as the name suggests, is defined via the angle ϑ subtended by the object,

$$D_A = l/\vartheta\,. \tag{2.23}$$

The comoving size of the object is l/a, and the comoving distance is given by Eq. (2.22), so that

$$D_A = a\,\chi = \frac{\chi}{1+z}. \tag{2.24}$$

Finally, distances can also be inferred from the flux F (i.e. the energy received per unit time per unit area) from a source at redshift z_S with a known luminosity L (i.e. the energy emitted per unit time); the luminosity distance is defined as

$$D_L(z_S) \equiv \left(\frac{L}{4\pi F}\right)^{1/2}. \tag{2.25}$$

The relation of this definition the angular diameter distance can be deduced by considering the energy emitted in a proper time interval of the source, $\mathrm{d}t_S = a(\tau_S)\mathrm{d}\tau$, which is $La(\tau_S)\mathrm{d}\tau$. This energy is then redshifted, by a factor of $1/(1+z_S) = a(\tau_S)$. It is also distributed over a spherical shell with the radius $\chi(z_S)$, so that flux per proper time of the observer at $a_{obs} = 1$ is

$$F = \frac{La^2(z_S)}{4\pi\chi^2(z_S)}. \tag{2.26}$$

Replacing F in the definition Eq. (2.25) yields the relation between the different distance measures in the flat Universe,

$$D_L = (1+z)\chi = (1+z)^2 D_A. \tag{2.27}$$

Using the Friedmann Equation to replace $H(z)$ in the definition of the comoving distance, Eq. (2.22), we can now relate the luminosity distance to the energy content of the Universe, and write relations like

$$d_L(z) = \frac{1+z}{H_0} \int_0^z \mathrm{d}z' \left[\Omega_\gamma^0 (1+z')^4 + \Omega_m^0 (1+z')^3 + \Omega_d(z')\right]^{-1/2}, \qquad (2.28)$$

where Ω_r^0 and Ω_m^0 are the fractions of the total energy density today of radiation and matter with the standard scaling behavior, and we anticipate the existence of a dark energy component with an - at least a priori - arbitrary time evolution of the energy density $\Omega_d(z)$.

Supernovae of Type Ia

The relation Eq. (2.28) is a powerful tool to infer the composition of our Universe, if we can determine the left-hand side from observations, and historically, it were exactly such measurements (Perlmutter et al. 1999; Riess et al. 1998) that made the need for $\Omega_d \neq 0$ apparent, namely the observation of supernovae of type Ia. Supernovae can be classified by their spectra, where type Ia supernovae are those that do not have any hydrogen or helium lines, together with an absorption structure due to Si II lines at wavelengths of about $\lambda \approx 610\,nm$. They are the result of the explosion of white dwarf stars when their mass grows to near the Chandrasekhar limit in a binary system. The measurements are usually discussed in terms of their absolute magnitudes M compared to the apparent magnitude m, which are related to fluxes by $m = -(5/2)\log(F) + \text{const.}$ As the flux scales like ${d_L}^{-2}$, the apparent magnitude is $m = M + 5\log(d_L) + \text{const}$, and one arrives at the distance modulus

$$m - M = 5\log\left(\frac{d_L}{10\,\mathrm{pc}}\right), \qquad (2.29)$$

which is the main quantity of cosmological interest determined from supernovae surveys. The usefulness of SnIa comes from the fact that they are 'standard candles', a fancy term to indicate that they have the same absolute magnitudes, or are at least 'standardizable candles', i.e. the intrinsic differences can be corrected for. While the original samples contained about ~ 50 supernovae covering a redshift range up to $z \lesssim 1$, current compilations cover between 300 and 400 SnIa (Kowalski et al. 2008), and the outlook is that future probes will increase the number to tens of thousands of supernovae discoveries (for a recent overview of future observational prospects, see e.g. Howell et al. 2009), so that the statistical errors are bound to decrease significantly, and understanding the systematic errors in SnIa data becomes increasingly important.

The crucial piece of evidence for dark energy from the first SnIa observations then was the discovery that at recent cosmological times, the deceleration parameter $q \equiv \ddot{a}/aH^2 < 0$. From Eq. (2.9) we see that during matter and radiation domination, $q > 0$ and $\ddot{a} < 0$, i.e. gravity slows down the expansion. Only a component that has $p < -\rho/3$, and therefore $w < -1/3$, can cause the expansion to accelerate, $\ddot{a} > 0$. This is the defining property of the dark energy.

Baryon Acoustic Oscillations

Another way of measuring distances are the baryon acoustic oscillation, which we mention here as one example of the many other cosmological probes that have confirmed the picture of the accelerating universe.

When measuring the large-scale correlation function of galaxies, one finds a peak at a separation of about $100\,h^{-1}$ Mpc. This peak is a remnant of the sound waves in the photon-baryon fluid in the early universe, the acoustic oscillations. In the coupled photon-baryon fluid, these waves can propagate, until at recombination, the wave propagation effectively stops. The comoving distance that a sound wave can travel from the initial seed of a perturbation to the time of recombination is a characteristic length scale, known as the 'sound horizon', denoted by s. It is this scale that is responsible for the observed peak. Its size depends both on the expansion history, and the properties of the photon-baryon plasma, encoded in its speed of sound c_s, and is given by

$$s = \int_{z_{dec}}^{\infty} dz \frac{c_s}{H(z)}, \tag{2.30}$$

where $z_{dec} \sim 1100$ is the redshift of decoupling between the photons and the baryons. Measuring this scale in the in clustering of galaxies in the transverse and line-of-sight directions yields a determination of $\chi(z)/s$ and of $s\,H(z)$, respectively. The power of measurements of the baryon acoustic oscillations now lies in the fact that we can observe the imprint of the acoustic oscillations in the CMB, thereby calibrating the sound horizon at a very high redshift, and then measure this length scale at different redshifts in the large-scale baryon power spectrum. The ratios of these distances then determine the angular-diameter-distance to redshift relation, yielding a powerful geometric measurement of the expansion history of the Universe. The main observational obstacle is the weakness of the acoustic feature in the correlation function ($\approx 10\%$ contrast), and so the first detection (at $z \approx 0.35$) was only reported a few years ago, by Eisenstein et al. (2005). A crucial ingredient for the correct interpretation of these distance ratios is obviously the precise determination of the size of the sound horizon from the CMB, and we will come back to this issue in Chapter 4 in the context of early dark energy models.

The detection of the baryon acoustic peak, however, is not only significant due to its potential for accurate geometric measurements, but also because it provides a confirmation of the paradigm that large scale inhomogeneities grow from small perturbations at $z \sim 1100$ by gravitational clustering, and because the observed size of the feature cannot be reproduced without dark matter, and therefore confirms its existence.

2.3 Scalar Field Dark Energy

If we assume that the measured acceleration is not due to a cosmological constant, but caused by a dynamical dark energy component, then the most natural candidate is a scalar field. We can write down the action of such a scalar field

ϕ with potential V, as

$$\mathcal{S} = -\int \mathrm{d}^4x\sqrt{-g}\left[\frac{1}{2}\partial_\mu\phi\partial^\mu\phi + V(\phi)\right]. \tag{2.31}$$

Varying the action with regard to the metric yields the energy momentum tensor

$$T_{\mu\nu} = \frac{-2}{\sqrt{-g}}\frac{\partial}{\partial g^{\mu\nu}}\left(\sqrt{-g}\mathcal{L}\right) \tag{2.32}$$

$$= \partial_\mu\phi\,\partial_\nu\phi - \left[\frac{1}{2}\partial_\alpha\phi\partial^\alpha\phi + V\right]g_{\mu\nu}, \tag{2.33}$$

and, in the homogeneous background case where spatial derivatives vanish, to an energy density

$$\rho_\phi = -T_0{}^0 = \frac{1}{2a^2}\,\phi'^2 + V(\phi), \tag{2.34}$$

and pressure

$$p_\phi = \frac{1}{3}T_i{}^i = \frac{1}{2a^2}\,\phi'^2 - V(\phi). \tag{2.35}$$

Hence, defining the kinetic energy $T \equiv \dot{\phi}^2/2$, the equation of state becomes

$$w_\phi \equiv \frac{p}{\rho} = \frac{T-V}{T+V}. \tag{2.36}$$

The equation of motion for the field becomes

$$\phi'' + 2\frac{a'}{a}\,\phi' + a^2\frac{\partial V}{\partial\phi} = 0. \tag{2.37}$$

Furthermore, by inserting the expression for the pressure in Eq. (2.9), we can see that in order to get $w_\phi < -1/3$, the condition

$$\dot{\phi}^2 < V(\phi) \tag{2.38}$$

needs to be fullfilled, which in standard quintessence models is reached by very flat potentials, but can theoretically also be obtained by any other mechanism that makes $\dot{\phi}$ small, i.e. slows or completely stops the evolution of the field.

One of the prototypical quintessence potentials is the exponential potential (Wetterich 1988b, 2008),

$$V(\phi) = M_\mathrm{P}^4\exp(-\alpha\,\phi/M_\mathrm{P}), \tag{2.39}$$

which admits scaling solutions for the evolution of the field, where the equation of state follows the dominating component, i.e. radiation or matter. In the scaling regime, the constant α determines the fraction that the dark energy contributes to the total energy density via

$$\Omega_\phi = \frac{n}{\alpha^2}, \tag{2.40}$$

where $n = 4$ (3) during radiation (respectively matter) domination. However, the scaling solutions do not simply convert to the accelerated solutions where

dark energy dominates today. Modifications of a pure exponential potential, such as a polynomial prefactor (Albrecht & Skordis 2000),

$$V(\phi) = V_P(\phi)\exp(-\alpha\,\phi/M_{\rm P}), \tag{2.41}$$

where the prefactor is for example of the form

$$V_P(\phi) = (\phi - B)^\beta + A \tag{2.42}$$

with constants B, β and A. Such modifications can lead to a local minimum in the potential, in which the field can be trapped and cause the onset of acceleration. In Chapter 7, we will encounter a dynamical mechanism that combines the pure exponential potential with a possibility to obtain late-time acceleration, thereby making any additional modifications of the exponential redundant.

A second prototypical potential is the inverse power law (Ratra & Peebles 1988)

$$V(\phi) = A\left(\frac{\phi}{M_{\rm P}}\right)^{-\alpha}, \tag{2.43}$$

which has been widely studied in the literature (e.g. Caldwell, Dave, & Steinhardt (1998); Zlatev, Wang, & Steinhardt (1999); Binetruy (1999); see also Copeland et al. (2006) and references therein). The dynamics in these models can lead to a tracking regime where the equation of state is given by

$$w_\phi \approx \frac{\alpha\, w_{\rm Bgrnd} - 2}{\alpha + 2}, \tag{2.44}$$

where $w_{\rm Bgrnd}$ is the equation of state of the dominant (background) component. The observed quintessence equation of state today restricts the combination of A and α in these models, requiring $0 < \alpha \lesssim 1$. The scale A is then set by the fraction of quintessence observed today - for smaller and smaller α this is akin to finetuning the value of the cosmological constant. Owing to the popularity of this class of models, we will use this potential as a starting point for a set of example models with a dark matter dark energy interaction in Chapter 6.

One can also consider modifying the kinetic term of scalar field dark energy models, and write more general scalar field actions formulated as functions of the field ϕ and of $X \equiv -(1/2)\partial_\mu\phi\partial^\mu\phi$. In these 'k-essence' theories (Armendariz-Picon et al. 2000, 2001), we have

$$S = \int {\rm d}^4x\sqrt{-g}\,p(\phi, X), \tag{2.45}$$

where the cosmic pressure is given by the lagrangian density, p. The corresponding energy density is

$$\rho = 2X\frac{\partial p}{\partial X} - p. \tag{2.46}$$

Certain choices of p, for which the field tracks the radiation component with $w_\phi = 1/3$ early on, but transitions to w_ϕ at the onset of the matter era, have been proposed as solutions to the coincidence problem. An often-employed simplification in the choice of $p(\phi, X)$ is to only consider

$$p(\phi, X) = f(\phi)\tilde{p}(X), \tag{2.47}$$

and tracker models similar to the standard quintessence case can then also be found for example (Chiba et al. 2000) by choosing $f(\phi) \propto \phi^{-\alpha}$ and $\tilde{p}(X) = (-X + X^2)$. For $0 < \alpha < 2$, the k-essence is characterized by a constant equation of state, $w_\phi = -1 + (\alpha/2)(1 + w_{\rm Bgrnd})$, until it starts to dominate the energy density budget, at which point $w_\phi \to -1$. In this work, we will not consider the general case of k-essence cosmology, but study a particular example in Chapter 5.

2.3.1 Parameterizations

Since a clear front runner for a complete particle physics model of dark energy has not yet emerged, it is often times convenient to consider the dark energy not directly in terms of a specific potential for the scalar field, but instead starting from a parameterization of the time evolution of its energy density $\Omega_d(a)$, or of its equation of state $w(a)$. In this way, one can hope to capture the important physical properties and study their consequences, and employ observations to search for hints towards the underlying fundamental theory; we will make extensive use of this approach in Chapter 4.

Converting from the equation of state to the energy density and vice versa can easily be done analytically, using Eq. (2.15). For a universe with certain fractions of the total energy density stored in dark energy, matter, and relativistic species, we have $\Omega_{tot} = \Omega_d + \Omega_m + \Omega_{rel}$, and find the derivative of Ω_d with respect to the scale factor,

$$\begin{aligned} \frac{\mathrm{d}\Omega_d}{\mathrm{d}a} &= \frac{\mathrm{d}}{\mathrm{d}a}\frac{\rho_d}{\rho_{crit}} \\ &= \frac{1}{\rho_{crit}^2}\left[-\frac{3\rho_d}{a}(1+w)\rho_{crit} - \frac{\rho_d}{a}\left(-3\rho_{crit} - \rho_{rel} - 3w\,\rho_d\right)\right], \end{aligned} \tag{2.48}$$

which simplifies to

$$\frac{\mathrm{d}\Omega_d/\mathrm{d}a}{\Omega_d} = 3(1-\Omega_d)a^{-1}w + \Omega_{rel}a^{-1}. \tag{2.49}$$

Dividing both sides by $(1-\Omega_d)$, using $\Omega_d = 1-\Omega_m-\Omega_{rel}$ on the right hand side and re-expressing Ω_{rel} via the scale factor of equality a_{eq} as $\Omega_{rel} = (a_{eq}/a)\Omega_m^0$, one finds that the equation of state is related to the energy density via

$$w_d(a) = \frac{-\mathrm{d}\Omega_d/\mathrm{d}\ln a}{3(1-\Omega_d)\Omega_d} + \frac{1}{3}\frac{1}{1+\frac{a}{a_{eq}}}. \tag{2.50}$$

When neglecting radiation, which is a good approximation in the late universe, this is equivalent to

$$w_d(a) = \frac{-\mathrm{d}\Omega_d/\mathrm{d}\ln a}{3(1-\Omega_d)\Omega_d}. \tag{2.51}$$

In the same vein, the potential $V(a)$ of the scalar field ϕ with a canonical kinetic term can be reconstructed from a given functional form of the equation

of state via

$$V(a) = \frac{1}{2}\left[1 - w(a)\right]\rho(a), \tag{2.52}$$

$$\phi(a) = \int \mathrm{d}a \frac{\sqrt{1+w(a)}}{aH(a)}\sqrt{\rho(a)}, \tag{2.53}$$

which holds as long as $\dot{\phi} \neq 0$.

3 Perturbations

This chapter gives a short summary of the theory of linear perturbations around the homogeneous background described in Chapter 2. As we have stated from the beginning, we expect this treatment to yield useful results, simply because the Universe looks more and more homogeneous the larger the scales become. Even more importantly, gravity should usually cause inhomogeneities to grow, so that the structures that we do observe have evolved out of very small initial fluctuations. That in turn means that linear perturbation theory should be a rather good description especially of the early times of the cosmological evolution. The theory that we - very briefly - review in this chapter indeed yields a remarkably precise description of many cosmological observables, and in particular of the fluctuations visible in the CMB, which are still very small even at the present day, and can to a very good accuracy be calculated entirely in linear theory.

The results of these discussions will not be a prediction for e. g. the exact pattern of the temperature anisotropy that we observe on the sky, nor for the particular matter distribution in the Universe; this would be pointless, as we assume that the initial fluctuations present at the end of inflation are a particular realization of random variables set by a stochastic process. Instead, the predictions will be about statistical properties of these quantities, such as their correlation functions. If the perturbations of the model under consideration are Gaussian, which we are going to assume, then the full information is contained in the Fourier transform of the two-point correlation function, the power spectrum. For a scalar quantity $X(\mathbf{x})$, the power spectrum P_X is defined in terms of its Fourier transform $X(\mathbf{k})$ as

$$\left\langle X(\mathbf{k})\, X^*(\mathbf{k}')\right\rangle = (2\pi)^3 \delta_D(\mathbf{k}-\mathbf{k}') P_X(k), \tag{3.1}$$

where letters in bold face denote 3-vectors. We assume that inflation generates the initial perturbations, and we describe this by the initial perturbation for the metric perturbation Ψ[1], with a power spectrum parameterized as

$$P_\Psi(k) = \frac{2\pi^2}{k^3} A_s \left(\frac{k}{k_\star}\right)^{n_s-1}. \tag{3.2}$$

The parameters are the initial scalar amplitude A_s, given at a pivot scale $k_\star$ (our choice is usually $k_\star = 0.05$ Mpc^{-1}, but $k_\star = 0.002$ Mpc^{-1} is also popular), and the scalar spectral index n_s. We will restrict the discussion here to scalar perturbations, and therefore do not consider e.g. the initial amplitude of tensor fluctuations A_T. This shape of the initial power spectrum is a fundamental input, justified a posteriori by its ability to fit observations; in our parameter

[1] The precise definition of the perturbation variables will be given below.

estimation analysis in Chapter 4, both n_s and A_s will be free parameters, to be determined from observational data. For the analysis of the evolution of perturbations, we only assume that the initial values of all perturbation variables can be set from this input; the method to obtain these initial conditions is then discussed at the end of this Chapter, in Section 3.4.

To motivate the following mathematical considerations, we start by introducing the CMB and the power spectrum of the temperature and polarization anisotropy; together with the matter power spectrum, these are the observable quantities that we want to compute. The purpose of the theoretical machinery in this chapter therefore is to relate the initial power spectrum P_Ψ to these observables. This overview of the theoretical framework is rather brief, since we focus only on the modeling of the dark energy fluctuations together with dark matter and neutrinos, as this is the foundation for the treatment of coupled dark energy models in Chapters 6 & 7. At the end of this chapter, we introduce CMBEASY, the numerical tool we will use in the subsequent chapters to actually compute predictions for dark energy models and compare them with observations, using the framework outlined here.

3.1 The Cosmic Microwave Background

At early times, when the cosmic fluid is dominated by radiation, reaction rates are much faster than the expansion rate, so that the fluid is in thermal equilibrium. The neutrinos are the first to decouple, since they are kept in equilibrium via their weak interaction with electrons. For the photons, the scattering off of free electrons via Thomson scattering is the dominant process. The scattering rate of Thomson scattering is

$$\Gamma_T = \sigma_T n_e, \tag{3.3}$$

where $\sigma_T = 6.6524 \times 10^{-25}\mathrm{cm}^2$ is the Thomson scattering cross section. The scattering rate depends also on the number density of free electrons, n_e. As long as the recombination process,

$$p + e^- \leftrightarrow H + \gamma \tag{3.4}$$

is rapid compared to the expansion, the ionization fraction $x_e \equiv n_e/(n_e + n_H)$, i.e. the number density of free electrons divided by the total number density of neutral hydrogen and electrons, will be given by an equilibrium distribution (well described by the Saha equation). The mean free path of a photon λ_C is given by

$$\lambda_C^{-1} \equiv \tau' \equiv n_e \sigma_T \, a, \tag{3.5}$$

which also defines an absorption coefficient τ'; the integral over conformal time of this coefficient is the optical depth, τ. As long as the ionization fraction is close to unity, $x_e \approx 1$, the mean free path of a photon is $\lambda_C \sim 2.5$ Mpc, which is about two orders of magnitude smaller than the horizon at recombination. For scales larger than this, $\lambda \gg \lambda_C$, the photons are tightly coupled to the electrons

by Thomson scattering (and the electrons are in turn tightly coupled to the protons by Coulomb interactions).

As the Universe expands there will be a certain point in time, when there are not enough photons with energies above the binding energy to ionize the hydrogen. At a temperature of about $T \sim 4000K \sim 0.4$ eV, $z_{rec} \sim 1400$, the protons begin to recombine to neutral hydrogen, the free electron fraction drops, and the mean free path of a photon becomes larger than the Hubble scale. The exact evolution of $n_e(\tau)$, during this time depends on the details of the reactions by which the electrons and protons recombine to neutral Hydrogen and Helium, and can only be solved numerically. Computer codes like CMBEASY usually employ numerical approximations calibrated by more detailed simulations of the recombination processes, such as RECFAST (Seager et al. 2000; Wong et al. 2007), in order to obtain the ionization history for a given background cosmology. Eventually, the photons decouple from the electrons, and the Universe becomes transparent (at $T \approx 0.26$ eV or redshift $z \approx 1100$). Hence, the fluctuations of the energy density in the photon/baryon plasma before recombination are reflected in the temperature anisotropies that we measure today.

However, there is one important caveat: observations find very little neutral hydrogen in the intergalactic medium (Fan et al. 2006), apart from so-called Ly-α-clouds, i.e. clouds of neutral hydrogen that lead to absorption features in the spectra of distant quasars (see Sec. 4.2.4). One is therefore led to conclude that the Universe became reionized at low redshifts. In practice, we account for this by introducing the optical depth to the last scattering surface,

$$\tau = \sigma_T \int_{t_{lss}}^{t_0} a(t) n_e(t) dt, \tag{3.6}$$

as an additional cosmological parameter. So far, we have only mentioned the temperature anisotropies. Yet, the CMB contains much more information. Since the Thomson scattering cross section depends on the polarization of the outgoing photon in the scattering process, information is not only contained in the temperature anisotropies, but also in the polarization of the CMB photons.

Polarization

In Thomson scattering, for an outgoing photon that has a polarization vector that lies in the scattering plane, the cross section is reduced by a factor $\cos^2\beta$, where β is the scattering angle. There is no such reduction for a polarization normal to the scattering plane. Hence, if the incoming photons are isotropically distributed, the polarization will still average out, but if we are in a situation where there is a higher intensity of photons coming in from one direction than from a direction perpendicular to it, a net polarization will build up; therefore, a quadrupole anisotropy (in the electron reference frame) will produce a polarization of the outgoing photon beam.

The polarization that we observe on the microwave sky is described by the Stokes parameters (see e.g. Dodelson 2003), $\mathcal{Q}$, U, and V. In a basis ϵ_1, ϵ_2 that forms a right-handed orthonormal system with the incoming beam, $\mathcal{Q}$ and U measure linear polarization. $\mathcal{Q}$ is the difference of linear polarization along ϵ_1

and ϵ_2, U is the same, but along vectors ϵ_1' and ϵ_2' rotated by 45° each. The fourth Stokes parameter known from electrodynamics, V, which describes circular polarization, is zero for the CMB - Thompson scattering does not produce circular polarization.

The Power Spectra

The temperature anisotropies $\Delta(\mathbf{n})$ of the microwave sky, observed today in a direction $\mathbf{n}$, can be expanded in spherical harmonics,

$$\Delta(\mathbf{n}) \equiv \frac{\Delta T}{T}(\mathbf{n}) = \sum_{l,m} a_{lm} Y_l^m(\mathbf{n}). \tag{3.7}$$

The two-point correlation then is

$$\left\langle \Delta(\mathbf{n})\Delta(\mathbf{n}') \right\rangle = \sum_{l,l',m,m'} \langle a_{l,m} a^*_{l',m'} \rangle Y_l^m(\mathbf{n}) \left(Y_{l'}^{m'}(\mathbf{n}') \right)^*. \tag{3.8}$$

For a distribution of $\Delta T/T$ that is independent of $\mathbf{n}$, we have

$$\langle a_{lm} a^*_{l'm'} \rangle = \delta_{ll'} \delta_{mm'} C_l, \tag{3.9}$$

which defines the coefficients C_l. For the temperature anisotropy, we have

$$\begin{aligned} \left\langle \Delta(\mathbf{n})\Delta(\mathbf{n}') \right\rangle &= \sum_l C_l \sum_{m=-l}^{l} Y_l^m(\mathbf{n}) \left(Y_{l'}^{m'}(\mathbf{n}') \right)^* && (3.10) \\ &= \frac{1}{4\pi} \sum_l (2l+1) C_l^{TT} P_l(\mathbf{n}\cdot\mathbf{n}') && (3.11) \end{aligned}$$

For the polarization, we expand the combination $\mathcal{Q} \pm iU$ in terms of spin-weighted spherical harmonics, ${}_s Y_{lm}$ of weight $s = \pm 2$, which defines the coefficients e_{lm} and b_{lm},

$$(\mathcal{Q} \pm \mathrm{i}U)(\mathbf{n}) = \sum_{l=2} \sum_{m=-l}^{l} (e_{lm} \pm i b_{lm})_{\pm 2} Y_{lm}(\mathbf{n}). \tag{3.12}$$

and corresponding power spectra

$$\begin{aligned} C_l^E &= \langle |e_{lm}|^2 \rangle, && (3.13) \\ C_l^B &= \langle |b_{lm}|^2 \rangle, && (3.14) \\ C_l^{TE} &= \langle a^*_{lm} e_{lm} \rangle && (3.15) \end{aligned}$$

The next step now is to use perturbation theory to connect the initial fluctuations to the power spectra of the CMB.

3.2 Metric and Fluid Perturbations

The mathematical framework of linear perturbations theory in cosmology is well-known. The use of gauge-invariant variables in cosmology is for example reviewed in a seminal article by Bardeen (1980). The formalism that we use here (and in the numerical implementation in CMBEASY) follows Kodama & Sasaki (1984). Our notation is identical to Doran (2005); a very detailed and pedagogical review of perturbation theory (and the CMB) is given by Durrer (2008), where the only notational difference is the opposite sign of the gravitational potential Φ.

The general strategy will be to compute the perturbed versions of the metric as well as of the energy momentum tensor, so that one can then use Einstein's equation and the conservation equations to relate the metric to the energy-momentum perturbations. This yields evolution equations for the perturbation variables, which can for special cases be solved analytically, but in general need to be computed numerically - in our case by CMBEASY.

Decomposition of Perturbation Variables

The metric and energy-momentum perturbations on constant-time hypersurfaces can decomposed into Eigenfunctions of the 3-dimensional Laplacian,

$$\mathbf{\Delta} Q_{\mathbf{k}} = -k^2 Q_{\mathbf{k}}. \tag{3.16}$$

separating the perturbations into scalar, vector and tensor parts, which evolve independently. In a flat universe, we have

$$Q_k = \exp(i\,\mathbf{k}\,\mathbf{x}), \tag{3.17}$$

so that the decomposition is nothing else than a Fourier transform, and therefore e.g. the energy density is given by

$$\rho(\tau, \mathbf{x}) = \rho + \frac{1}{(2\pi)^3} \int \mathrm{d}^3k\, \delta\rho(\tau, \mathbf{k})\, Q_{\mathbf{k}}(\mathbf{x}) \tag{3.18}$$

This decomposition also works for vectors $\mathbf{V}$, since they can be written as the sum of a gradient and a rotation part,

$$\mathbf{V} = \mathrm{grad}\varphi + \mathrm{rot}\mathbf{B}, \tag{3.19}$$

where φ is a scalar function. Together with the definitions of

$$Q_i \equiv -k^{-1} Q_{,i} \quad \text{and}$$
$$Q_{ij} \equiv k^{-2} Q_{,ij} + \frac{1}{3}\delta_{ij} Q,$$

the contribution of a scalar perturbation $B(\tau, \mathbf{k})$ to a vector field B_i can be expressed as

$$B_i(\tau, \mathbf{x}) = B(\tau, \mathbf{k}) Q(\mathbf{k}, \mathbf{x}). \tag{3.20}$$

Correspondingly, the scalar contributions to a tensor field are given by

$$H_{ij}(\tau, \mathbf{x}) = H_L(\tau)Q\delta_{ij} + H_T(\tau)Q_{ij}. \tag{3.21}$$

This only gives the basis functions for scalar type perturbations, but basis functions for vector and tensor perturbations can be derived accordingly. Since we will focus on scalar perturbations in this work, we do not repeat their definition here, and specialize our treatment to the scalar case - the general case can be found in any of the reviews referenced above.

Gauge Transformations

In the context of linear perturbation theory around a Friedmann-Robertson-Walker background, the application of general coordinate transformations (diffeomorphisms) becomes problematic. One could still make use of the usual transformation laws of general relativity, but a given coordinate transformation will, in general, not keep the FRW background invariant, which, in our context, is too high a price to pay. If we consider small perturbations $h_{\mu\nu}$ around the FRW background metric $\bar{g}$,

$$g_{\mu\nu} = \bar{g}_{\mu\nu} + a^2 h_{\mu\nu}, \tag{3.22}$$

we only allow transformations that leave $\bar{g}$ invariant, and therefore deviate only in first order from the identity. One can show (see Doran 2005, for a step-by-step calculation) that such an infinitesimal coordinate transformation,

$$x^\mu \to \tilde{x}^\mu = x^\mu + \epsilon(\tau, \mathbf{x}), \tag{3.23}$$

can be written using the Lie derivative L_ϵ, so that for example the metric perturbation h transforms as

$$h \to h + a^{-2} L_\epsilon \bar{g}. \tag{3.24}$$

In cosmology, these infinitesimal coordinate transformations are called 'gauge transformations'. Conventionally, the transformation vector ϵ is parameterized by its scalar and vector parts, T and L,

$$\begin{aligned} \tilde{\tau} &= \tau + T(\tau)Q(\mathbf{x}) \\ \tilde{x}^i &= x^i + L(\tau)Q^i(\mathbf{x}. \end{aligned} \tag{3.25}$$

The usefulness of these transformations will become obvious in a moment, since we now define the perturbations of the metric and the energy-momentum tensor; one can then choose the functions T and L such that the general forms of the perturbed metric and energy-momentum tensor have the most convenient form.

Metric Perturbations

For the case of scalar perturbations, Eq. (3.20) and Eq. (3.21) are the definitions that can be inserted into the general form of the line element in a perturbed FRW-metric, which is given by (Bardeen 1980)

$$\mathrm{d}s^2 = a(\tau)^2 \left[-(1+2AQ)\,\mathrm{d}\tau^2 - 2B_i\,\mathrm{d}\tau\mathrm{d}x^i + (\delta_{ij} + 2H_{ij})\,\mathrm{d}x^i\,\mathrm{d}x^j\right]. \tag{3.26}$$

We can now apply the general transformation Eq. (3.25) to obtain the behavior of A, B^i and $H_{i,j}$ under gauge transformations. From the explicit calculation, one finds that T and L can be chosen in such a way that two of the perturbation variables vanish. Common choices are the synchronous gauge, defined by setting $A = B = 0$, and the longitudinal, or conformal Newtonian gauge, which is defined by the choice $H_T = B = 0$. In this thesis, we always use quantities in longitudinal gauge, or gauge-invariant quantities, which can be constructed by combining the gauge-dependent quantities in a suitable way. Such gauge invariant quantities were constructed by Bardeen (1980), namely

$$\Psi \equiv A - \frac{a'}{a}k^{-1}\sigma - k^{-1}\sigma', \quad \text{and} \tag{3.27}$$

$$\Phi \equiv H_L + \frac{1}{3}H_T - \frac{a'}{a}k^{-1}\sigma, \tag{3.28}$$

which are called the Bardeen potentials. In longitudinal gauge, we have

$$\sigma \equiv k^{-1}H'_T - B = 0. \tag{3.29}$$

so that the line element corresponding to the perturbed metric becomes

$$\mathrm{d}s^2 = a(\tau)^2\left[-(1+2\Psi)\mathrm{d}\tau^2 + (1+2\Phi)\delta_{ij}\mathrm{d}x^i\mathrm{d}x^j\right], \tag{3.30}$$

where we do not write out the basis functions Q and its counterparts explicitely anymore.

Starting from the perturbed metric, it is now an algebraic exercise to calculate the perturbed version of the left hand side of the Einstein Equation, Eq. (2.7). The next step then is to compute the perturbations of the energy momentum tensor.

The Perturbed Energy-Momentum Tensor

For the energy-momentum tensor, we consider a fluid, for which

$$T^\mu_\nu = p\,\delta^\mu_\nu + (p+\rho)u^\mu u_\nu + \pi^\mu_\nu\,. \tag{3.31}$$

The four-velocity u here is the velocity of the fluid restframe with respect to the coordinate frame. From the condition $u^\mu u^\nu\, g_{\mu\nu} = -1$, the components of u can be shown to be

$$\begin{aligned} u_0 &= -a(\tau)(1+A(\tau)), \\ u_i &= a\,(v(\tau) - B(\tau))\,Q_i\,. \end{aligned} \tag{3.32}$$

The spatial part contains the definition of the velocity perturbation v. Similarly, the density perturbation δ to the background value $\bar\rho$ is defined by

$$\rho \equiv \bar\rho\,(1+\delta\,Q)\,, \tag{3.33}$$

but we ususally drop the overbar for background quantities, since there is little potential for confusion. The spatial trace and the traceless part, in turn, define the perturbations π_L and Π via

$$\begin{aligned} p\delta^i_j &\equiv \bar p\,[1+\pi_L Q]\,\delta^i{}_j, \\ \pi^i_j &\equiv \bar p\,\Pi\,Q^i{}_j. \end{aligned} \tag{3.34}$$

After inserting these definitions of the perturbations δ, v, π_L and Π in Eq. (3.31), we can - just like we did for the perturbed metric - apply the general transformation Eq. (3.25) to determine these perturbation variables in the different gauges; a very useful reference for the comparison between the longitudinal gauge that we employ here and the also very popular synchronous gauge is the review by Ma & Bertschinger (1995).

As we will often switch between gauge-invariant combinations V and D_g of these variables and the longitudinal gauge, the explicit conversion between these two sets is useful enough to write out explicitely, and is given by (e.g. Kodama & Sasaki 1984)

$$V \equiv v - \frac{1}{k}H_T' = v^{longit} \tag{3.35}$$

$$D_g \equiv \delta + 3(1+w)\left(H_L + \frac{1}{3}H_T\right) \tag{3.36}$$

$$= \delta^{longit} + 3(1+w)\Phi \tag{3.37}$$

$$\Gamma \equiv \pi_L - \frac{1}{w}\frac{\bar{p}'}{\bar{\rho}'}\delta. \tag{3.38}$$

Since we either use gauge-invariant quantities, or longitudinal gauge, we drop the explicit '*longit*' designation for v and δ from now on.

Evolution of Perturbations

After these preparations, the final steps are to first use Einstein's Equations to relate the perturbed metric perturbations to the energy-momentum perturbations, and then, to write down the conservation equations for the energy-momentum. This yields the differential equations that govern the evolution of the perturbations. The perturbed Einstein Equations yield:

$$a^2\,\rho\,\delta = 2M_{\rm P}^2\left[k^2\Phi + 3\frac{a'}{a}\left(\Phi' - \frac{a'}{a}\Psi\right)\right], \tag{3.39}$$

$$a^2 v\,(\rho + p) = 2M_{\rm P}^2\,k\left(\frac{a'}{a}\Psi - \Phi'\right), \tag{3.40}$$

$$a^2\,p\,\Pi = -M_{\rm P}^2\,k^2\,(\Phi + \Psi)\,. \tag{3.41}$$

Converting the longitudinal variables to their gauge-invariant counterparts, one finds the perturbed Einstein Equations in gauge-invariant variables:

$$a^2\rho\,D = 2M_{\rm P}^2\,k^2\Phi \tag{3.42}$$

$$a^2(\rho + p)V = 2M_{\rm P}^2 k\left(\frac{a'}{a}\Psi - \Phi'\right) \tag{3.43}$$

$$a^2\,p\,\Pi = -M_{\rm P}^2\,k^2\,(\Phi + \Psi)\,. \tag{3.44}$$

We can combine these equations to obtain expressions for Φ and Ψ,

$$\Psi = -\Phi - M_{\rm P}^{-2}k^{-2}a^2\,p\,\Pi \tag{3.45}$$

$$\Phi = \frac{\sum_\alpha a^2\rho_\alpha D_g^\alpha}{2M_{\rm P}^2k^2 + \sum_\alpha 3\rho_\alpha a^2(1+w_\alpha)}. \tag{3.46}$$

This formulation is useful for the numerical integration, as the right hand side only contains known variables at each timestep, and hence one can also compute Φ' and Ψ' from these expression already during the integration.

Finally, $T^{\mu}{}_{\nu;\mu} = 0$ leads to

$$(\rho + p)\left[3\Phi' + k\,v\right] + 3\frac{a'}{a}\rho(\delta + w\,\pi_L) + \frac{\mathrm{d}}{\mathrm{d}\tau}(\rho\,\delta) = 0, \tag{3.47}$$

together with

$$p\left[\frac{2}{3}\Pi - \pi_L\right] + (\rho + p)\left(4\frac{a'}{a}\frac{v}{k} + \frac{v'}{k}\right) + \frac{v}{k}(\rho' + p') - (\rho + p)\Psi = 0. \tag{3.48}$$

We can define the adiabatic sound speed as $c_s^2 = \dot{\rho}/\dot{p}$ and isolate δ' and v', so that we find an expression suitable for numerical integration:

$$\delta' = -(1+w)\left[kv + 3\Phi'\right] - 3\frac{a'}{a}w\Gamma + 3\frac{a'}{a}\delta\,(w - c_s^2), \tag{3.49}$$

$$v' = \frac{a'}{a}\left(3c_s^2 - 1\right)v + k\,\Psi + \frac{c_s^2}{1+w}\,k\,\delta + \frac{w}{1+w}k\left(\Gamma - \frac{2}{3}\Pi\right). \tag{3.50}$$

These expressions can also be converted to the gauge invariant variables defined in Eq. (3.35), where we find

$$D_g' = -3(c_s^2 - w)\frac{a'}{a}D_g - kV(1+w) - 3\frac{a'}{a}w\Gamma \tag{3.51}$$

$$V' = k\left(\Psi - 3c_s^2\Phi\right) + \frac{a'}{a}(3c_s^2 - 1)V + \frac{c_s^2 k}{1+w}D_g + \frac{wk}{1+w}\left[\Gamma - \frac{2}{3}\Pi\right].$$

As these equations in the fluid-language are derived from the energy-momentum tensor Eq. (3.31), they are valid for any component individually, provided its energy-momentum is conserved, since it was the conservation of energy momentum that yields the evolution equations Eq. (3.47) and Eq. (3.48). A particularly simple case, for example, are perturbations of cold dark matter, for which we have $w = c_s^2 = 0$, so that Eq. (3.51) reduces to:

$$D_g'^{c} = -kV_c \tag{3.52}$$

$$V_c' = -\frac{a'}{a}V_c + k\,\Psi. \tag{3.53}$$

To model the dark energy, it is useful to formulate the system in terms of an arbitrary speed of sound (Bean & Dore 2004; Caldwell & Doran 2005; Erickson et al. 2002) . In the rest frame of the fluid, we define

$$\mu^2 \equiv \frac{\delta\tilde{p}}{\delta\tilde{\rho}}, \tag{3.54}$$

which describes the actual speed with which perturbations propagate, which in general is different from the adiabatic sound speed c_s^2. In this expressions, $\tilde{p}$ and $\tilde{\rho}$ denote quantities in the rest frame of the fluid. From there, we can transform to a random frame (Kodama & Sasaki 1984),

$$\tilde{\delta} = \delta + 3\mathcal{H}(1+w)\frac{v}{k}, \tag{3.55}$$

and find that the pressure perturbation δp is given by

$$\delta p = \mu^2 \delta\rho + \rho \frac{V}{k} \left[4\mathcal{H}(\mu^2 - w) + \frac{w'}{1+w} \right]. \tag{3.56}$$

A canonical scalar field has $\mu^2 = 1$, whereas in more general dark energy theories, like k-essence, the speed of sound can be time and scale dependent. Together, the equations combine to give the evolution equations for the perturbations of the dark energy, namely

$$\delta'_\phi = -3(1+w_\phi)\Phi' - k(1+w_\phi)V_\phi - 3\mathcal{H}(\frac{\delta p_\phi}{\rho_\phi} - w\delta_\phi), \tag{3.57}$$

$$v'_\phi = (3w_\phi - 1)\mathcal{H}(1+w_\phi)v_\phi + k\left[(1+w_\phi)\Psi + \frac{\delta p_\phi}{\rho_\phi}\right]. \tag{3.58}$$

When dark matter is coupled to the dark energy, the case we consider in Chapter 6, only the combined energy momentum tensor is conserved, but the individual conservation equations will obtain a source term that accounts for the coupling - the changes to the formalism presented here will be outlined in Section 6.1.

3.3 The Distribution Function

The fluid formulation is only appropriate for the dark energy and matter perturbations; neutrinos and photons can only be described by following their full distribution function. As an example of this treatment, we review the case of massive neutrinos here, in anticipation of the study of a dark energy - neutrino coupling in Chapter 7, which will be based on this formalism.

When writing down the perturbed distribution function, one usually chooses the comoving momentum $q_i = a p_i$ as a coordinate in phase space, instead of the proper momentum p_i measured by an observer at a fixed spatial coordinate x^i, and splits q_i into magnitude q and direction $\mathbf{n}$, $q_j = q n_j$, with $n^i n_i = \delta_{ij} n^i n^j = 1$. We follow Ma & Bertschinger (1995), and denote the perturbation to the zeroth-order f_0 by $\mathbf{\Psi}_{ps}$ and write

$$f(x^i, \tau, q, n_j) = f_0(q)\left[1 + \mathbf{\Psi}_{ps}(x^i, \tau, q, n_j)\right]. \tag{3.59}$$

We can recover the energy momentum tensor via

$$T_{\mu\nu} = \int \mathrm{d}^3 P \frac{1}{\sqrt{-g}} \frac{P_\mu P_\nu}{P^0} f(x^i, P, \tau), \tag{3.60}$$

noting that in longitudinal gauge the conjugate momenta P_i of the coordinates x^i are related by

$$P_i = a(1+\Phi)p_i. \tag{3.61}$$

For example, this relation leads to Eq. (2.18) in the unperturbed case for neutrinos; here, we will use this relation to recover the perturbations to the density

and pressure from the perturbation of the distribution function, $\mathbf{\Psi}_{ps}$. The time evolution of the distribution function is described schematically by

$$\frac{\mathrm{d}f}{\mathrm{d}\tau} = C[f]. \tag{3.62}$$

This is the Boltzmann Equation, where the right hand side describes changes in the distribution function due to collision between species. The detailed computation of this term is crucial when considering the change in f for the coupled photon-baryon fluid before decoupling. Luckily, since we concentrate on the neutrinos, we do not need to worry about this term, and only need to compute the collisionless Boltzmann equation:

$$\frac{\mathrm{d}f}{\mathrm{d}\tau} = \frac{\partial f}{\partial \tau} + \frac{\mathrm{d}x^i}{\mathrm{d}\tau}\frac{\partial f}{\partial x^i} + \frac{\mathrm{d}q}{\mathrm{d}\tau}\frac{\partial f}{\partial q} + \frac{\mathrm{d}n_i}{\mathrm{d}\tau}\frac{\partial f}{\partial n_i} = 0. \tag{3.63}$$

The last term is a second order quantity, and is therefore neglected in the linear calculation (without perturbations, the distribution function does not depend on direction, and the momenta - and their direction - can only change in the presence of a potential, which is also a first order quantity). The $\mathrm{d}x^i/\mathrm{d}\tau$ can be computed using $P^\mu \equiv \mathrm{d}x^\mu/\mathrm{d}\lambda$. The geodesic equation

$$P^0\frac{\mathrm{d}P^\mu}{\mathrm{d}\tau} + \Gamma^\mu{}_{\alpha\beta}P^\alpha P^\beta = 0, \tag{3.64}$$

can be used to obtain the momentum derivative

$$\frac{\mathrm{d}q}{\mathrm{d}\tau} = -\Phi' - \epsilon(q,\tau)n_i\partial_i\Psi, \tag{3.65}$$

and we recall the definition of $\epsilon^2 = q^2 + m_\nu^2\, a^2$ from Chapter 2. We have spelled out the momentum derivative explicitely, since we already have the case of neutrinos with a varying mass in mind, where $m_\nu = m_\nu(\phi)$, so that this term in the Boltzmann Equation will acquire extra terms in Chapter 7. Combining the results for the individual terms, the Boltzmann Equation then can be expressed as

$$\frac{\partial \Psi_{ps}}{\partial \tau} + i\frac{q}{\epsilon}(\mathbf{k}\cdot\mathbf{n})\Psi_{ps} + \frac{d\ln f_0}{d\ln q}\left[-\Phi' - i\frac{\epsilon}{q}(\mathbf{k}\cdot\mathbf{n})\Psi\right] = 0. \tag{3.66}$$

The only directional dependence of this equation comes via $(\mathbf{k}\cdot\mathbf{n})$, which motivates the expansion using Legendre polynomials. Defining

$$\xi \equiv k^{-1}\mathbf{k}\cdot\mathbf{n}, \tag{3.67}$$

To solve the Boltzmann Equation for massive neutrinos, Ψ_{ps} is now expanded in a Legendre series,

$$\Psi_{ps} = \sum_{l=0}^{\infty}(-i)^l(2l+1)\Psi_{ps,l}P_l(\xi) \tag{3.68}$$

with Legendre Polynomials P_l. The relation between the perturbation variables in k-space and the expansion of the perturbed distribution function is then given

by:

$$\delta\rho_\nu = 4\pi a^{-4} \int q^2 \mathrm{d}q\, f_0(q) \epsilon \Psi_{ps,0} \tag{3.69}$$

$$\delta p_\nu = \frac{4\pi}{3} a^{-4} \int q^2 \mathrm{d}q\, \frac{q^2}{\epsilon} f_0(q) \Psi_{ps,0} \tag{3.70}$$

$$(\rho_\nu + p_\nu) v = 4\pi a^{-4} \int q^2 \mathrm{d}q q f_0(q) \Psi_{ps,1} \tag{3.71}$$

$$(\rho_\nu + p_\nu) \sigma_\nu = \frac{8\pi}{3} a^{-4} \int q^2 \mathrm{d}q \frac{q^2}{\epsilon} f_0(q) \Psi_{ps,2} \tag{3.72}$$

However, we still need to solve the Boltzmann Equation, and express the solution in a form that can be numerically evaluated. The well-known procedure to do exactly that operates along the following lines:

- First multiply the k-space version of Eq. (3.66) by $P_l(\xi)$,
- insert the expansion of Ψ_{ps},
- integrate both sides of the equation over ξ: $\int_{-1}^{1} \mathrm{d}\xi$,
- and then consider the orthonormality relations of the Legendre polynomials, and their recurrence relation $(l+1)P_{l+1}(\xi) = (2l+1)\xi P_l(\xi)$.

The end result of this calculation is a hierarchy of expressions for the conformal time derivatives of the moments $\Psi_{ps,l}$, namely:

$$\begin{aligned}
\Psi'_{ps,0} &= -\frac{qk}{\epsilon} \Psi_{ps,1} + \mathbf{\Phi}' \frac{d \ln f_0}{d \ln q}, \\
\Psi'_{ps,1} &= \frac{qk}{3\epsilon} (\Psi_{ps,0} - 2\Psi_{ps,2}) - \frac{\epsilon k}{3q} \mathbf{\Psi} \frac{d \ln f_0}{d \ln q}, \\
\Psi'_{ps,l} &= \frac{qk}{(2l+1)\epsilon} \left[l \Psi_{ps,l-1} - (l+1) \Psi_{ps,l+1} \right] \ , \ l \geq 2.
\end{aligned} \tag{3.73}$$

This is an infinite set of equations, one for each moment $l = 0..\infty$. Fortunately, higher multipole moments decay rapidly, and in practice only the first few multipoles need to be evolved numerically (~ 30 already yields an accuracy that is sufficient for most purposes). Instead of setting the last multipole to zero, approximating the behavior of the first non-evolved one helps to improve the accuracy; there are a few approximation schemes that have been proposed in the literature, but the original one by Ma & Bertschinger (1995) works quite well, setting

$$\Psi_{ps,l_{max}+1} \approx \frac{(2l_{max}+1)\epsilon}{qk\tau} \Psi_{ps,l_{max}} - \Psi_{ps,l_{max}-1}. \tag{3.74}$$

This completes the set of equations necessary to numerically compute the evolution of the Boltzmann hierarchy for massive neutrinos from some suitable initial conditions.

Photons, Baryons, and Electrons

What remains is the derivation of the evolution of the perturbations for the photons, and the baryons. Conceptually, the derivation of the photon evolution follows the same steps as for the massive neutrinos (indeed, for massless particles the phase space integrals in the equations can be simplified considerably). What makes photons more interesting, however, are their interactions with the baryons and electrons.

The mathematical description of the CMB polarization is one of the more intricate parts of the theory of the Cosmic Microwave Background. However, none of our considerations in the following introduce any changes to the standard treatment (literature that uses the same notation as the numerical implementation in CMBEASY includes Durrer 2008; Doran 2005). When considering a dark energy component coupled either to dark matter (Chapter 6) or to neutrinos (Chapter 7), only the perturbation equations that we have outlined above will be modified. Nevertheless, since the physical observables are the photons of the CMB, let us briefly sketch the remaining steps towards the description of the anisotropies that we see today.

Boltzmann Equations

Instead of using the photon distribution function directly, we use the temperatrue perturbation Δ as a more intuitive variable. This is, of course, directly connected to the distribution function of the photons, so that we can relate the first few moments of the temperature perturbation Δ to the fluid perturbation variables in a given gauge in a way similar to the neutrino case, namely via

$$\delta_\gamma = 4\Phi + \Delta_0, \tag{3.75}$$

$$V_\gamma = \Delta_1, \tag{3.76}$$

$$\Pi_\gamma = \frac{12}{5}\Delta_2. \tag{3.77}$$

Instead of Δ, which is again a gauge-dependent variable, we can also define a gauge-invariant quantity,

$$\mathcal{M} \equiv \Delta + 2\left(H_L + \frac{1}{3}H_T\right) + \mathrm{i}\xi k^{-1}H_T' - \xi^2 H_T, \tag{3.78}$$

which, if Δ is in longitudinal gauge, reduces to

$$\mathcal{M} = \Delta + 2\Phi, \tag{3.79}$$

and can be expanded in terms of Legendre polynomials [2]

$$\mathcal{M}(\tau, \mathbf{x}, \mathbf{n}) = \sum_l (-\mathrm{i})^l \mathcal{M}_l(k,\tau) P_l(\mathbf{n}) Q. \tag{3.80}$$

The polarization is expanded via spin-weighted spherical harmonics,

$$(\mathcal{Q} \pm \mathrm{i}U)(\tau, \mathbf{x}, \mathbf{n}) = \sum_{l=2} (-\mathrm{i})(E_l \pm \mathrm{i}B_l) \times \sqrt{\frac{4\pi}{2l+1}}{}^{\pm 2}Y_l{}^0(\mathbf{n}) Q. \tag{3.81}$$

[2] Note that $\mathcal{Q}$ is different from the eigenfunctions of the 3-d Laplacian Q; see Eq. (3.17).

For scalar perturbations, $B_l = 0$[3]. The Boltzmann equation for $\mathcal{M}$ is given by

$$\begin{aligned}&\mathcal{M}' + \mathrm{i}k\xi\mathcal{M} + \kappa'\mathcal{M} \\ &\quad = \mathrm{i}\xi k\left(\Phi - \Psi\right) + \kappa'\left(\frac{1}{4}\Delta_g^\gamma - \mathrm{i}\xi V_b + \frac{1}{10}P_2(\xi)\left[\sqrt{6}E_2 - \mathcal{M}_2\right]\right),\end{aligned} \tag{3.82}$$

whereas for the polarization one finds

$$\mathcal{Q}' + \mathrm{i}k\xi\mathcal{Q} + \kappa'\mathcal{Q} = \frac{\kappa'}{10}\left(P_2(\xi) - 1\right)\left[\sqrt{6}E_2 - \mathcal{M}_2\right]. \tag{3.83}$$

These two equations need to be solved in addition to the evolution equations for neutrinos, baryons and dark matter and the dark energy, which is again done by inserting the multipole expansions Eq. (3.80) and Eq. (3.81), and then of projecting out multipoles, resulting in a hierarchy of equations for $\mathcal{M}_l$ and E_l.

Mapping Anisotropies onto the Sky

The actual observed quantity, of course, is the temperature (and polarization) anisotropy today, so we want to know $\mathcal{M}(\tau_0, \xi)$; the clever and now standard way of how to compute this from the hierarchies for $\mathcal{M}_l$ and E_l is due to Seljak & Zaldarriaga (1996), who showed how it is possible to cleanly separate the integration into a geometrical term and a source term, where only the source term depends on the E_l and $\mathcal{M}_l$ (and only on the first few of them). This *line of sight* approach allows to calculate the source terms, which depend on the system of evolution equations for all the perturbation variables we have considered so far, for only relatively few k-modes, as they only vary slowly with the wavenumber. The integration over the geometrical part can then be done afterwards; this approach saves a large amount of computational time - about two orders of magnitude on then-standard CPUs.

The first step in this approach is to define a function L,

$$L \equiv \exp(\mathrm{i}\xi k\tau)\exp(\kappa(\tau)\mathcal{M} \tag{3.84}$$

and then note that in terms of this function, the Boltzmann equation Eq. (3.80) is given by:

$$L' = e^{\mathrm{i}\xi k\tau}e^{\kappa(\tau)}\left[\mathrm{i}\xi k(\Phi - \Phi) + \kappa'\left(\frac{1}{4}D_g^\gamma - \mathrm{i}\xi V_b - \frac{1}{2}(3\xi^2 - 1)\mathcal{C}\right)\right], \tag{3.85}$$

where $\mathcal{C} = (M_2 - \sqrt{6}E_2)/10$. The temperature anisotropy today then is

$$\mathcal{M}(\xi, \tau_0) = e^{\mathrm{i}\xi k\tau_0}e^{-\kappa(\tau_0)}L(\tau_0), \tag{3.86}$$

so L' needs to be integrated over conformal time; the integration can be rewritten (i.e. integrated by parts) to eliminate any dependence on ξ that appeared on the right hand side of Eq. (3.80). It is also useful to define the visibility function,

$$g \equiv \kappa'\exp\left[\kappa(\tau) - \kappa(\tau_0)\right]. \tag{3.87}$$

[3] Weak lensing of the CMB introduces a B-mode component, which we do not discuss here; see Lewis & Challinor (2006) for a review of CMB lensing, and Robbers (2006) for a discussion of the numerical implementation in CMBEASY. An example B-mode power spectrum is shown in Fig. 4.8.

This function is sharply peaked at the time of recombination, and will encode the fact that we see the CMB (almost) as it was at that time. These manipulations result in the final expression of the temperature anisotropy,

$$\mathcal{M}(\xi,\tau_0) = \int_0^{\tau_0} \exp\left[\mathrm{i}\xi k(\tau-\tau_0)\right] S_T(k,\tau)\mathrm{d}\tau, \tag{3.88}$$

with the source term

$$\begin{aligned} S_T &= -e^{k(\tau)-k(\tau_0)}\left[\Phi'-\Psi'\right] + g'\left[\frac{V_b}{k}+\frac{3}{k^2}\mathcal{C}'\right] + g''\frac{3}{2k^2}\mathcal{C} && (3.89)\\ &+ g\left[\frac{1}{4}D_g^\gamma + \frac{V_b'}{k} - (\Phi-\Psi) + \frac{\mathcal{C}}{2} + \frac{3}{2k^2}\mathcal{C}''\right] && (3.90)\end{aligned}$$

In this expression, the most important features the temperature anisotropies that we observe today are already apparent: the last term has a prefactor of g, therefore the anisotropies get their largest contribution from the density contrast in the photon gas from that time - in fact, the behavior of D_g^γ is the main contribution towards the oscillations in the C_l spectrum. The V_b term (Doppler term) describes the relative motion of emitter and observer. The term with $[\Phi'-\Psi']$ is the integrated Sachs-Wolfe effect, describing the red- or blue-shift of a photon that travels through an evolving gravitational potential; finally the $[\Phi-\Psi]$ term is responsible for the ordinary Sachs-Wolfe effect, the main contribution to the power spectrum on very large scales.

The Multipole Spectrum

This brings us full circle, as we can now express the C_ls that we had introduced in Section 3.1 (p. 20) in terms of the temperature anisotropy. First, we note that the evolution of the perturbation quantities does not depend on the direction of $\mathbf{k}$, so that for a perturbation $A(\mathbf{k},\tau_0,\mathbf{n})$ we can write

$$A(\mathbf{k},\tau_0,\mathbf{n}) = \psi^{\mathrm{ini}}(\mathbf{k})A(k,\tau_0,\mathbf{n}), \tag{3.91}$$

where the power spectrum of $\psi^{\mathrm{ini}}(\mathbf{k})$,

$$\langle\psi^{\mathrm{ini}}(\mathbf{k})\,\psi^{\mathrm{ini}}(\mathbf{k}')^*\rangle = \frac{2\pi^3}{k^3}P_\Psi(k)\delta_D(\mathbf{k}-\mathbf{k}'), \tag{3.92}$$

is the input spectrum of Eq. (3.2) and encodes the initial correlation. To obtain the C_l, we first project out the individual a_{lm}, and then insert the Fourier decomposition,

$$\begin{aligned} a_{lm} &= \int \mathrm{d}\mathbf{n}\,[Y_l^m(\mathbf{n})]^*\,A(\mathbf{x_0},\tau_0,\mathbf{n}) && (3.93)\\ &= \int \mathrm{d}\mathbf{n}\,[Y_l^m(\mathbf{n})]^* \int \frac{\mathrm{d}^3k}{(2\pi)^3}A(\mathbf{k},\tau_0,\mathbf{n})\exp(\mathrm{i}\mathbf{kx}). && (3.94)\end{aligned}$$

We can find the expression for the temperature anisotropy, $\mathcal{M}$, by substituting A by the integral expression we found for $\mathcal{M}$ in Eq. (3.88), and use the definition

of the C_l in terms of the a_{lm}, so that we have finally have an expression for the temperature power spectrum:

$$C_l^{TT} = \frac{1}{2l+1}\sum_m \langle a_{lm}^* a_{lm}\rangle \tag{3.95}$$

$$= \frac{1}{2l+1}\int \frac{\mathrm{d}^3k}{(2\pi)^3} P_\Psi(k) \tag{3.96}$$

$$\times \sum_m \left| \int \mathrm{d}\tau\, \mathrm{d}\mathbf{n}\, Y_l^m(\mathbf{n})\, \exp(\mathrm{i}k\xi[\tau-\tau_0])\, S_T(k,\tau)\right|^2 . \tag{3.97}$$

The last step then is to use the following relation for the spherical Bessel functions j_l:

$$\int \mathrm{d}\mathbf{n}\, Y_l^m(\mathbf{n}) \exp(\mathrm{i}\xi x) = \sqrt{4\pi(2l+1)}\, i^l j_l(x)\delta_{0m}. \tag{3.98}$$

The integral over $\mathbf{n}$ in Eq. (3.95) will therefore give a spherical Bessel function in the final result. If we define

$$\mathcal{M}_l^T = (2l+1)\int \mathrm{d}\tau j_l\left(k[\tau_0-\tau]\right) S_T(k,\tau), \tag{3.99}$$

the C_l^{TT} can be written in the following way:

$$C_l^{TT} = \frac{4\pi}{(2l+1)^2}\int \frac{\mathrm{d}^3k}{(2\pi)^3} P_\Psi(k)\left[\mathcal{M}_l(k)\right]^2 . \tag{3.100}$$

From this expression, the recipe for a numerical computation of the C_l is obvious:

- evolve the perturbation equations for a suitably chosen set of Fourier modes k from their initial conditions to today and save the source term S_T at a sufficient number of timesteps τ_i
- compute the result of folding the source terms with the spherical Bessel functions
- square the result, and obtain the final C_l^{TT} by integrating over Fourier modes k times the initial power spectrum $P_\Psi(k)$.

As to polarization, it is remarkable that the final result can be expressed just as concisely as for the temperature, even though the complete derivation is more involved than for the temperature (among other things, we have to deal with spin-weighted spherical harmonics, which also depend on the chosen polarization basis orthogonal to $\mathbf{n}$). The source term for the polarization can be written as

$$S_E = 3g\frac{\mathcal{C}}{4\left[k(\tau-\tau_0)\right]^2}, \tag{3.101}$$

where $\mathcal{C} = (M_2 - \sqrt{6}E_2)/10$ as above, and together with the definition for Δ_l^E,

$$\Delta_l^E = (2l+1)\sqrt{\frac{(l-2)!}{(l+2)!}}\int \mathrm{d}\tau j_l\left(k[\tau_0-\tau]\right) S_E(k,\tau), \tag{3.102}$$

the polarization power spectrum and the cross correlation with temperature are given by

$$C_l^{EE} = \frac{4\pi}{(2l+1)^2}\int \frac{\mathrm{d}^3k}{(2\pi)^3} P_\Psi(k)\left[\Delta_l^E(k)\right]^2 \tag{3.103}$$

$$C_l^{TE} = \frac{4\pi}{(2l+1)^2}\int \frac{\mathrm{d}^3k}{(2\pi)^3} P_\Psi(k)\Delta_l^E(k)\mathcal{M}_l(k). \tag{3.104}$$

The only missing piece now is how to set the initial values of the perturbation variables, i.e. relating the initial fluctuations in the densities, velocities and so forth at early times to the initial curvature perturbation and its power spectrum, Eq. (3.2).

3.4 Initial Conditions

The strategy for finding the initial conditions is to consider the evolution equations for each $k-$mode at early times, during radiation domination, in the limit where $x \equiv k\tau \ll 1$ when the mode is still far outside the horizon. One can then expand the evolution equations for the perturbation variables in powers of x, and write down the system with the perturbed Einstein Equations. The solutions to these equations are classified using the gauge-invariant entropy perturbation $S_{\alpha,\beta}$ between two species α and β (see e. g. Kodama & Sasaki 1984)

$$S_{\alpha,\beta} \equiv \frac{D_g^\alpha}{1+w_\alpha} - \frac{D_g^\beta}{1+w_\beta}. \tag{3.105}$$

Adiabatic initial conditions correspond to the case when all $S_{\alpha,\beta}$ vanish. To classify the remaining modes, one introduces the curvature perturbation[4] on hyper-surfaces of uniform energy density of the component α,

$$\zeta = \left(H_L + \frac{1}{3}H_T\right) + \frac{\delta\rho_\alpha}{3(1+w_\alpha)\rho_\alpha}, \tag{3.106}$$

where the total curvature perturbation on slices of uniform total energy density is given by

$$\zeta_{tot} = \left(H_L + \frac{1}{3}H_T\right) + \frac{\sum_\alpha \delta\rho_\alpha}{\sum_\alpha 3(1+w_\alpha)\rho_\alpha}, \tag{3.107}$$

and for a constant w, we have $\zeta_{tot} \propto \Psi$. Besides the adiabatic initial conditions, one defines the 'isocurvature' modes by requiring $\zeta_{tot} = 0$, while one species σ has $S_{\alpha,\beta} \neq 0$, and for all other species we still require $S_{\alpha,\beta} = 0$. In the remainder of this work, we only consider adiabatic initial conditions, for which explicit expressions in a universe with quintessence are given by Doran et al. (2003)

$$D_g^\nu = D_g^\gamma = \frac{4}{3}D_g^b = \frac{4}{3}D_g^c = \frac{4}{3}(1+w_\phi)^{-1}D_g^\phi, \tag{3.108}$$

[4]There are slightly different definitions of this quantity in the literature; we follow Doran et al. (2003).

and

$$V_c = V_\gamma = V_\nu = V_\phi = -\frac{5}{4}\mathcal{P}, \tag{3.109}$$

where $\mathcal{P} = (15 + 4\Omega_\nu)^{-1}$. The overall amplitude of the perturbations for each $k-$mode is then set by calculating Ψ via Eq. (3.45), and normalizing according to the amplitude of the initial power spectrum of Eq. (3.2), determined by the specific values of A_s and n_s.

3.5 Numerical Tools

3.5.1 Cmbeasy

We have now all the ingredients to numerically evaluate the background history, the evolution of perturbations, and the CMB power spectra for cosmologies with a dark energy component, and this will be the topic of the next chapters. The results that we discuss there have been computed using CMBEASY (Doran 2003), updated and extended by implementing the respective models, e.g. coupled dark energy cosmologies (Chapter 6) and growing neutrino quintessence models (Chapter 7).

CMBEASY is implemented in the C++ programming language, and is based on CMBFAST (Seljak & Zaldarriaga 1996), but almost all of its code has been re-implemented; it is, however, not a completely independent implementation.

From the discussion of the theory of the homogeneous background in Chapter 2 and of the perturbations around this background in this chapter, it is clear that the computation of model predictions can be split in separate parts:

- computing the expansion history for a given model,
- calculating the thermal history; as discussed on p. 19, we rely on a version of RECFAST (Seager et al. 2000; Wong et al. 2007) ported to C++,
- evolving the perturbations from their initial conditions, and compute the 'observables', such as the CMB spectra following the recipe outlined on p. 32, and e.g. the matter power spectra.

The output generated by this procedure can then be compared to observational data, in order to asses the viability of a given model. The predictions of a particular model depend on the input parameters, of which the ΛCDM-model has at least six: the baryon and cold dark matter densities today, the value of the Hubble paramater, the slope and amplitude of the initial fluctuations, and the optical depth to the last scattering surface. Then there are the neutrino masses, possibly a running of the spectral index, the amplitude of tensor fluctuations and so forth, so that the dimensionality of the parameter space quickly becomes rather high, especially when considering dark energy models that are characterized by additional parameters; we therefore need methods to reduce the amount of computational resources needed to explore the parameter space.

3.5.2 AnalyzeThis!

Specifically, when we study cosmological models in the following, we want to quantify how likely it is that a particular model, with a specific set of values for its parameters, denoted m, is the true description of our Universe, given a set of observational data d_i with associated errors σ_i. That is, we want to find the propability $\pi(m|\{d_i, \sigma_i\})$. However, this is not exactly the quantity that we can compute directly. Rather, the results of our computation are either quantities like the luminosity distances, or expectation values and variance for e.g. the temperature of the CMB in different directions for a given model, that is to say we compute $\pi(\{d_i, \sigma_i\}|m)$. The connection between these two quantities is of course Bayes' theorem, which states

$$\pi(m|\{d_i, \sigma_i\}) = \frac{\pi(\{d_i, \sigma_i\}|m)\,\pi(m)}{\pi(\{d_i, \sigma_i\})}, \tag{3.110}$$

where $\pi(m)$ is the prior, encoding our prior knowledge of the parameter space, e. g. the bounds on the values that the model parameters can take, and $\pi(\{d_i, \sigma_i\})$ is the evidence. In the following, we will estimate the confidence intervals for parameters within the context of one cosmological theory (e.g. ΛCDM) at a time, so that the total probability should be normalized to unity, and the evidence is only an overall normalization factor and hence unimportant. It is, however, the crucial quantity in the context of Bayesian model comparison techniques (see e.g. Trotta 2008).

The most obvious way to compute the posterior distribution would be to interpolate it from a sufficient number of likelihood evaluations on a grid. This approach is however infeasible for a high dimensionality of the parameter space. There are several techniques that solve this problem, and the method of choice for cosmological parameter estimation is the Markov Chain Monte Carlo (MCMC) approach, made popular in cosmology by the implementation in CosmoMC (Lewis & Bridle 2002), which employs Camb (Lewis et al. 2000) as its underlying Boltzmann code. In the following, we use the MCMC implementation of Cmbeasy, christened 'AnalyzeThis!', as originally presented in Müller (2005) as well as Doran & Müller (2004), with several extensions and modifications.

4 Early Dark Energy

In the previous chapters, we have covered the foundations necessary to study specific dark energy models, to compute their predictions, and to compare those predictions with observational data. In this chapter, we will apply this machinery to the investigation of 'early dark energy' models, i.e. cosmological models in which the dark energy contributes a non-negligible fraction to the total energy budget even at high redshifts. In this regard, this class of early dark energy models is distinct not only from ΛCDM cosmologies, but also from many standard scalar field models of dark energy, where the dark energy component is assumed to be of no importance at all for redshifts higher than a few. We will now briefly review the effect of early dark energy on the cosmological evolution. We then compare a sample of early dark energy models to observational data and compute upper bounds for the amount of early dark energy. At the same time, we compare these early dark energy models to the standard ΛCDM case and other scalar field dark energy models.

In the second part of this chapter, we ask the question whether it is possible to detect early dark energy in the CMB power spectra. We show quantitatively how assuming a negligible fraction of early dark energy for the analysis of observations of the baryon acoustic oscillations leads to a substantially biased (i.e. wrong) interpretation of the data, and to the incorrect inference of cosmological parameters.

4.1 Cosmological Implications

The presence of early dark energy (EDE) can potentially have an impact on all three levels of cosmological evolution, the background, the linear perturbations, and possibly even on the non-linear formation of structure. These effects have been studied in the literature, for example the structure formation in the linear regime by Ferreira & Joyce (1997); Doran et al. (2001). The effect on the CMB power spectrum was investigated by Doran & Lilley (2002), and then by Caldwell et al. (2003), who considered the compatibility of the CMB spectra of these models with the results from the WMAP satellite obtained through one year of observations. For a more recent review of dark energy models that includes a discussion of early dark energy, see e.g. Linder (2008) and references therein.

On the background level, the presence of early dark energy changes the evolution of the Hubble parameter. This is easy to see if we assume that the dark energy scales as a constant fraction of the energy density, i.e. contributes a constant fraction of Ω_{EDE} to the total energy budget. The Hubble parameter

then depends on the energy density as

$$\begin{aligned} H^2(z) &= \frac{1}{3M_{\rm P}^2}[\rho_{\rm matter,radiation}(z) + \rho_{\rm EDE}(z)] \\ &= \frac{1}{3M_{\rm P}^2}\rho_{\rm matter,radiation}(z) + H^2(z)\Omega_{\rm EDE}(z) \\ &= \frac{1}{3M_{\rm P}^2}\frac{\rho_{\rm matter,radiation}(z)}{1-\Omega_{\rm EDE}(z)} \end{aligned} \tag{4.1}$$

At high redshifts the Hubble parameter therefore scales as $H(z) \sim (1-\Omega_{EDE})^{-1/2}$. This also means that cosmological distance scales in an early dark energy universe are changed compared to e.g. a ΛCDM-universe - this will, for example, change the angle under which we see the acoustic peaks in the CMB.

The change in the expansion rate induced by the presence of early dark energy during the radiation era (at $T \sim 1$ MeV) affects Big Bang Nucleosynthesis, and hence the light element abundance inferred from observations, can constrain the amount of early dark energy. Current limits are $\Omega_{EDE}(T \sim 1\text{MeV}) \lesssim 0.2$ (Cyburt et al. 2005), considerably weaker than the bounds we will find from our analysis.

Early dark energy also affects structure formation - the growth of linear perturbations is suppressed (Ferreira & Joyce 1998). Hence, in a universe in which dark energy is important when structures form, these structures grow slower. To quantify the effect, we consider an average of the dark energy contribution towards the total energy density during structure formation Doran et al. (2001),

$$\bar{\Omega}^d_{\rm sf} \equiv [\ln\, a_{tr} - \ln\, a_{eq}]^{-1} \int_{\ln\, a_{eq}}^{\ln\, a_{tr}} \Omega_d(a)\, {\rm d}\ln\, a, \tag{4.2}$$

where the scale factor a_{tr} is chosen as $a_{tr} = 1/3$. The suppression of growth can be understood by considering the sub-horizon limit of the equation of motion for the dark matter perturbations (Ferreira & Joyce 1998),

$$\delta_m'' + \mathcal{H}\delta_m' - \frac{3}{2}\mathcal{H}^2\Omega_m\delta_m = 0. \tag{4.3}$$

If the dark energy is negligible during structure formation, we have $\Omega_m \approx 1$, and $\delta_m \propto a$. In an early dark energy cosmology $\Omega_m < 1$, and the solution of Eq. (4.3) is

$$\delta_m \propto a^{\left[\sqrt{25-24\bar{\Omega}^d_{\rm sf}}-1\right]/4} \approx a^{1-3\bar{\Omega}^d_{\rm sf}/5}. \tag{4.4}$$

Hence, all $k-$modes inside the horizon at a given time will suffer this suppresion. Modes that had already been inside the horizon around matter-radiation equality will all suffer the same suppression. As an approximation to the effect on σ_8, the rms density fluctuations averaged over $8\,h^{-1}$ Mpc spheres, Doran et al. (2001) suggested

$$\frac{\sigma_8(EDE)}{\sigma_8(\Lambda)} \approx (a_{eq})^{3\bar{\Omega}^d_{\rm sf}/5}(1-\Omega_0^\Lambda)^{-(1+\bar{w}^{-1})/5}\sqrt{\frac{\tau_0(EDE)}{\tau_0(\Lambda)}}, \tag{4.5}$$

where $\bar{w}$ is a suitable average of the dark energy equation of state from matter radiation equality until today; this estimate roughly gives a decrease of σ_8 by about 50%, if $\bar{\Omega}^d_{\rm sf}$ is increased by 10%.

4.2 Constraints on Early Dark Energy

4.2.1 Models and Parameterizations

The aim of our study is to determine the amount of early dark energy that is compatible with observations. In order to obtain robust results, we do not choose one specific dark energy model, but consider a broad sample of models and parameterizations. We also include models that by construction do not have an early dark energy component, in order to assess potential differences in the inferred parameter bounds on the standard cosmological parameters. Naturally, we include the ΛCDM models for comparison purposes.

Leaping Kinetic Term Quintessence

The first model we consider is a quintessence model with a 'Leaping Kinetic Term' (the 'LKT' model). The LKT model was introduced by Hebecker & Wetterich (2001), who discussed the naturalness of different quintessence scenarios from a field theoretical point of view by writing the scalar field Lagrangian as

$$\mathcal{L}(\phi) = \frac{1}{2}(\partial\phi)^2 k^2(\phi) + M_{\rm P}^4 \exp(-\phi/M_{\rm P}), \tag{4.6}$$

and considering specific forms of the ϕ-dependent kinetic coefficient $k(\phi) > 0$. As one particular case for our comparison of different dark energy models we choose the example $k(\phi)$ to be given by

$$k(\phi) = k_{min} + \tanh(\phi - \phi_1) + 1. \tag{4.7}$$

Reasonable values for the constants k_{min} and ϕ_1 that lead to a typical quintessence evolution of the scalar field are e.g. $k_{min} \approx 0.1$ and $\phi_1 \approx 276$. The scalar field will then first track the component that dominates the background (first radiation, then matter), and finally, at a time close to today, the 'leap' in the kinetic coefficient will cause the quintessence component to become dominant and lead to late-time acceleration. It is noteworthy that one can rewrite Eq. (4.6) as a completely equivalent Lagrangian, but one that has a standard kinetic term by defining a function $K(\phi)$ such that

$$k(\phi) = \frac{\partial K(\phi)}{\partial \phi}, \tag{4.8}$$

and introducing a new field variable $\chi = K(\phi)$, so that Eq. (4.6) becomes

$$\mathcal{L}(\phi) = \frac{1}{2}(\partial\phi)^2 + M_{\rm P}^4 \exp\left[-K^{-1}(\chi/M_{\rm P})\right]. \tag{4.9}$$

In the numerical implementation in CMBEASY we use this rewritten form of the potential.

Parameterizing the Energy Density I

As the first of two examples of parameterizations of the energy density of the quintessence component, we consider the form proposed by Wetterich (2004), with $\Omega_d(a)$ given as

$$\Omega_d(a) = \frac{e^R}{1+e^R}, \tag{4.10}$$

where $R(a)$ is defined by

$$R(a) \equiv \ln \frac{\Omega_d(a)}{1-\Omega_d(a)}, \tag{4.11}$$

and can be written in terms of a parameter b and a constant R_0,

$$R(a) = R_0 - \frac{3w_0 \ln(a)}{1 - b\ln(a)}. \tag{4.12}$$

The introduction of the parameter b is advantageous because it is directly related to the asymptotic early-time value of the energy density, $\Omega_\star$, by the relation

$$b = -3w_0 \left(\ln \frac{1-\Omega_\star}{\Omega_\star} + \ln \frac{\Omega_d^0}{1-\Omega_d^0} \right)^{-1}. \tag{4.13}$$

Additionally, this also allows to give a simple form of the equation of state $w(a)$,

$$w(a) = \frac{w_0}{\left[1 - b\ln(a)\right]^2}, \tag{4.14}$$

so that this parameterization can also be considered a particularly simple parameterization of the equation of state, which allows for the possibility of early dark energy, completely specified by the parameter set of $(\Omega_d^0, w_0, \Omega_\star)$. In this class of models, the energy density Ω_d rather slowly relaxes from today's Ω_d^0 to its asymptotic value of $\Omega_\star$ at early times. Observational constraints on the parameters of this model, including $\bar{\Omega}_{\rm sf}^d$, were computed by (Doran et al. 2005); our investigation here extends this study by the inclusion of more (and updated) data.

Parameterizing the Energy Density II

As a second way to parameterize the evolution of the fraction of dark energy, we include in our analysis the class of models proposed in Doran & Robbers (2006), which are discussed at length in Robbers (2006). Here, $\Omega_d(a)$ is given by

$$\Omega_d(a) = \frac{\Omega_d^0 - (1-a^{-3w_0})\Omega_d^e}{\Omega_d^0 + (1-\Omega_d^0)a^{3w_0}} + \Omega_d^e(1-a^{-3w_0}). \tag{4.15}$$

This specific form of $\Omega_d(a)$ (which we will call the '$\Omega(w_0, \Omega_d^e)$' model) is motivated by two considerations: firstly, that the late-time behavior should be as close as possible to a cosmological constant, and secondly, that the fraction of dark energy at early times should be given by a single number, Ω_d^e (and is therefore necessarily constant at early times, before changing to a cosmological-constant-like behavior for redshifts $z \lesssim 2$). The amount of dark energy therefore is never smaller than a given Ω_d^e, which is one of the three input parameters $\Omega_d^0, w_0, \Omega_d^e$ for this parameterization.

Interpolating model

Allowing more freedom in the time-evolution of the energy density, we also consider a case where Ω_d is linearly (in $\ln a$) interpolated between values at different redshifts z_i; we choose the z_i as $z_i = 1, 3, 10, 100, 1100$. In particular, this includes the possibility of a non-monotonic evolution.

Parameterizing the Equation of State I

Instead of parameterizing the energy density, we can also choose a specific form for the equation of state, as we have seen in Section 2.3. A very popular choice to parameterize the equation of state is

$$w(a) = w_0 + w_1(1-a) = w_0 + w_1 \frac{z}{1+z}, \tag{4.16}$$

which has originally been discussed in the context of cosmology by Chevallier & Polarski (2001) and Linder (2003). This particular $w(a)$ is characterized by a a linear redshift behavior at low redshifts while at high redshifts $w \to w_0 + w_1$; early dark energy models cannot be described by this parameterization. It is, however, a very useful tool for the description of models with a dynamical dark energy component, but no early dark energy.

Parameterizing the Equation of State II

Another widely used version of a parameterization for the equation of state of the dark energy (the 'C&C' parameterization) has been introduced by Bassett et al. (2002), and later been generalized by Corasaniti & Copeland (2003). The evolution of $w(a)$ is in this case being written as

$$w(a) = w_0 - w_0 \times \frac{1 + e^{\frac{a_c^m}{\Delta_m}}}{1 + e^{-\frac{a - a_c^m}{\Delta_m}}} \times \frac{1 + e^{-\frac{a-1}{\Delta_m}}}{1 - e^{\frac{1}{\Delta_m}}}, \tag{4.17}$$

where we have set an additional parameter w_m, which in the original version of Eq. (4.17) describes the value of w during matter domination, to zero. An equation of state described by this formula features two distinct phases; it first stays close to its value today w_0, and for small scale factors it is essentially zero. This evolution is described by two parameters apart from w_0, the equation of state today: A scale factor a_c^m, which signifies the scale factor where $w(a)$ turns from w_0 to zero, and a width, Δ_m, which is a measure for the width of this transition.

4.2.2 Observational Data

The cosmological predictions for all of these models are computed using CMBEASY, and then compared with a variety of observational data. We first compare only with the CMB data from WMAP (the release after three years of data). In a second step, we additionally include more sets of CMB data (which extend to higher C_l in the TT-spectra), data from SnIa surveys, as well as from large scale

structure. Specifically, we use the data from the extended *Very Small Array*, a radio telescope located at the Teide Observatory site in Tenerife, which provides data points for the TT spectrum out to $l \sim 1500$ (Dickinson et al. 2004), as well as data from the *Cosmic Microwave Background Imager* (CBI) extending out to even slightly higher multipoles closer to $l \sim 2000$, where we use data released in 2004 (Readhead et al. 2004). Our set also includes data from ACBAR (the *Arcminute Cosmology Bolometer Array Receiver*, observed from the Viper telescope at the South Pole (Kuo et al. 2004), and finally from the 2003 flight of the balloon-borne Boomerang probe (MacTavish et al. 2005). While ACBAR's highest-l binned data point is at $l = 2500$, the Boomerang data is the most accurate of our set in the range $600 < l < 1200$ for the TT-spectrum.

The distribution of matter in our models is probed by comparing the linear matter power spectra with data from the *Sloan Digital Sky Survey* (Tegmark et al. 2004b) and the *2dF Galaxy Redshift Survey* (Percival et al. 2001). For this analysis, we marginalize over the bias between the galaxy power spectrum observed by these surveys and the underlying distribution of cold dark matter, i.e. we do not use any information on the normalization of the measured power spectra. As we will see below, the inclusion of measurements of the overall normalization can provide quite powerful additional constraints on the allowed fraction of early dark energy, which is to be expected from its influence on the growth of perturbations as we have discussed at the beginning of this chapter.

Finally, we also make use of the results of SnIa surveys, where we include the first-year data from the *Supernovae Legacy Survey* (Astier et al. 2005) and the *Gold Set* of Riess et al. (2004).

4.2.3 Parameter Constraints

After these preparations, we use CMBEASY and its MCMC implementation ANALYZETHIS! to finally compute the parameter constraints on the standard cosmological parameters, including the quantity that we are most interested in, the fraction of dark energy during structure formation, $\bar{\Omega}^d_{\rm sf}$. Looking first at our interpolated model, we can see in Fig. 4.1 that already from the WMAP data alone the time evolution of dark energy is quite well constrained. It is also apparent that also for the combined set of data, the values typical for a ΛCDM cosmology are always inside the one-sigma bounds from the MCMC analysis. However, at redshifts $z = 3$ and higher, the amount of dark energy is allowed to be considerably larger.

As a general result from our Monte-Carlo analysis, we find that cosmological models with a dynamical dark energy component fit the observational data as well as ΛCDM, but not better - the addition of more degrees of freedom in the form of additional parameters for the evolution of the dark energy component does not lead to correspondingly better likelihood values. Our complete results are shown in Fig. 4.2, which includes both the constraints on the standard cosmological parameters, as well as their scatter between the different models. In our analysis, we compute the predictions of our sample of cosmological models depending on the standard cosmological parameters: the present matter energy fraction Ω^0_m and baryon energy fraction Ω^0_b, the Hubble parameter

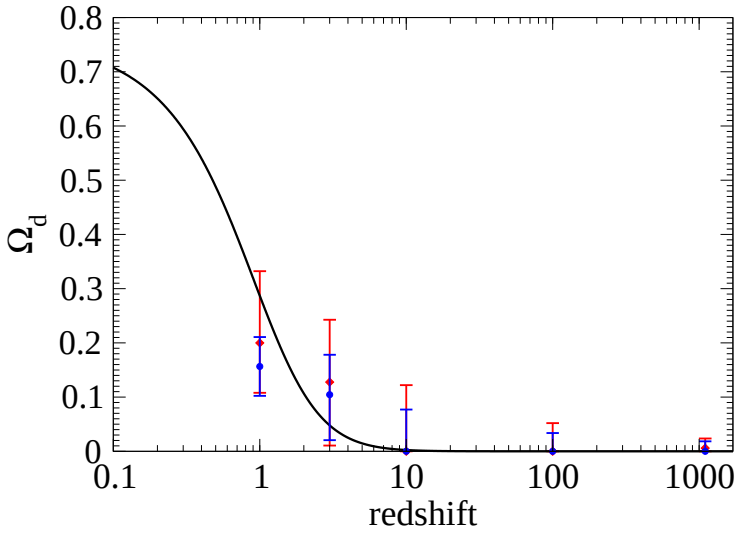

Figure 4.1: The fraction of dark energy compatible with observations in the interpolated model. Shown are the one-sigma confidence intervals at the different redshifts. Red bars correspond to the result from the WMAP data alone, whereas the blue bars correspond to the combined set described in the text. The black line shows the evolution of Ω_Λ in a ΛCDM-Universe with the WMAP 3-year best fit values for the standard cosmological parameters.

h, optical depth τ, scalar spectral index n_s and the initial scalar amplitude A_s, which we took into account using the observationally relevant combination $\ln(10^{10}A_s) - 2\tau$. Fig. 4.2 summarizes the results for these parameters for our choice of flat priors on all parameters. Fig. 4.2 also includes the results for $\bar{\Omega}^d_{\rm sf}$ and σ_8. Naturally, all models additionally depend on their respective dark energy parameters.

The results for the standard cosmological parameters show little deviation from their values in ΛCDM-cosmologies - the choice of a particular dark energy model does not lead to any significant shift of the confidence intervals. The trend for models that allow for comparatively large fractions of early dark energy to have correspondingly lower σ_8 is clearly visible. Most surprising though are the confidence intervals for $\bar{\Omega}^d_{\rm sf}$ for the interpolated model. While we have seen in Fig. 4.1 that the preferred amount of dark energy at the redshift points z_i always includes the ΛCDM-value, this model allows for considerably larger dark energy fractions at higher redshifts than the other models, and in particular much higher values than a ΛCDM universe. This is mainly due to the fact that the evolution of the dark energy density in this model is not required to be monotonic, which can lead to substantial contributions to the integrated Sachs-Wolfe effect. In fact, the free Ω_d at the different redshift points z_i can in a sense 'manufacture' the shape of the large-scale TT-spectrum to be compatible with the WMAP data even for rather large values of $\bar{\Omega}^d_{\rm sf}$. The relative independence of Ω_d in a given redshift bin from its neighboring values in effect allows for a

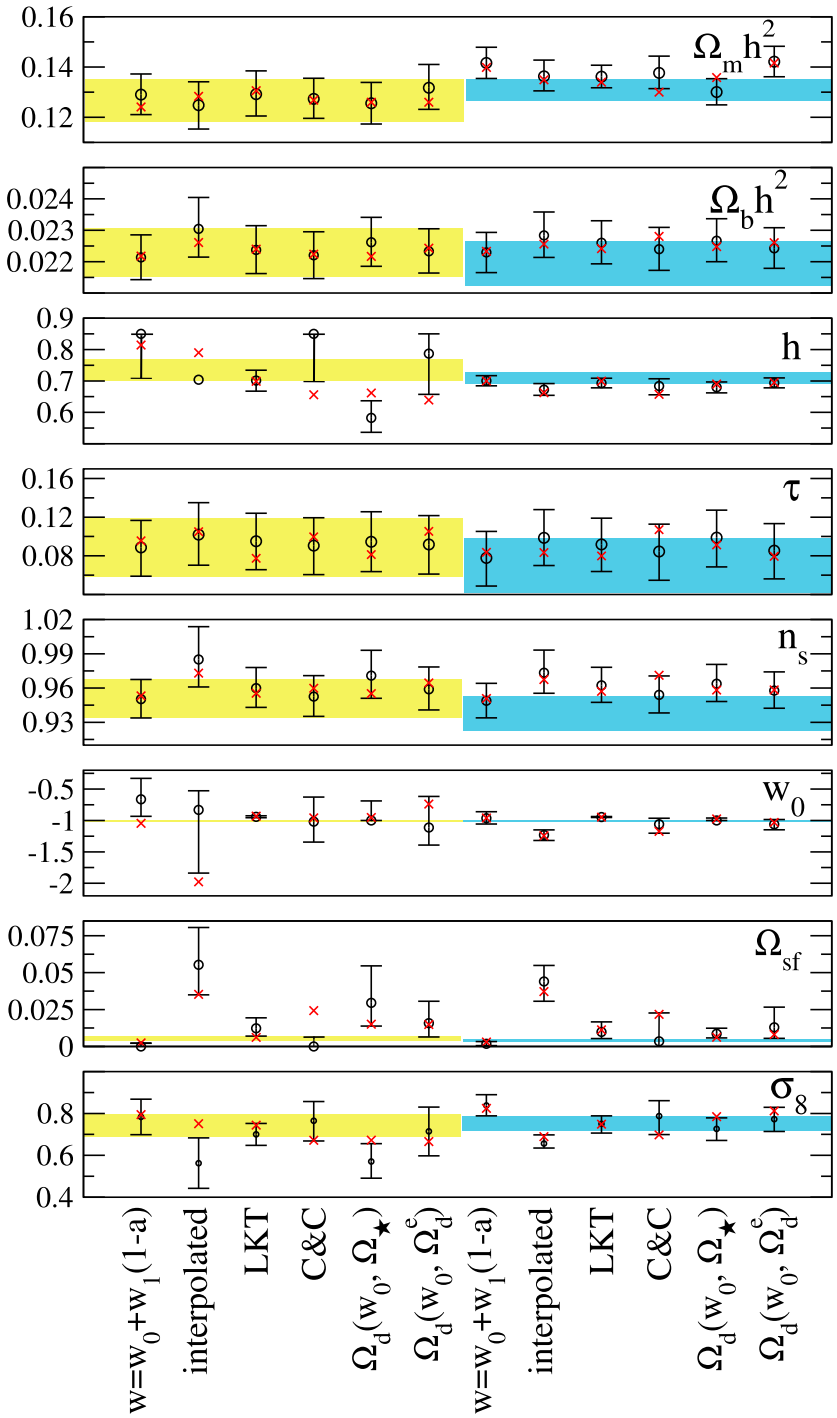

Figure 4.2: Monte-Carlo results for the cosmological parameters. The results shown on the left-hand side are for the comparison to WMAP 3-year data alone, the right-hand side corresponds to the results for the combined set described in the text. The errorbars depict the one-sigma bounds for the different models; the shaded regions show the corresponding bounds for ΛCDM-cosmologies. The crosses mark the parameter values for the best-fit models in the respective Monte-Carlo chains.

	68% confidence limit	95% confidence limit	best fit
$\Omega_m h^2$	$0.144^{(-)0.004}_{(+)0.004}$	$0.144^{(-)0.008}_{(+)0.009}$	0.144
$\Omega_b h^2$	$0.0227^{(-)0.0006}_{(+)0.0006}$	$0.0227^{(-)0.0012}_{(+)0.0013}$	0.0224
h	$0.66^{(-)0.02}_{(+)0.02}$	$0.66^{(-)0.03}_{(+)0.03}$	0.67
τ	$0.11^{(-)0.03}_{(+)0.03}$	$0.11^{(-)0.05}_{(+)0.05}$	0.09
n_s	$0.97^{(-)0.01}_{(+)0.02}$	$0.97^{(-)0.03}_{(+)0.03}$	0.96
$\ln(10^{10}A_s) - 2\tau$	$2.91^{(-)0.02}_{(+)0.02}$	$2.91^{(-)0.03}_{(+)0.03}$	2.92
Ω_e	< 0.008	< 0.017	0.0006
w_0	< -0.92	< -0.84	-1

Table 4.1: Marginalized one-dimensional likelihood constraints for the cosmological parameters for our complete data set described in the text, including SnIa observations, matter power spectra, and CMB observations, together with Ly-α data from Seljak et al. (2006); McDonald et al. (2005). The corresponding $2d$-plots for the early dark energy parameter Ω_e are shown in Fig. 4.3.

relatively large number of models in the Monte-Carlo chains with these high $\bar{\Omega}^d_{\rm sf}$ values. The models with a high $\bar{\Omega}^d_{\rm sf}$ then have a substantially lower σ_8, and the combination of the CMB data with the other observations in our combined data set then leads to a clear decrease in the allowed range for $\bar{\Omega}^d_{\rm sf}$ also for the interpolated model, but the upper $2-\sigma$ limit is still only $\bar{\Omega}^d_{\rm sf} \lesssim 6.5\%$ for our combined set.

Summarizing the results for the other models, we find the expected very small upper (2σ) bound of $\sim 0.5\%$ for the amount of early dark energy for the $w(a) = w_0 + w_1(1-a)$ parameterization, which is 'by design' limited to have dark energy fractions close to the ΛCDM values. For all other models, the combined sets a constraint of less than about three percent, and the $\Omega(w_0, \Omega^e_d)$ model yields $\bar{\Omega}^d_{\rm sf} \lesssim 4\%$.

4.2.4 Constraints from Ly-α data

We now consider the constraints on the abundance of early dark energy that can be inferred from observations of the Lyman-α forest, using the data set of Seljak et al. (2006), which is obtained from the absorption of the Ly-α line in quasar spectra by the *Sloan Digital Sky Survey* (McDonald et al. 2005).

These observations provide a constraint on the linear matter power spectrum, and given the effect of early dark energy on the perturbation growth, one would expect that Ly-α data can improve the constraints on $\bar{\Omega}^d_{\rm sf}$ that we have obtained in the last section; that this is indeed the case was first pointed out in Afshordi

et al. (2007a).

The dataset essentially provides a measurement of the amplitude and the slope of the linear power spectrum at a scale of ~ 1 Mpc^{-1} and at a redshift of $z \simeq 3$. The measurement is derived from the observation of the absorption of the Ly-α lines of ~ 3000 spectra of quasars by the neutral hydrogen in the intergalactic medium.

The conversion from the observed spectra to a 'measured' linear power spectrum involves the use of numerical simulations that assume that the underlying cosmological model is a ΛCDM model. Hence, there is a potential that the application to early dark energy models could introduce additional errors, especially if the non-linear growth of density perturbations behaved substantially different in early dark energy models (as suggested by analytic estimates in Bartelmann et al. (2006)). On the other hand, the constraints on the early dark energy abundance that we have found above are already relatively substantial (so that an eventual error would expected to be small compared to the present observational uncertainties), and at the scale of consideration, linear effects should dominate. Additionally, results from N-body simulations (Francis et al. 2008a,b; Grossi & Springel 2008) suggest that correctly taking into account the change in the linear growth factor is sufficient to capture the non-linear effects. We therefore proceed with the analysis, keeping this potential caveat in mind.

We use the $\Omega(w_0, \Omega_d^e)$ model as the model for an early dark energy cosmology, and add the Ly-α data to the full set of observational data that we used in the last section; the resulting confidence intervals for the cosmological parameters are shown in Tab. 4.1, and the two dimensional contours for the early dark energy parameter Ω_d^e in Fig. 4.3. The decrease in the upper bound for the early dark energy abundance is quite significant, as we find $\Omega_d^e \lesssim 1.7\%$ for the 95% confidence limit, compared to about 4% without the Ly-α data. The addition of a constraint on the linear overdensity provides the strongest of the limits for early dark energy.

Other Constraints

The power of measurements of the amplitude of the (linear) growth of perturbations was also illustrated by Xia & Viel (2009). They parameterized the dark energy equation of state as

$$w(a) = -1 + \left[1 - \frac{w_0}{1 + w_0} a^C\right]^{-1}, \tag{4.18}$$

where w_0 is the value of the equation of state today, and the parameter C determines the change in the equation of state from its present day value to its asymptotic value of zero in the past. This is a particular version of the parameterization discussed by Linder & Huterer (2005); that version also allows to specify an arbitrary asymptotic value for the equation of state in the past, and added a parameter to independently specify the redshift of the transition and its rapidity, while still providing an analytic expression for $H(z)$.

Using a combination of CMB and BAO data, together with SnIa, Xia & Viel quote 95% confidence upper limits on the amount of dark energy at the last

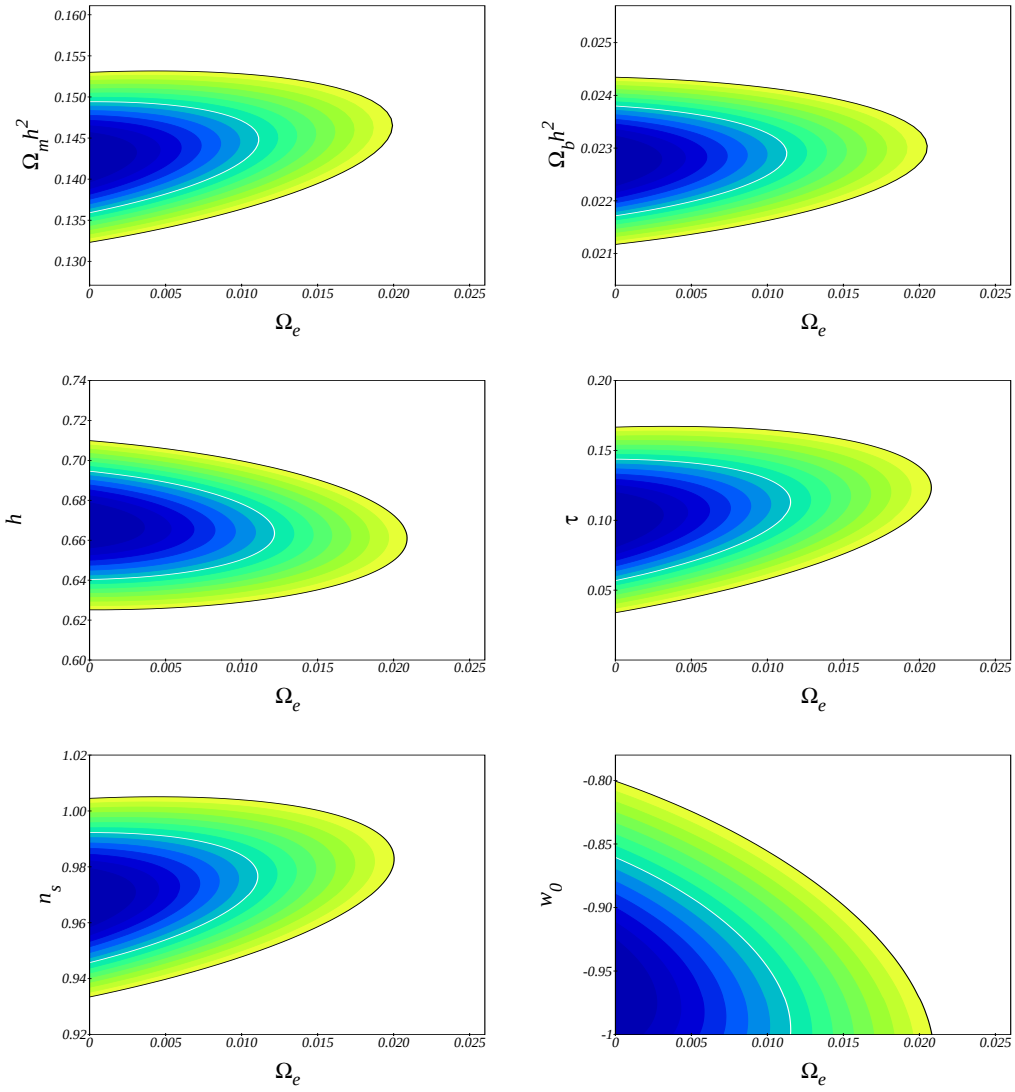

Figure 4.3: Likelihood constraints for the $1\sigma-$ (blue shades delimited by the white line) and 2σ (green shades delimited by a black line) confidence levels for the cosmological parameters in the $\Omega_d^e - x$ plane, where $x \epsilon \{\Omega_m h^2,\, \Omega_b h^2,\, h,\, \tau,\, n_s,\, w_0\}$, for our complete data set described in the text, including SnIa observations, matter power spectra, and CMB observations, together with the Ly-α data set (Seljak et al. 2006; McDonald et al. 2005).

scattering surface of about 2%, and of about 6% during structure formation, with a somewhat different definition of the average amount of dark energy during structure formation, so that these results are compatible with what we had found above. They also find that adding information on the power spectra from Ly-α observations improves their constraint on the amount of dark energy at last scattering by a factor of at least five, and when using measurements of the growth factor (and not only the power spectra), by a factor of fifteen, showing how crucial the inclusion of high-redshift probes of the growth of perturbations is. Apart from the different dark energy parameterization, the higher improvement on the constraint compared to what we have found above can be attributed to the choice of Ly-α data sets, since they also included the dark matter power spectrum information inferred from Ly-α by Viel et al. (2004) in addition to the SDSS data in our analysis. Furthermore, they include the values of the growth factor from these data, so that the smaller upper bound is not surprising. However, the caveat still applies that the conversion from the observed Ly-α flux power spectrum to the 'measured' linear dark matter power spectrum involves numerical simulations of the cosmological and astrophysical processes is based on a ΛCDM cosmology.

The analysis by Xia & Viel also uses luminosity distances inferred from 69 Gamma-Ray Bursts (GRBs) reaching up to redshift of $z > 6$, (Schaefer 2007), but notes that the use of GRBs as 'standard candles' is still in its infancy, and the procedures currently in use to derive luminosity distances do involve assumptions of the input cosmology, i.e. assume a ΛCDM model.

While the upper bounds that we have discussed in this section might seem small, especially when compared to today's value of Ω_d, one should keep in mind that in the concordance ΛCDM model, the cosmological constant contributes less than half a percent to the energy density during structure formation (i.e. to the average $\bar{\Omega}^d_{\rm sf}$), while its importance before the time of last scatter is of the order of 10^{-9}. In Section 4.4, we will discuss the prospects of how constraints on early dark energy are expected to improve in the future.

4.3 Early Dark Energy and the CMB

Having computed bounds on early dark energy from a compilation of cosmological observations, we now return to considering only the CMB without adding any other data. The CMB alone yields strong constraints on the fraction of early dark energy, as we have just seen from the WMAP-only constraints. But is CMB data enough to unambiguously detect the presence of an early dark energy? Since we can easily decrease the amount of early dark energy in a suitable parameterization of $\Omega_d(a)$ down to the limiting case of a cosmological constant, we are actually interested in finding out whether an early dark energy cosmology with a physically significant amount of early dark energy is detectable by CMB observations alone. The results obtained in the last section clearly demonstrate that for current CMB data, this is not the case - an early dark energy fraction on the percent-level is certainly compatible with the data, as is a pure ΛCDM model, so that we cannot cleanly distinguish between these cases relying on the

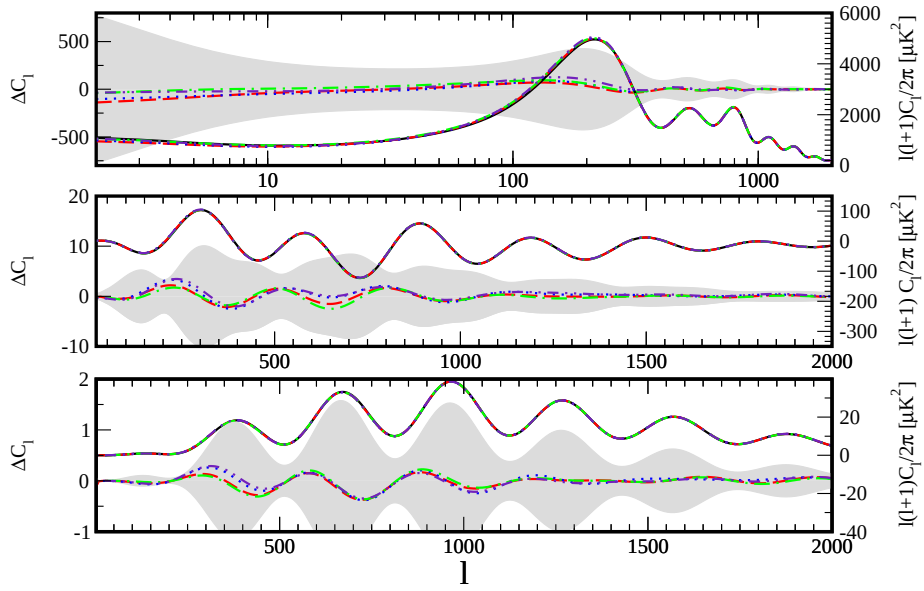

Figure 4.4: CMB power spectra for TT (top panel), TE (middle), and EE (bottom) modes of different $\Omega_d^e = 0.03$ EDE models (listed in Table 4.2) are plotted using the right axis scale. Their differences relative to the fiducial ($w_0 = -0.95, w_a = -0.1$) model are shown using the left axis scale, and lie within the grey shading surrounding the zero difference level that shows the cosmic variance limit.

data that is available today.

However, this might soon change, as the precision of CMB observations approaches the fundamental limit dictated by cosmic variance. The question then is whether this increased precision will allow for a clear distinction between early dark energy models and theories with a 'fading' dark energy, i.e. theories that predict a negligible dark energy component at early times, or even a cosmological constant.

To answer this question, we will now investigate whether the CMB power spectra in two dark energy models, one with and the other without early dark energy, can be similar enough to be indistinguishable, even if we already had CMB measurements only limited by cosmic variance up to $C_l = 2000$.

The two example models we chose are the $(\Omega_d^0, w_0, \Omega_d^e)$ parameterization of Eq. (4.15) introduced in 4.2.1 as an example of an early dark energy (EDE) model, and the (w_0, w_1) described in 4.2.1 as a representative for the family of fading dark energy models.

The result is shown in Fig. 4.4, demonstrating that EDE models can indeed reproduce the power spectra of a reference model with a fading dark energy component. In particular, each panel in Fig. 4.4 shows the respective power spectrum (TT, TE and EE) of a fiducial fading dark energy model with $(w_0, w_1) = -0.95, w_1 = -0.1)$, and on top the corresponding spectra of EDE models with $\Omega_d^e = 0.03$ and $w_0 = -0.95$ and their difference to the fiducial spectra. The differences are always well within cosmic variance limits.

fiducial	———	$w_0 = -0.95$, $w_a = -0.1$, no EDE
A	— —	matching $2 < C_\ell^{TT} < 2000$
B	• • •	$\Omega_m^0 = 0.28$, matching $2 < C_\ell^{TT} < 2000$
C	• — •	matching $2 < C_\ell^{TT,EE} < 2000$
D	— • •	$\Omega_m^0 = 0.28$, matching $2 < C_\ell^{TT,EE} < 2000$

Table 4.2: Fitting requirements for the models shown in Fig. 4.4.

The matching spectra were found by running MCMC chains with CMBEASY, using the power spectra of the fading model as the 'observed' data, and then varying the other cosmological parameters of the EDE model. For the chains used to obtain the spectra in Fig. 4.4, we allowed the baryon density $\Omega_b^0 h^2$ to vary, as well as the overall matter density $\Omega_m^0 h^2$, the Hubble parameter h, optical depth τ and the scalar spectral index n_s. The amplitude of the fluctuation was also allowed to vary, by including the conventional combination of $A_s \exp^{-2\tau}$ as a Monte-Carlo parameter for the chains. In particular, we have not included a potential running of the spectral index, do not allow w_0 to vary, and have assumed neutrinos to be massless, so there exist considerably more degeneracies that make it even more difficult to look for a clear signal of early dark energy in the CMB.

The matching EDE spectra shown are examples from Monte-Carlo chains with four different matching requirements summarized in Tab. 4.2 - matching either the temperature-temperature spectrum only, or both the TT and the EE-polarization spectra, as well as additionally requiring the matter density Ω_m^0 to be in exact agreement with the value in the fiducial fading model ($\Omega_m^0 = 0.28$). The precision of the hypothetical future CMB experiment assumed to have 'measured' the fiducial spectrum was set to be cosmic-variance limited up to $l = 2000$ for a observed sky-fraction of 81%.

These matching spectra then are not cleanly distinguishable: e.g. for model A, the overall χ^2 relative to the fiducial fading model for all $C_l < 2000$ and six cosmological parameters is only 14 - the corresponding numerical value for unbinned multipoles e.g. for the five-year data from WMAP is a $\chi^2 \sim 1000$ comparing to their best-fit ΛCDM-model over the range $33 \leq \ell \leq 1000$ (Nolta et al. 2009). When looking at binned multipoles, the WMAP team obtains a reduced $\chi^2 = 1.04$, compared to a $\chi^2 = 0.3$ for the EDE model relative to the fiducial fading model, when using the same binning.

We can therefore conclude that even a CMB observation able to deliver accurate C_l-measurements up to $\ell = 2000$ does not enable us to detect a clear signal of early dark energy in the CMB power spectra. In 4.4 we will show an example B-mode polarization spectrum, which would discriminate between our example models, but might be difficult to measure due to its much lower amplitude. We will now study the consequences of the results we have obtained so far for the interpretation of data from measurements of the baryon acoustic oscillations.

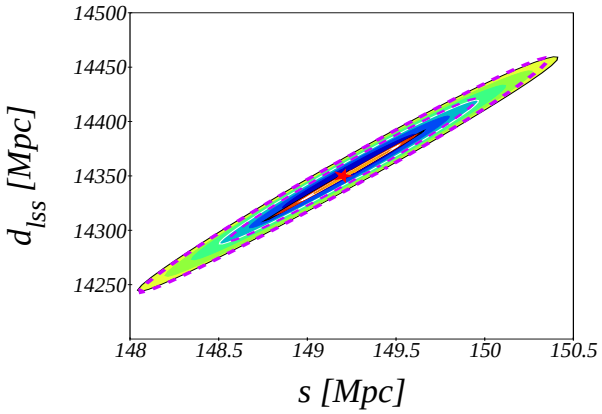

Figure 4.5: The distance to last scattering, $d_{\rm lss}$ and the sound horizon scale s as determined by the CMB power spectrum. Their ratio, i.e. the slope of the contours is particularly well constrained. The white and black lines give the 68.3% and 95.4% confidence limits for a CMB experiment limited only by cosmic variance up to $l = 2000$. The outer contours light green to dark blue) are the result when using only the temperature power spectrum and the dashed lines correspond to using only multipoles of $l \geq 40$. The smaller contours from dark red to light gold include the polarization E-mode spectra and the TE cross-correlation spectra for a cosmic variance limited experiment. The star marks the input values used for generating the "observed" spectrum

4.3.1 Baryon Acoustic Oscillations

As we have seen in the introduction in Chapter 2, the information one can deduce from the BAO measurements relies on an accurate determination of the standard ruler. On the other hand, since early dark energy changes the distance scales according to Eq. (4.1), both the distance to the last scattering surface, $d_{\rm lss}$, and the sound horizon s will be modified in an universe with an early dark energy component. The size of the sound horizon mainly depends on the sound speed c_s of the coupled photon-baryon fluid, and therefore on baryon and photon densities, and the redshift z_{dec} when the photons and baryons decouple. The redshift of decoupling is the result of atomic physics and remains unaffected by an early dark energy component. Hence we can directly deduce from the expression for the sound horizon s,

$$s = \int_{z_{dec}}^{\infty} dz \frac{c_s}{H(z)}, \tag{4.19}$$

that the influence of early dark energy on the scale of the sound horizon is determined by the change in $H(z)$. Indeed, we see that Eq. (4.1) yields

$$\frac{s_{\rm EDE}}{s_{\rm noEDE}} \sim (1 - \Omega_E DE)^{1/2}\,. \tag{4.20}$$

for the shift in the sound horizon caused by the presence of a non-negligible early dark energy component (for a detailed discussion see Doran et al. 2007b). The conformal distance also changes, of course, as

$$d(z) = \int_0^z \frac{dz'}{H(z')}, \tag{4.21}$$

which directly gives the change of the distance to the last scattering surface, $d_{\rm lss}$. That we could accurately match the CMB spectra of cosmologies with and without EDE in Section 4.3 is simply a consequence of the fact that the CMB power spectra measure the ratio, $d_{\rm lss}/s$, much more precisely than the individual distances themselves, as seen in Fig. 4.5, which depicts the likelihood contours in the $d_{\rm lss}$-s plane for a cosmic variance limited experiment (here for a ΛCDM universe). Since the contribution of the dark energy to $H(z)$ is time-dependent, the change in the distances and scales also depends on time, so that an early dark energy cosmology can match the angular scale given by $d_{\rm lss}/s$ at the time of last scattering of a model with fading dark energy, and produce matching CMB spectra, while the ratio will be distinctly different at other times.

The same experiment can be done with our two example cosmologies with matching CMB spectra from Section 4.3. As we have shown there, both the EDE and the non-EDE model can produce matching spectra, and therefore the same $d_{\rm lss}/s$. However, we cannot recover the distances individually from the CMB spectra alone, as we would like for the BAO measurements. Since we do not know a priori what the true cosmology is, and specifically, whether it has an EDE component or not, this has to be taken into account when determining the scale of the standard ruler in BAO measurements. For example, assuming that the our real Universe has only fading dark energy and is described by the fiducial ($w_0 = -0.95, w_1 = -0.1$) model from Section 4.3, then trying to determine cosmological parameters by fitting an EDE model will lead to biased results, as can be seen in Fig. 4.6. In particular, neglecting the possibility of early dark energy when calibrating the standard ruler for BAO studies will bias the values of the cosmological parameters obtained from such observations.

We can now calculate the propagation of the error introduced by assuming a wrong cosmology and subsequently miscalibrating the standard ruler. This error propagates into the cosmological parameters as determined in BAO measurements - and this calculation then shows that the effects of such a miscalibration is indeed important for the interpretation of future cosmological observations, as we will now show in the next section.

4.3.2 Miscalibrating the Standard Ruler

To asses the magnitude of the error introduced by a miscalibrated standard ruler due to ignoring the effect of early dark energy, we use the Fisher information matrix for a data set consisting of a vector $\mathbf{O} = \{O_1, ..., O_k\}$ of observed quantities. The probability distribution f of these quantities then depends on the cosmological parameters $\mathbf{p} = \{p_1, ..., p_n\}$ that we want to estimate. The Fisher

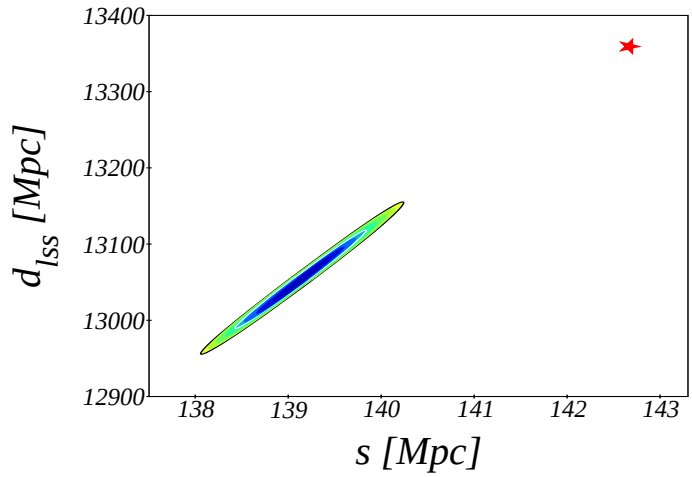

Figure 4.6: Likelihood contour at 95.4% cl in the $s-d_{\rm lss}$ plane for EDE cosmologies with $\Omega_d^e = 0.03$ that match the CMB temperature power spectrum of the fiducial $(w_0 = -0.95, w_a = -0.1)$ model without early dark energy. Note that the matching almost automatically preserves the geometric shift factor, i.e. the slope $d_{\rm lss}/s$, but not the individual distance scales. The red star marks s and $d_{\rm lss}$ of the fiducial model; the shift in the standard ruler amounts to 2.5%.

matrix F_{ij} is defined by

$$F_{ij} \equiv -\left\langle \frac{\partial^2 \ln f(\mathbf{O};\mathbf{p})}{\partial p_i \partial p_j} \right\rangle, \tag{4.22}$$

and its inverse F_{ij}^{-1} gives the best possible covariance matrix for the measurement errors on these parameters. We can then quantify how a miscalibration in the O_k propagates to the inferred values for the cosmological parameter p_i via

$$\delta p_i = (F^{-1})_{ij} \sum_k \Delta O_k \frac{\partial O_k}{\partial p_j} \frac{1}{\sigma^2(O_k)}. \tag{4.23}$$

In our case, the quantities observed by the radial and transverse BAO modes, O_k, are the ratio $\tilde{d} = d/s$ of the angular diameter distance at redshifts z_k to the sound horizon, as well the ratio of the proper distance interval to the sound horizon, $\tilde{H}^{-1} = H^{-1}/s$. We will assume a future BAO experiment that will be able to measure these quantities to 1% precision at four different redshifts, $z_k = 0.4, 0.6, 0.8, 1$, a precision that will require surveys beyond the planned WFMOS survey (Bassett et al. 2005), or e.g. the BOSS survey (The SDSS-III Collaboration 2008). For the accuracy of the determination of the sound horizon at high redshift, we use the precision of the Planck satellite (Tauber 2000). If our real Universe has an EDE component, and if we were then to deduce the value of cosmological parameters of this EDE-universe (we assume $\Omega_d^e = 0.03, w_0 = 0.95$), but incorrectly assumed that the dark energy evolution could be fit using the $w(a) = w_0 + w_1(1-a)$ parameterization, the result would

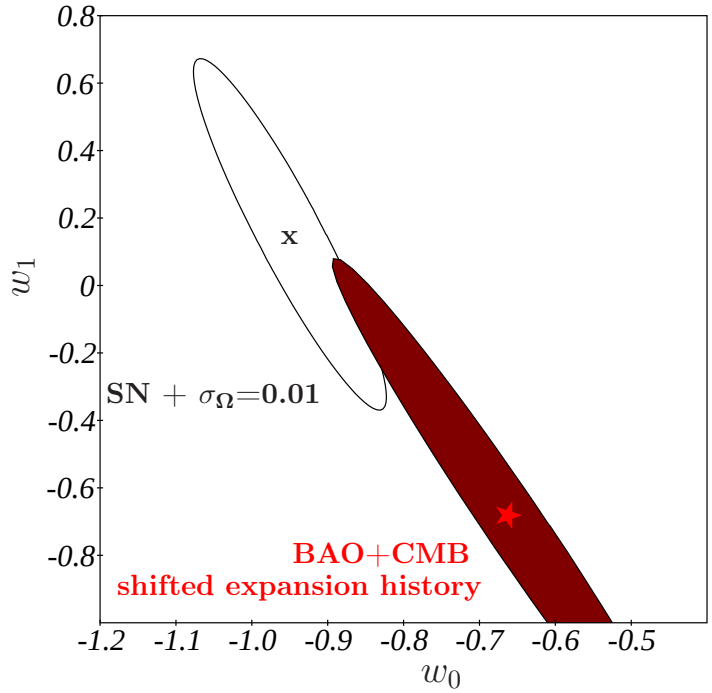

Figure 4.7: Early dark energy density Ω_d^e can cause miscalibration of the standard ruler used by the baryon acoustic oscillation probe. Assumed here is a true model with $\Omega_d^e = 0.03$ - this shifts the dark energy properties derived with BAO+CMB data from their true values (black x) to those marked by the red star, with the dark red confidence contour. The contours indicate the 68% confidence limit. Distance probes such as supernovae that do not rely on the standard ruler recover the true expansion history (here shown with a prior on Ω_m).

be that of Fig. 4.7. We would obtain a value of $w_1 \equiv w_a = -0.66$ instead of the true -0.95, and even the 68% confidence limits overlap only slightly.

In contrast, supernovae observations would be able to recover the true value w_0 today, as would other observations that do not rely on the calibration of a high-z quantity influenced by the dark energy - shown in the plot are results that could be obtained by a survey like SNAP (Aldering et al. 2002), that would measure the luminosity distance at low redshift ($0 < z \lesssim 1.7$) through SnIa, and yield a constraint σ_Ω on the matter density through weak lensing measurements. This is the direct result of the fact that at low redshifts, the luminosity distances expansion histories of both models are the same to a precision of 0.02%, as the best-fit (w_0, w_1) model can replicate the expansion history of the EDE model very well at low redshifts (for about $z \lesssim 2$ in our case), and it is only at high redshifts where the difference becomes substantial.

To avoid misleading conclusions from BAO observations, one has has to account for this uncertainty. This will effectively increase the confidence limits on the derived cosmological parameters, but allow to recover the true cosmology. In the context of BAO observations, this is easily done by also fitting for the absolute ruler scale, i.e. including the uncertainty δs in the sound horizon as an

additional parameter in the analysis (see also Linder 2007).

For the model example models considered here, accounting for the possibility of early dark energy in this way increases the area of the error contours in Fig. 4.7 by a factor of 2.3. This shows that the potential presence of an early dark energy component considerably weakens the potential power of BAO constraints.

4.4 Prospects

We have restricted our discussion of early dark energy almost entirely to the regime accessible by linear perturbation theory, and not investigated the effects of an early dark energy component on the non-linear regime of structure formation at all. Semi-analytical calculations within the spherical collapse model (Bartelmann et al. 2006) find that in early dark energy models, the linear collapse parameter δ_c is lowered, leading e.g. to a significant increase in clusters at redshifts above unity. The effect on the statistics of gravitational arcs have been studied by Fedeli & Bartelmann (2007), and the impact on the cluster sample that forthcoming surveys will observe has been discussed by Fedeli et al. (2008); Waizmann & Bartelmann (2008) specifically study the cluster sample that the Planck satellite will measure, and find that a fraction $\bar{\Omega}^d_{\rm sf} \gtrsim 4\%$ would be necessary for a clear detection, but also that EDE cosmologies lead to cluster samples that are considerably less contaminated by false detections than in ΛCDM. In contrast to the analytical estimate, numerical studies performing N-body simulations (Francis et al. 2008a; Grossi & Springel 2008; Francis et al. 2008b) conclude that standard estimates for the abundance of dark matter halos continue to work in EDE cosmologies, provided the change in linear growth is properly taken into account. This would suggest that finding a clear signal of EDE might be harder than originally thought.

Independently of this debate, probes sensitive to the linear structure growth remain a viable observational path. For example, when discussing the degeneracy of the CMB spectra between EDE and fading dark energy models in Section 4.3, we have skipped the B-mode polarization, which is one such possibility.

The B-mode polarization is not intrinsically present in the CMB, but is generated by the gravitational deflection of the photons by the large scale structure between the last scattering surface and the observer (for a review, see Lewis & Challinor 2006). The effect of the lensing of the CMB can roughly be described as smearing out the acoustic peaks, and has an effect of a few percent at high multipoles ($l \sim 2000$) on the TT spectra. The total angle by which the photons are deflected is on the order of a few arcminutes, but since the deflection angles are correlated over scales of typically about two degrees, the acoustic peaks are broadened by a few percent. The largest contribution to the lensing potential comes from redshifts of a few (see e.g. Acquaviva & Baccigalupi 2006), and therefore provides a probe of the changed growth in early dark energy models.

A method combining gravitational lensing of the CMB with cosmic shear surveys in a way that yields a measurement of the ratio of comoving distances to different redshifts was proposed by Das & Spergel (2008). The authors concluded

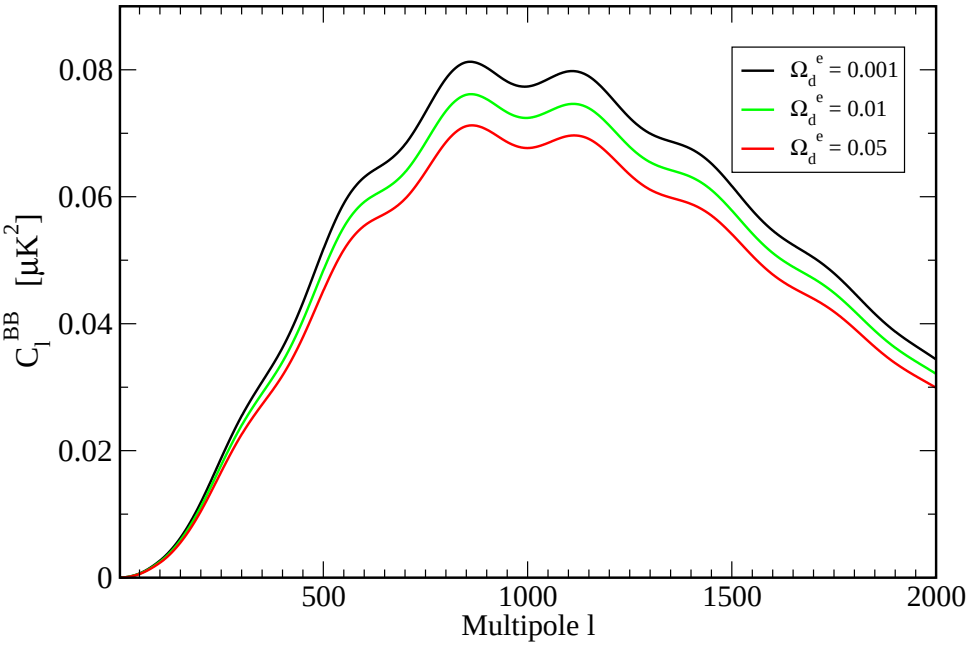

Figure 4.8: Power spectra of the B-mode polarization for three $\Omega(w_0, \Omega_d^e)$-models with the same initial fluctuation amplitude and different values of Ω_d^e, while all other parameters are kept fixed, as computed by CMBEASY. Normalizing all models to the same σ_8 today would show the inverse effect, i.e. an enhancement of the B-mode signal by early dark energy.

that their method is unfortunately rather insensitive to the early dark energy contribution, particularly to the parameterization in terms of the $\Omega(w_0, \Omega_d^e)$-model. Nevertheless, it is very useful for determining the late-time behavior of dark energy, and could potentially yield tighter constraints when the early dark energy behaves differently than the parameterization of the $\Omega(w_0, \Omega_d^e)$ model.

As for the B-mode spectra, the biggest observational difficulty is their low overall amplitude, which can be seen from the example spectra in Fig. 4.8; this is well beyond the reach of current experiments. That might change with future probes, though. Experiments that are contemplated include for example CMBpol (Zaldarriaga et al. 2008), which is designed to measure the polarization spectra, including the B-mode, with 'ultra-high' precision. Two groups, de Putter et al. (2009) as well as Hollenstein et al. (2009), have computed forecasts for the expected constraints on Ω_d^e that could be achieved, finding a sensitivity down to $\Omega_d^e \lesssim 0.002$ for CMBpol; a combination with weak lensing data from future weak lensing surveys (Amara & Refregier 2007) is projected to be able to constrain Ω_d^e to $\sim 10^{-4}$, so that the outlook of possibly detecting an early dark energy component in the future seems promising.

5 The Planck Mass at the Cosmological Horizon Scale

The last chapter presented an overview of different models of early dark energy, and their general features in comparison with 'fading' dark energy and the concordance ΛCDM - model. In this chapter, we will explore the 'boundary region' between these scalar field dark energy models and modifications to the law of gravitation as formulated by the Theory of General Relativity. The specific question we are asking here is: Does the Planck Mass change at the cosmological horizon scale? This question immediately requires that the Planck Mass, which in General Relativity quantifies the strength of the coupling between the space-time metric and the matter and energy content of the Universe, now becomes a scale-dependent quantity, an 'effective' Planck Mass. In the limit of a vanishing scale dependence, we then recover standard General Relativity. In Section 5.2 we will see that we can reinterpret the tracker models of the dark energy that we have studied in the last chapter as causing such a change in the value of the effective Planck Mass, leading to a 'glitch' in the value between sub-horizon and super-horizon scales; it is this direct connection that motivates the investigations in this chapter.

In early dark energy cosmologies, however, this feature, while interesting enough to merit closer study, is more of a by-product of the presence and the dynamics of the scalar field; there exists however, a class of theories, called 'Cuscuton' models (Afshordi et al. 2007b), where this mismatch between small-scale and large-scale values of the Planck Mass emerges as a central property of a theory that does not contain a new scalar field dark energy component, but instead describes a modification of the law of gravity that leads to this mismatch, and therefore is a much more natural setting for this discussion. Additionally, as we will see below, one can still describe 'Cuscuton' models in a language that is indeed very similar to the scalar field dark energy we have used so far, showing the direct relation to the models we have discussed in Chapter 4, and pointing out yet another aspect of the close connection of (scalar field) dark energy and modified gravity models.

Since $M_{\rm P} = (8\pi G)^{-1/2} \simeq 2.44 \times 10^{18}$GeV, a change in the Planck Mass can equivalently be described in terms of Newton's constant G as a fifth-force modification to the inverse square law,

$$V(r) = -G\frac{m_1 m_2}{r}\left(1 + \alpha e^{-r/\lambda}\right), \tag{5.1}$$

where m_1 and m_2 are the masses of (point-like) gravitating objects, while α and λ quantify the strength and the scale of the new interaction. In this formulation, the effective Newton's constant smoothly goes from G on large scales ($r \gg \lambda$)

to $G(1+\alpha)$ on small scales ($r \ll \lambda$). Current constraints from torsion-balance experiments (e.g. Kapner et al. 2007) to solar-system/planetary dynamics and lunar laser-ranging (e. g. Williams et al. 2004) severely limit α in the range $10^{-2}\text{cm} < \lambda < 10^{16}\text{cm}$, (see Adelberger et al. 2003, for an overview), and large-scale structure in the Universe has been used to obtain constraints on α even on scales of $\lambda \sim 10^{25}\text{cm}$ (Sealfon et al. 2005).

With a numerical implementation of the Cuscuton models in CMBEASY, we will then be able to compute observational constraints on the possible running of the Planck mass, which, together with the constraints on the abundance of early dark energy from Chapter 4, show that current observational data constrain deviations from Einstein gravity even on the scale of the cosmological horizon, or the Hubble radius ($\lambda \sim c/H \sim 10^{28}\text{cm}$).

5.1 Effective Planck Mass

In order to quantify the size of the possible change of the Planck Mass as we approach and cross the cosmological horizon, General Relativity's constant Planck Mass $M_{\rm P}$ in Einstein's Equation,

$$G^{\mu}_{\nu} = M_p^{-2} T^{\mu}_{\nu}, \tag{5.2}$$

should be replaced by a scale dependent function. The effective Planck Mass $M_{p,\rm eff}(|\mathbf{k}|)$, which we define in Fourier space as a function of the vector $\mathbf{k}$ as

$$M^{-2}_{p,\rm eff}(|\mathbf{k}|) \equiv \frac{\langle \delta G^0_{0,\mathbf{k}} \delta T^{0*}_{0,\mathbf{k}} \rangle}{\langle \delta T^0_{0,\mathbf{k}} \delta T^{0*}_{0,\mathbf{k}} \rangle}, \tag{5.3}$$

where $\delta T^0_{0,\mathbf{k}}$ and $\delta G^0_{0,\mathbf{k}}$ are the spatial Fourier transforms of δT^0_0 and δG^0_0 on a given spatial hypersurface, and '$\langle\,\rangle$' represent ensemble averages. Another possible definition would have been

$$M^{-2}_{p,\rm eff} \equiv \frac{\delta G^0_0}{\delta T^0_0}, \tag{5.4}$$

taking $M^{-2}_{p,\rm eff}$ as a direct measure of the response of G^0_0 to perturbations of the energy density. But this simple definition becomes ill-defined when the denominator crosses zero; additionally, our choice of definition has the advantage of making the scale-dependence explicit, being a function of a single physical scale $|\mathbf{k}|$.

Obviously, the definition of Eq. (5.3) depends on the gauge we choose to compute the perturbations. However, on small scales we recover Newtonian gravity, and the effective Planck Mass will therefore be gauge independent. On super-horizon scales ($k \ll H$), gauge transformations can change the effective Planck mass only if the Planck mass associated with the background expansion is different from the Planck mass associated with the perturbations; for our analysis, we assume that this is not the case, and the large-scale value of the Planck Mass will be identical to the Planck Mass value in the Friedmann Equation,

and therefore gauge independent. Only the details of the transition will depend on the choice of gauge.

Referring to the cosmological sub-horizon ($k \gg H$) and super-horizon ($k \ll H$) scales as the UV and IR scales, respectively, we denote the corresponding values of the effective Planck mass by $M_{p,\mathrm{UV}}$ and $M_{p,\mathrm{IR}}$. In this notation, the UV-IR mismatch can then be expressed by the dimensionless parameter α:

$$M^2_{p,\mathrm{IR}} = M^2_{p,\mathrm{UV}}(1+\alpha). \tag{5.5}$$

One can, of course, imagine many other forms of variations of the Planck Mass and equivalently, Newton's constant. When we consider possible couplings between the scalar field dark energy and matter, as we will do in the next chapter, one also finds an effective Newton's Constant, modified by the strength of this coupling. Theories of gravity other than General Relativity in general predict a time- and/or space-dependent G, as do e.g. scalar-tensor theories (Linde 1990; Garcia-Bellido et al. 1994; Clifton et al. 2005; Nagata et al. 2004; Pettorino et al. 2005). In other words, possible deviations from Einstein gravity, or alternatively, other energy components that are not accounted for in the total energy momentum tensor, $T_{\mu\nu}$, may lead to an effective (or dressed) Planck mass that could run with time and/or the energy/length scale of the interactions. In fact, the isolated consideration of the gravity theory under the assumption that the other 'constants' of nature are indeed constants, is already a very strong simplification (see e.g. Stern 2008; Dent et al. 2009, and references therein).

In our investigation here, we concentrate on cases where α does not depend on redshift, and where the scale at which this transition occurs is the only natural macroscopic scale of the problem, namely the cosmological horizon size; the only time dependence of the transition scale therefore is through the evolution of the cosmological horizon.

A scale dependence of the Planck Mass that can be written in the form of Eq. (5.5) can also be found in "Einstein-Aether" theory, where the "aether" is a Lorentz-violating, fixed-norm and time-like vector field (Jacobson & Mattingly 2001; Foster & Jacobson 2006; Carroll & Lim 2004). In contrast to both the tracking dark energy models and the Cuscuton that we consider below, the coupling of the vector field to the metric renormalizes both the IR and UV values of the effective Planck mass, so that the 'bare' value is seen neither on small nor on super-horizon scales.

5.2 The Planck Mass and Early Dark Energy Models

The connection between early dark energy models and a rescaled Planck Mass is easy to see on the background level. Assuming an exponential potential for the scalar field,

$$V(\phi) = M_p^4 e^{-\lambda\phi/M_p}, \tag{5.6}$$

the constant fraction of early dark energy Ω_ϕ is during matter domination given by

$$\Omega_\phi = \frac{3}{\lambda^2}, \tag{5.7}$$

as we had seen in Section 2.3. As long as Ω_ϕ is a constant, we see that with the definition

$$M^2_{p,\mathrm{IR}} = M^2_{p,UV}\left(1 - \frac{3}{\lambda^2}\right), \tag{5.8}$$

the Friedmann Equation can be written as

$$H^2 = \frac{\rho_m}{3M^2_{p,IR}}, \tag{5.9}$$

interpreting the early dark energy as a simple rescaling of the Planck Mass. This interpretation is consistent with our definition of the effective Planck Mass by Eq. (5.3), which gives

$$M^{-2}_{p,\mathrm{eff}}(k) = \frac{\delta\rho_\phi + \delta\rho_m}{\delta\rho_m}, \tag{5.10}$$

if we assume adiabatic initial conditions, as given in Section 3.4; the choice of adiabatic initial conditions is a precondition for the validity of this analysis.

5.3 Cuscuton Cosmologies

Leaving the early dark energy models aside for a moment, we now turn to the 'Cuscuton' models, in order to see how a UV-IR mismatch in the values of the Planck Mass appears in this framework. Introduced by Afshordi et al. (2007b), this theory is a scalar field dark energy model with a particular action for the field φ that results in several intriguing characteristics. Most importantly, even though the action is formulated as the action of a scalar field, the form of the action dictates that the field degree of freedom is merely a non-dynamical auxiliary field. The equation of motion does not have any second-order time derivatives, and the behavior of φ is completely determined by the fields it couples to. In other words, φ does not introduce an additional degree of freedom, like conventional dark energy models do. Instead, it merely acts as a constraint, changing the dynamics of the theory. This explains the name 'Cuscuton', which is the Latin name for dodder, a genus of parasitic plants. Then, as there is no additional degree of freedom in the theory, it is indeed more a theory of modified gravity, and this makes it a suitable framework to explore a possible mismatch of the Planck Mass between the UV and IR regimes.

Formally, the Cuscuton action is given by

$$S_Q = \int d^4x\sqrt{-g}\left(\kappa^2\sqrt{|\partial^\mu\varphi\partial_\mu\varphi|} - V(\varphi)\right), \tag{5.11}$$

where φ is a scalar field, and κ and m are constants of theory with the dimensions of energy. The general cosmological aspects of the Cuscuton have been outlined by Afshordi et al. (2007a). The first main property of interested to us here is the behavior in the homogeneous limit of the field, i.e. the cosmological background evolution. In this limit, the definition of the Cuscuton action Eq. (5.11) implies that the kinetic term of the field is a total derivative, so that the action for φ is simply

$$S_\phi^{\mathrm{homog.}} = -\int \mathrm{d}^4x\, V(\varphi), \tag{5.12}$$

as long as the field does not couple to any other fields, which we assume here. Then, the field equation can be written in the form

$$3\kappa^2 H \mathrm{sgn}(\dot{\varphi}) + V_{,\varphi}(\varphi) = 0. \tag{5.13}$$

Together with the Friedmann Equation, this relation leads to

$$\left(\frac{M_\mathrm{P}^2}{3\kappa^4}\right) V_{,\varphi}^2(\varphi) - V(\varphi) = \rho_{bkg}, \tag{5.14}$$

where ρ_{bkg} is the total energy density without the contribution from the Cuscuton. This relation shows how, once $V(\varphi)$ is chosen, the field does not have its own dynamics, but has its value determined by the background density. We can also use this equation to rewrite the Friedmann Equation (for $\dot{\varphi} < 0$) as

$$H^2 = \frac{1}{3M_\mathrm{P}^2}\left\{\rho_{bkg} + V\left[V_{,\varphi}^{-1}(3\kappa^2 H)\right]\right\}, \tag{5.15}$$

with $V_{,\varphi}^{-1}$ denoting the inverse function of $V_{,\varphi}$. The nature of the Cuscuton as a modification of gravity is evident here. Even though we use the same field-theoretical language as for our scalar field models, writing down the action for a Cuscuton 'field' φ, this variable can be eliminated from the resulting equations, and the cosmology is described by a modified Friedmann equation which is fixed once we specify the potential $V(\varphi)$.

For our investigation, we set

$$V(\varphi) = V_0 + \frac{1}{2}m^2\varphi^2, \tag{5.16}$$

i.e. a simple quadratic potential. Other possibilities are discussed in Afshordi et al. (2007a). With this choice, V_0 will simply contribute to the cosmological constant. The quadratic part, instead, maintains a constant fraction Ω_Q of the total energy density, which can easily be seen by taking the square of Eq. (5.13), which together with the Friedmann Equation shows that this fraction is

$$\Omega_Q = \frac{\frac{1}{2}m^2\varphi^2}{\rho_{tot}} = \frac{3\kappa^4}{2M_\mathrm{P}^2 m^2}. \tag{5.17}$$

Inserting this in Eq. (5.15) then shows that the Friedmann Equation, modified by the Cuscuton constraint, can be written in its usual, un-modified way, but with a rescaled Planck Mass,

$$M_{p,\mathrm{IR}}^2 = M_{p,\mathrm{UV}}^2 - \frac{3\kappa^4}{2m^2}. \tag{5.18}$$

As the Cuscuton does not represent a real degree of freedom, it is not surprising that the Cuscuton perturbation is a direct function of the metric perturbations (assuming $\Phi = \Psi$), and can be written as (Afshordi et al. 2007a):

$$\delta\varphi = \frac{3\dot{\varphi}(\dot{\Phi} + H\Phi)}{k^2/a^2 - 3\dot{H}}, \tag{5.19}$$

which makes it possible to eliminate the Cuscuton perturbation from the perturbed Einstein Equations, so that e.g. in a matter dominated universe,

$$\left(\frac{k^2}{a^2}\right)\Phi + \left[3H + \frac{9H(2\dot{H}+3H^2\Omega_m)}{2\left(k^2/a^2 - 3\dot{H}\right)}\right]\left(\dot{\Phi}+H\Phi\right) + (2M_{\rm P}^2)^{-1}\delta\rho_m = 0. \quad (5.20)$$

The quantity of interest for us, however, is the effective Planck Mass, and since we take the Cuscuton as not contributing to the energy-momentum tensor but as part of the gravitational action, we can use these expressions and Eq. (5.10) to find that

$$M^2_{p,\rm eff} \simeq M^2_{p,\rm UV} - \frac{3\kappa^4}{2m^2}\left(1+\frac{k^2}{3H^2}\right)^{-1}\left(1-\frac{k^2}{3\dot{H}}\right)^{-1}, \quad (5.21)$$

to the lowest order in κ, in a flat matter-dominated Universe, which again shows that the IR limit of our definition of the effective Planck Mass is consistent with the background result above, and that in our numerical calculations below, only the exact transition between the IR and UV regimes will depend on our choice of gauge.

5.3.1 Cuscuton and k-Essence

For completeness, let us very briefly mention the connection between the k-essence models introduced in Section 2.3 and the Cuscuton. If we consider k-essence actions written as

$$S_\varphi = \int \mathrm{d}^4x\sqrt{-g}\left[\frac{1}{2}F(X,\varphi) - V(\varphi)\right], \quad (5.22)$$

with $X \equiv \partial_\mu\varphi\partial^\mu\varphi$, we see that the Cuscuton action corresponds to a particular choice for F. Important in our context is the relation for the speed of sound μ (as defined in Section 3.2), which can in k-essence theories be computed by

$$\mu^2 = \frac{1}{1+2XF''/F'}, \quad (5.23)$$

where only for this subsection we use $'$ to denote the derivative with respect to X. Inserting the definition of the Cuscuton action in this equation, one finds that $\mu = \infty$. Cuscuton models therefore are a very specific limiting case of k-essence theories, namely the limit of an infinite speed of sound. On one hand, this is intimately connected to the fact that the scalar degree of freedom can be eliminated from the dynamical equations, on the other hand, it immediately raises questions about the causality of the theory (see Bonvin et al. 2006; Babichev et al. 2008; Adams et al. 2006; Bruneton 2007; Vikman 2007, for the debate of whether or not $\mu > 1$ is a fundamental problem in k-essence theories in general). We will not repeat the very detailed discussion of this question carried out in the original article by Afshordi et al. (2007b), but merely state the result, namely that perturbations of the Cuscuton cannot carry any microscopic information, and therefore do not violate causality. This again expresses the fact that $\delta\varphi$ is

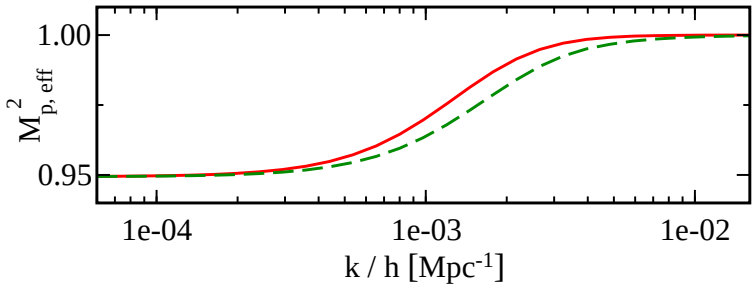

Figure 5.1: Transition between the IR and UV regimes for the effective Planck mass (in units of $M_{p,\mathrm{UV}}$) for the quadratic Cuscuton with $\alpha = -0.05$ (red, straight line). The transition for a canonical scalar field model ($\mu^2 = 1$) is depicted in green (dashed line). For $\mu^2 \gtrsim 10$, the transitions virtually coincide with the quadratic Cuscuton (for which $\mu^2 = \infty$).

given by a constraint equation, and cannot individually carry any information. It could, in principle, change causal properties of other fields that it couples to, but again, Afshordi et al. (2007a) show explicitely that for metric perturbations coupled to the Cuscuton, which is the case we are interested in here, the infinite speed of sound is not equivalent to an instantaneous interaction which would directly violate causality, and that there is no (at least no obvious) violation of causality in Cuscuton cosmologies.

5.4 Running of the Planck Mass?

In order to compute the observational constraints on the possible UV-IR mismatch of the Planck Mass, parameterized by α in Eq. (5.5)f, we have implemented the Cuscuton models in CMBEASY. An example of the transition is shown in Fig. 5.1, where we can see that for a canonical scalar field model with $\mu^2 = 1$, the transition shifts to slightly smaller scales, by about 30%. As we will see belowe, this slight shift has only a marginal effect on the allowed size of α.

The phenomenology of the quadratic Cuscuton model is very similar to the early dark energy models of Chapter 4, as the infinite speed of sound introduces no significant changes (but see Afshordi et al. 2007a, for the explicit calculations for the Cuscuton models). In particular, with $\alpha \equiv -\Omega_Q \ll 1$, the dependence of the growing mode of the matter density perturbations and the gravitational potential during matter domination is identical to the one in an early dark energy model,

$$\delta \propto t^{\frac{2}{3}+\frac{2}{5}\alpha} \Rightarrow \Phi \propto t^{\frac{2}{5}\alpha}. \tag{5.24}$$

The notable distinction though, is the fact that unlike the fractional energy density in a tracking dark energy model, α is not a priory required to be negative, so instead of the general suppression of growth that perturbation modes in early dark energy models would experience, we now have either a suppression or an enhancement. This directly translates to the matter power spectra, and also to the CMB, where for example the contribution from the Integrated Sachs-Wolfe

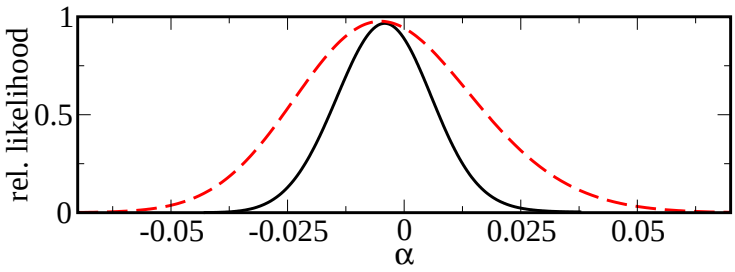

Figure 5.2: Observational constraints on the UV/IR Planck mass mismatch parameter, α, from 3 years of WMAP data alone Hinshaw et al. (2007)(red, dashed line), and our compilation (see the text) of cosmological observations (black straight line).

effect can now either lead to less power on the large angular scales (for $\alpha > 0$) or to an increase of the lower CMB multipoles (for $\alpha < 0$).

We compute the constraints that these effects impose on the allowed range for α using our modified version of CMBEASY, with the result shown in Fig. 5.2. The 3-year CMB power spectrum of WMAP (Hinshaw et al. 2007) constrains α to -0.005 ± 0.040 at the 95% confidence level, which is in line with the allowed size of α we would expect from our constraints on the abundance of early dark energy in Chapter 4.

We then also use data from the distribution of luminous red galaxies from the Sloan Digital Sky Survey (SDSS, Tegmark et al. 2006) to probe the effects of large scale structure data on our constraints. For the SDSS data, we marginalize over the bias. We also include constraints on the cold dark matter power spectrum from observations of the Lyman-α forest (Seljak et al. 2006), as we have done for the early dark energy models in Section 4.2.4. Adding the results from Supernovae Ia observations (Riess et al. 2007) as well as the observation of the baryon acoustic oscillations (BAO) (Eisenstein et al. 2005) to this large scale structure data (in order to decrease degeneracy with other cosmological parameters), together with the WMAP data. As our central result, we find the UV/IR mismatch parameter, α, to be tightly constrained to -0.004 ± 0.021 (95% confidence limit) by our complete set of observational data.

The effect of the sound speed of the scalar field on the bounds on a UV/IR glitch is marginal. If we recompute the constraints for a scalar field model with $\mu^2 = 1$, instead of the Cuscuton case of $\mu^2 = \infty$, the bounds on α are only slightly relaxed, namely to -0.004 ± 0.024 at the 95% confidence level. Together with the results for α from the early dark energy models, we therefore conclude that the constraints on α are insensitive to the details of UV/IR transition, since most of the observable consequences of the mismatch occur on small sub-horizon scales.

We can also compare our constraints to the Einstein-Aether theories that we had very briefly mentioned above; there, the glitch in the Planck Mass is a function of three constants of the theory $c_{1,2,3}$, i.e.

$$M^2_{p,\mathrm{IR}} = M^2_{p,\mathrm{UV}} - (2c_1 + 3c_2 + c_3), \tag{5.25}$$

but in contrast to our investigation, both $M^2_{p,\mathrm{IR}}$ and $M^2_{p,\mathrm{UV}}$ are 'screened' values of the bare Planck Mass in the theory. Recently, Zuntz et al. (2008) used a modified version of CMBEASY to obtain cosmological constraints from a combination of CMB and large scale structure data, finding 1σ bounds of $(c_1 = -0.26 \pm 0.12, c_2 = 0.20 \pm 0.09, c_3 = -0.12 \pm 0.05)$, so that an addition of the mean parameter values would yield $\alpha \sim -0.04$, broadly compatible with the constraints we found here.

As the precision of cosmological observations is continuously increasing, the bounds on any mismatch between UV and IR Planck Masses will improve accordingly, but already with current data, we have shown in this chapter that such a mismatch is constrained to less than 1.2% for the Planck Mass at the 95% confidence level, severely restricting any such deviation from Einstein Gravity at the largest cosmological scales.

6 Coupled Dark Energy

When considering scalar field dark energy in the previous chapters, we have always assumed that gravity is the only way of interaction between the scalar field and the other components in the Universe. In principle, there is no fundamental reason why we should postulate the absence of other interactions, and in fact, it is well known that such a possible interaction between the scalar field and other matter species could be an important part of any complete description of cosmology (Wetterich 1995; Amendola 2000). It is therefore not surprising that the literature on this 'Coupled Quintessence' is extensive, ranging from studies of Coupled Quintessence as a solution to the coincidence problem and similar questions (Quartin et al. 2008; Brookfield et al. 2008; Gromov et al. 2004; Mangano et al. 2003; Anderson & Carroll 1997), to its observational characteristics and implications (see e.g. Bertolami et al. 2007; Wang et al. 2007; Guo et al. 2007; Mainini & Bonometto 2007; Lee et al. 2006; Farrar & Peebles 2004; Gubser & Peebles 2004; Farrar & Rosen 2007, and references therein).

As one can a priori imagine many different forms of a dark energy coupling to other species, or e.g. an arbitrary time dependence, there is a vast theory space to explore, as one hopes to gain physical insight, and in the age of 'precision cosmology', quantitative numerical studies and comparison of their result with observations are indispensable; the number of such studies in the literature, however, is comparatively small (examples include Bean et al. 2008; Kesden & Kamionkowski 2006; Amendola & Quercellini 2004; Amendola 2001).

This chapter extends our previous consideration of scalar field dark energy models to cases with a coupling between cold dark matter and the scalar field. The formalism presented here has then been implemented in CMBEASY, and we will use this code to show the phenomenology of one specific example of coupled dark energy, i.e. for a specific choice of the scalar field potential and the dark matter - dark energy coupling. The numerical results for these specific models have then been used by Baldi (2009) as input for a modified version of the N-body code GADGET-2 (Springel 2005), in order to investigate the non-linear regime. Together with the extensions and modifications of CMBEASY described here, these two implementations form a complete numerical pipeline for the study of general coupled dark energy models, as presented in Baldi, Pettorino, Robbers, & Springel (2008).

Of course, dark energy could also interact with other particle species, not only the dark matter. The coupling to baryons is tightly contrained by experimental tests of gravity on scales of the solar system and below (see e.g. Carroll et al. 2009; Damour et al. 1990), but a dependence of the neutrino mass on the value of the scalar field is much less restricted by current observations. In fact, a neutrino with a time varying mass, depending on the scalar field, can have a very rich phenomenology, and suggest for example a very intriguing solution to

the 'why now?' question, together with substantial implications for structure formation. We will postpone the study of this particular kind of coupling to the next chapter, and focus on the dark matter - dark energy coupling here.

6.1 The Formalism

The action of the system of a dark energy scalar field coupled to matter fields ψ can be written as

$$\mathcal{S}_{coupled} = \int \mathrm{d}^4x\sqrt{-g}\left[-\frac{1}{2}\partial^\mu\phi\partial_\mu\phi - U(\phi) - m(\phi)\bar{\psi}\psi + \mathcal{L}_{kin}[\psi]\right] \tag{6.1}$$

The specific form of the interaction between dark matter and dark energy is encoded in the dependence of the mass of the matter fields on the value of the scalar field ϕ, i.e. the form of the coupling is specified by choosing a particular $m(\phi)$.

The coupling then naturally changes the evolution of the scalar field, which is now governed by a modified Klein-Gordon equation,

$$\phi'' + 2\mathcal{H}\phi' + a^2U_{,\phi}(\phi) \equiv -a^2S, \tag{6.2}$$

which is the result of varying Eq. (6.1) with respect to ϕ, and where $\mathcal{H} = a'/a$ is the conformal Hubble parameter and $U_{,\phi}$ is the derivative of the potential of the scalar field with respect to ϕ. The coupling changes the ordinary field equation through the appearance of an external source term S, which contains the ϕ-dependent mass term,

$$S \equiv \frac{\partial \ln m(\phi)}{\partial\phi}\langle m(\phi)\bar{\psi}\psi\rangle = \frac{\partial \ln m(\phi)}{\partial\phi}(\rho - 3p). \tag{6.3}$$

The energy density and pressure on the right hand side are the ones of the species that the dark energy couples to, so in the case considered here, they reduce to the energy density of cold dark matter, ρ_c. The energy-momentum tensor of the combined dark matter - dark energy fluid is conserved,

$$\sum_\alpha \nabla_\nu T_{(\alpha)}{}^\nu{}_\mu = 0, \tag{6.4}$$

but the divergences of the contributions of the individual species α (in this case dark matter and dark energy), do not vanish as they normally would, but are given by a source term $Q_{(\alpha)\mu}$.

$$\nabla_\nu T_{(\alpha)}{}^\nu{}_\mu = Q_{(\alpha)\mu}. \tag{6.5}$$

As the combined energy-momentum of this multifluid system is conserved, the sum of the source terms must vanish,

$$\sum_\alpha Q_{(\alpha)\mu} = 0, \tag{6.6}$$

model name	β
RP1	0.04
RP2	0.08
RP3	0.12
RP4	0.16
RP5	0.2

Table 6.1: Value of the coupling parameter β for our example models with an inverse power law potential.

which in the case considered here is equivalent to

$$Q_c = -Q_\phi. \tag{6.7}$$

We can combine this with the usual expression for the energy-momentum tensor of the scalar field and Eq. (6.2) to obtain the relation between the Q_α and S, which yields

$$Q_{(\phi)\mu} = S\nabla_\mu\phi. \tag{6.8}$$

The evolution of the background densities in a coupled cosmology is determined by the conservation equation Eq. (6.4). For notational convenience, we define

$$Q_\alpha \equiv -\frac{1}{a}Q_{(\alpha)0} \tag{6.9}$$

as well as

$$h_\alpha \equiv \rho_\alpha + p_\alpha = (1 + w_\alpha)\rho_\alpha, \tag{6.10}$$

so that the background densities then evolve according to

$$\rho'_\alpha = -3\mathcal{H}\rho_\alpha(1 + w_\alpha) + aQ_\alpha. \tag{6.11}$$

As we restrict our consideration here to a coupling between cold dark matter and ϕ, this is explicitely:

$$\begin{aligned} \rho'_\phi &= -3\mathcal{H}h_\phi + aQ_\phi \\ \rho'_c &= -3\mathcal{H}h_c + aQ_c. \end{aligned} \tag{6.12}$$

As examples for a particular coupled dark energy cosmology, we take a standard scalar field with an inverse power law potential (Ratra & Peebles 1988)

$$U(\phi) = U_0\,\phi^{-\alpha}, \tag{6.13}$$

and choose the coupling as

$$m(\phi) = m_0 e^{-\beta\phi/M_{\rm P}}. \tag{6.14}$$

The constant U_0 in the potential is then set such that we obtain a given present-day energy density of the dark energy, and the cold dark matter mass m_0 is determined by the dark matter energy density today. The slope of the potential and the coupling strength are chosen in as in Maccio et al. (2004), who carried

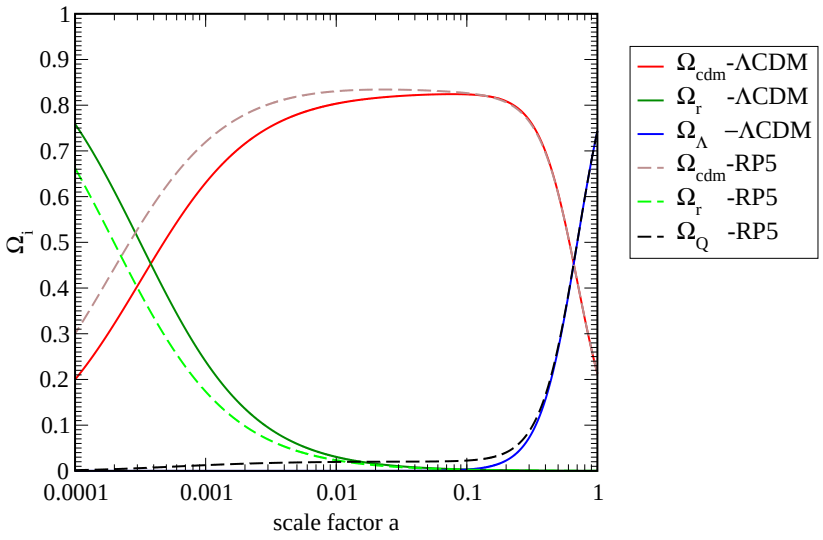

Figure 6.1: The evolution of energy densities in the coupled model RP5 with a coupling strength of $\beta = 0.2$ compared to a concordance ΛCDM cosmology. Both models have the same present-day values of the background densities (as determined from WMAP 5-year data for ΛCDM), but differ considerably in the past. The shift of matter-radiation equality is evident, as is the ϕMDE phase of the RP5 model. In the language of Chapter 4, this leads to an average fraction of dark energy during structure formation of $\bar{\Omega}^d_{\rm sf} \sim 2\%$.

out a first N-body simulation of these particular models. The example models are labeld RP1 through RP5, with $\alpha = 0.143$, and coupling strengths $\beta = \text{const}$ as shown in Table 6.1. Note that the numerical values of β differ from the ones in Maccio et al. (2004) due to a different convention in the definition of the coupling in Eq. (6.14).

This parameter choice then allows us to compare our numerical implementations to this previous work; the formalism here and the extension of CMBEASY and GADGET-2, however, are written in terms of a general coupling source S with the corresponding Q_α, as defined above.

For our example models with the coupling of Eq. (6.14), S is simply given by

$$S = -\frac{\beta(\phi)}{M_{\rm P}}\rho_c. \tag{6.15}$$

The resulting evolution of the background densities is illustrated by Fig. 6.1, which compares the example model RP5 to a concordance ΛCDM universe. A typical feature of this type of coupled dark energy cosmologies is the appearance of a phase of constant, but finite, Ω_ϕ before the scalar field begins to dominate - a particular realization of early dark energy. Assuming a vanishing energy density for all components other than cold dark matter and the scalar field, the dark energy density in this phase for a constant β is $\Omega_\phi = \frac{2}{3}\beta^2$. The phenomenology of this epoch with an early dark energy component, however, is substantially different from the uncoupled scalar field dark energy models

discussed in Chapter 4, as we will see below. In the nomenclature of the phase space analysis of coupled quintessence by Amendola (2000), this phase is called the ϕMDE, as this is not the pure matter dominated epoch (MDE) found in an ordinary ΛCDM, but contains also a fraction of dark energy that depends on the strength of the coupling. Also apparent in Fig. 6.1 is a shift of the time of matter-radiation equality to earlier times, which for the very high coupling strength of model RP5 is substantial.

6.2 Linear Perturbations

With the general formalism of the previous section at hand, one can now compute the linear perturbations around the homegeneous background, exactly as described in Chapter 3, but this time keeping the additional terms that result from the dark matter - dark energy coupling. The perturbed versions of energy-momentum conservation, Eq. (6.4), now are, in the longitudinal gauge,

$$(\rho_\alpha + p_\alpha)\left[3\Phi' + kv_\alpha\right] + 3\mathcal{H}\rho_\alpha(\delta_\alpha + w_\alpha\pi_{L\alpha}) + (\rho_\alpha + \delta_\alpha)' = -\delta Q_{(\alpha)0} \quad (6.16)$$

for the energy density perturbation of the species α, as well as

$$p_\alpha\left(\frac{2}{3}\Pi_\alpha - \pi_{L\alpha}\right)k + 4\mathcal{H}h_\alpha + (h_\alpha v_\alpha)' - h_\alpha\Psi = \delta Q_{(\alpha)i}, \quad (6.17)$$

for the velocity part. These equations are identical to the ones obtained in the uncoupled case, Eq. (3.47) and Eq. (3.48), but for the perturbations of the source terms on the right hand side, expressing the fact that instead of two independent sets of equations for cold dark matter and the dark energy fluid, we are dealing with one multicomponent fluid. In the evolution equations below, we substitute expressions that contain terms containing $\delta Q_{(\alpha)}$ by the corresponding expressions in terms of the gauge-invariant perturbation of the source S, denoted by DS. We now denote the adiabatic sound speed of species i by $c_i^2 = \dot{\rho}/\dot{p}$. Following Kodama & Sasaki (1984), and again using the same gauge-invariant variables and notation as Doran (2005) and Durrer (2008), Eq. (6.16) and Eq. (6.17) can be rewritten as evolution equations for the gauge-invariant density perturbations D_g^α (which, as a reminder, are related to the longitudinal δ via $D_g^\alpha = \delta_\alpha + 3(1+w)\Phi$). A tedious calculation leads to the following set of evolution equations:

$$\begin{aligned} D_g'^{\phi} &= -\left[3\mathcal{H}(1-w_\phi) + \frac{aQ_\phi}{\rho_\phi}\right]D_g^\phi \quad (6.18)\\ &\quad -\left[k^2(1+w_\phi) + 3\mathcal{H}(1-c_\phi^2)\left(3\mathcal{H}(1+w_\phi) - \frac{aQ_\phi}{\rho_\phi}\right)\right]V_\phi/k \\ &\quad +9\mathcal{H}(1+w_\phi)(1-c_\phi^2)(1-\frac{aQ_\phi}{3\mathcal{H}h_\phi})\Phi \\ &\quad +\frac{a}{\rho_\phi}\left[-\frac{\phi'}{a}DS - \frac{1}{a}SX' + Q_\phi\left(\frac{\mathcal{H}'}{\mathcal{H}^2} - 1\right)\Phi - Q_\phi\frac{\Phi'}{\mathcal{H}} - \frac{Q_\phi'}{\mathcal{H}}\Phi\right] \\ V_\phi' &= \frac{kD_g^\phi}{1+w_\phi} + \left[2\mathcal{H} - \frac{aQ_\phi}{h_\phi}\right]V_\phi - 3\left(1 - \frac{aQ_\phi}{3\mathcal{H}h_\phi}\right)k\Phi + k\Psi \quad (6.19) \end{aligned}$$

The evolution of cold dark matter perturbations is governed by the two equations:

$$\begin{aligned} D_g'^c &= -\frac{aQ_c}{\rho_c} D_g^c - kV_c + \frac{aQ_c}{\rho_c}\mathcal{A} - \frac{a}{\rho_c}\frac{Q_c'}{\mathcal{H}}\Phi + \frac{a}{\rho_c}Q_\phi\Psi + \frac{\phi'}{\rho_c}DS + \frac{SX'}{\rho_c}, \\ V_c' &= -\left(\mathcal{H} + \frac{S\phi'}{\rho_c}\right)V_c + \frac{S\phi'}{\rho_c}V_\phi + k\Psi, \end{aligned} \tag{6.20}$$

where $\mathcal{A}$ denotes a combination of the metric perturbations,

$$\mathcal{A} = \Psi - \left(1 - \frac{\mathcal{H}'}{\mathcal{H}^2}\right)\Phi - \frac{1}{\mathcal{H}}\Phi', \tag{6.21}$$

and X is the gauge-invariant perturbation of the scalar field, ϕ, for which we have

$$X = \frac{V_q}{k}\phi'. \tag{6.22}$$

In the equations above, only its derivative appears, which can be substituted by

$$X' = \left(-2\mathcal{H}\phi' - a^2 U_{,\phi} - a^2 S\right) V_\phi/k + \phi' V_\phi/k, \tag{6.23}$$

completing the set of evolution equations for the coupled dark matter - dark energy fluid. The other perturbation equations of Chapter 3 remain untouched, in particular the equations for the gravitational potentials Φ and Ψ.

These equations have been implemented in CMBEASY, allowing to compute CMB and matter power spectra for any coupling specified by an expression for S, and the corresponding perturbation, DS. For our example models, DS is given by

$$DS = -\frac{\beta(\phi)}{M_{\rm P}}\rho_c\left[D_g^c - 3\left(1 + \frac{\beta(\phi)\phi'}{3M_{\rm P}\mathcal{H}}\right)\Phi\right] - \frac{\beta_{,\phi}}{M_{\rm P}}\rho_c X. \tag{6.24}$$

The temperature-temperature CMB power spectrum of the set of example models is shown in Fig. 6.2. Even more pronounced than the shift of the peaks is the strong suppression of power with increasing coupling. A considerable part of this suppression is caused by the fact that a higher coupling also entails a higher initial energy density of cold dark matter, in order for all example models to reach identical fractional energy densities today. Already from this plot, it appears that it is very unlikely that a coupling strength as high as the one of RP5 could be compatible with present day observations, even if changes in other cosmological parameters could partly compensate for the change in the power spectra.

6.3 Matter Fluctuations

The effects of a coupling can also be very substantial for matter perturbations, as can be seen from the cdm-power spectrum of the example models in Fig. 6.3. At first, it seems surprising that the amplitude increases with higher coupling. After all, in Chapter 4 we had seen that the presence of an early dark energy

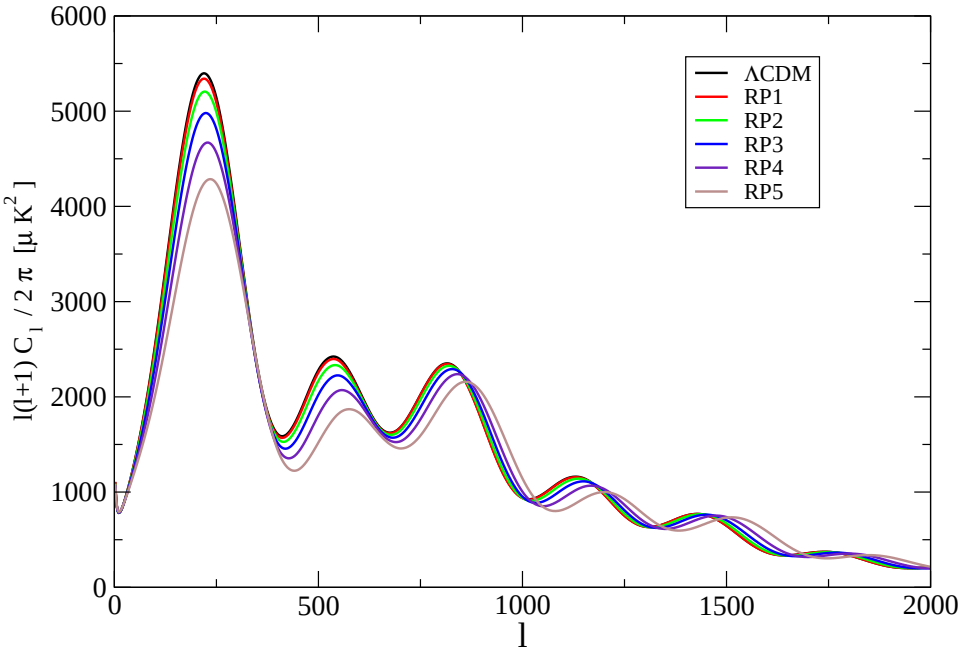

Figure 6.2: TT power spectra for models RP1 to RP5. Shown for comparison is a ΛCDM model with best fit parameter values determined from WMAP 5-year data.

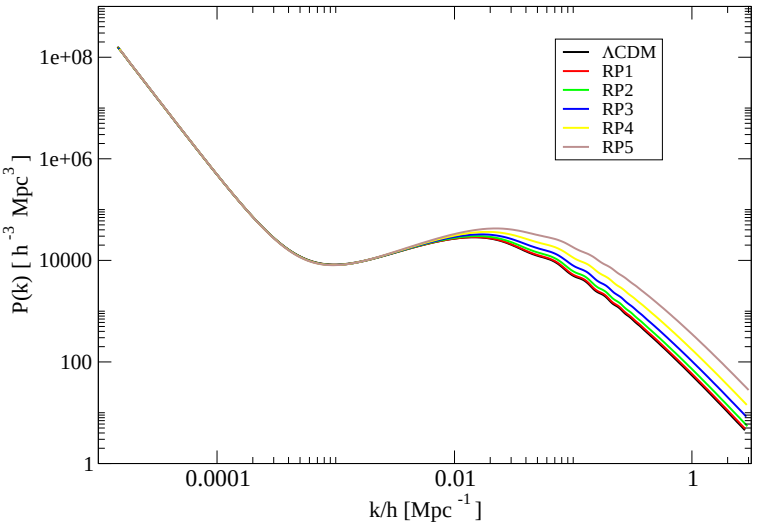

Figure 6.3: The power spectrum of linear cold dark matter perturbations for the example models RP1 to RP5. Shown in black is a fiducial ΛCDM model with best-fit parameter values from the 5-years of WMAP data. The enhanced structure growth in the linear regime is evident, in particular for model RP5 with the highest value of the coupling, $\beta = 0.2$.

component during the period of structure formation suppresses the growth of matter fluctuations, and from Section 6.1 we know that in the ϕMDE, we expect $\Omega_\phi \approx \frac{2}{3}\beta^2$. Of course, the higher matter fraction at early times in the example models could be partially responsible for the effect seen here, but the enhanced growth is actually a quite generic feature of our class of models, and can even be understood analytically, e.g. from the explicit solutions for the evolution of matter perturbations during the ϕMDE in the small-scale limit presented by Amendola & Tocchini-Valentini (2002). Deriving Eq. (6.20), and taking the limit $k \to \infty$, one arrives after some algebraic manipulations at the expression for the matter perturbation growth in terms of the time variable $\alpha = \log a$,

$$\ddot{D}_g^c + \left(1 + \frac{\dot{\mathcal{H}}}{\mathcal{H}} - \beta\dot{\phi}\right)\dot{D}_g^c - \frac{3}{2}(1+2\beta^2)D_g^c\Omega_c = 0, \tag{6.25}$$

where - only in this equation - overdots are derivatives with respect to α, and $\Omega_b = 0$ is assumed. This can be solved analytically (see also the discussion in Di Porto & Amendola 2008), and one finds

$$D_g^c \sim a^{1+2\beta^2}. \tag{6.26}$$

This behavior is illustrated in Fig. 6.4, which shows the numerical results of the growth factor D_g^c/a. In this figure, the growth factors are normalized to unity today, and it is apparent that the coupled models reach the same amplitude of the density contrast as the ΛCDM model starting from much lower values in the past.

6.4 The Growth Rate

We can also fit the growth of matter perturbations in our models by an analytic expression; such a phenomenological fit is especially useful when compared to the standard expressions commonly used for ΛCDM. Conventionally, one presents this kind of fit as an approximation of the the growth rate $f(a)$, which is defined as

$$f(a) \equiv \frac{d\ln D_g^c}{d\ln a}. \tag{6.27}$$

It is well known that for ΛCDM cosmologies the total growth rate is well approximated by a power of the total matter density

$$f \approx \Omega_M^\gamma, \tag{6.28}$$

with $\gamma = 0.55$, roughly independent of the cosmological constant density (Peebles 1980).

Amendola & Quercellini (2004) found that this fit can be extended to coupled dark energy models at low redshifts by setting $\gamma = 0.56(1-\beta^2)$. A more general fit, extending the validity to higher redshifts and to models with a growth faster than the standard ΛCDM case, was proposed by Di Porto & Amendola (2008). However, it is only valid for models with no admixture of uncoupled matter, whereas in our case we also have a baryonic component. We suggest here a fit

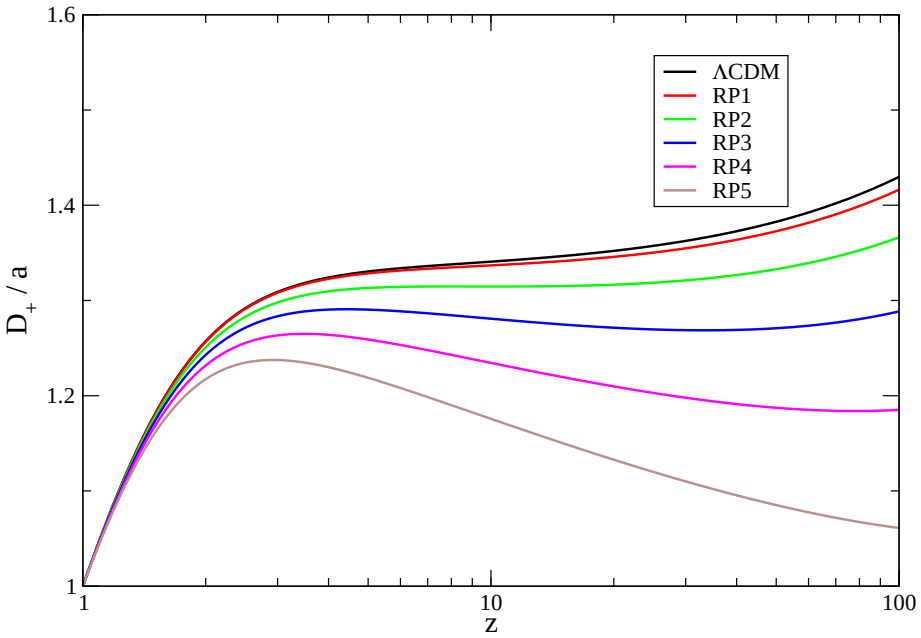

Figure 6.4: Growth factors for the example models compared to the reference ΛCDM model, for which the growth factor is approximately constant during matter domination. Plotted is the gauge-invariant D_g^c (labeled D_+ in the plot), numerically evaluated using CMBEASY, divided by the scale factor a.

for the combined growth rate, i.e. the one computed by weighting the matter fluctuations at any given redshift with the corresponding $\Omega_{(cdm,\,b)}$. For the class of our example models with $\alpha = 0.143$, we find that a phenomenological fit of the form

$$f(a) \sim \Omega_M^{\gamma}(1 + \gamma \frac{\Omega_{\rm CDM}}{\Omega_M} \epsilon_c \beta^2)\,, \tag{6.29}$$

with $\gamma = 0.56$ and $\epsilon_c = 2.4$ reproduces the growth rate with a maximum error of $\sim 2\%$ over a range of coupling values between 0 and 0.2 and for a cosmic baryon fraction Ω_b at $z = 0$ in the interval $0.0 - 0.1$. For models with a different slope of the potential the error is not much bigger, e.g. for $\alpha = 2.0$ the maximum error increases to $\sim 4\%$ in the same range of coupling and baryon fraction. Fig. 6.5 compares the result of this fitting formula to the numerical result, showing the good agreement, and compares this to the fit one would obtain from the fitting function Eq. (6.28), which is a good fits only for the ΛCDM case.

6.5 The Coupling Strength

Before we move on to the non-linear regime and the implications of a dark-matter dark energy coupling on smaller scales, we can ask the question of how realistic the size of β in our example models really is - and indeed the power spectra in Fig. 6.2 and Fig. 6.3 clearly suggested that the higher end of the range for β chosen for the examples can serve only as an illustration of the

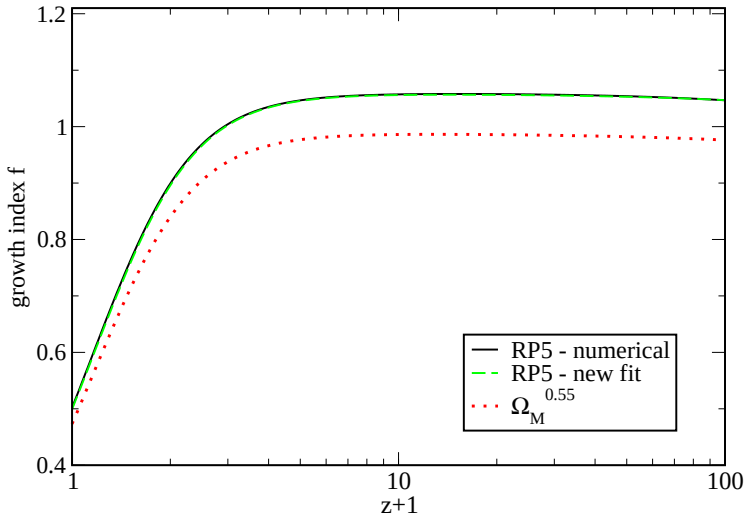

Figure 6.5: The growth rate $f(a)$, evaluated numerically for model RP5, and the phenomenological fit of Eq. (6.29), which at this scale is indistinguishable from the numerical computation. Also shown is the 'fit' $f = \Omega_M^{0.55}$, which is a very good approximation in ΛCDM cosmologies, but less so for coupled dark energy models.

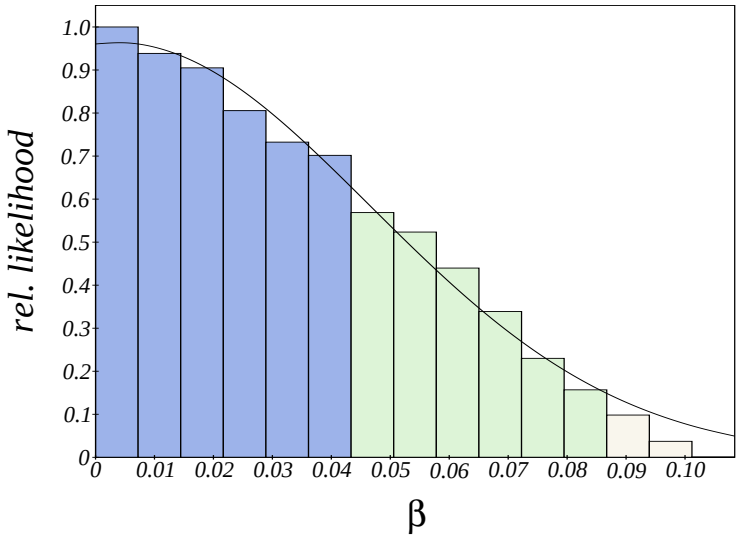

Figure 6.6: Observational constraints on the strength β of the dark matter - dark energy coupling for quintessence models with an inverse power law potential and $\alpha = 0.143$. The blue and light green bars show the 68% and 95% confidence limits. As expected from the example CMB and matter power spectra for the models RP1 through RP5, only the smaller coupling strengths of RP1 and RP2 are in the region that can give reasonable fits to our set of observational data.

	68% confidence limit	95% confidence limit
$\Omega_m h^2$	$0.136^{(-)0.003}_{(+)0.003}$	$0.136^{(-)0.006}_{(+)0.006}$
$\Omega_b h^2$	$0.0222^{(-)0.0005}_{(+)0.0006}$	$0.0222^{(-)0.0010}_{(+)0.0011}$
h	$0.69^{(-)0.01}_{(+)0.02}$	$0.69^{(-)0.03}_{(+)0.03}$
β	< 0.04	< 0.08
τ	$0.08^{(-)0.02}_{(+)0.02}$	$0.08^{(-)0.03}_{(+)0.03}$
n_s	$0.96^{(-)0.01}_{(+)0.01}$	$0.96^{(-)0.02}_{(+)0.03}$
$\ln(10^{10} A_s) - 2\tau$	$2.92^{(-)0.02}_{(+)0.02}$	$2.92^{(-)0.04}_{(+)0.04}$
σ_8	$0.81^{(-)0.03}_{(+)0.03}$	$0.81^{(-)0.05}_{(+)0.06}$

Table 6.2: Observational constraints on the cosmological parameters for coupled dark energy models of the type of our set of examples and the set of cosmological probes described in the text.

effects induced by the coupling, and that e.g. RP5 does not represent a realistic description of the Universe we observe.

Observational constrains on β are shown in Fig. 6.6, from comparing the predictions of the class of our example models (i.e. an inverse power law potential with $\alpha = 0.143$ and a constant, positive coupling as defined by Eq. (6.14)), to the CMB data from five years of observations from WMAP (Nolta et al. 2009), the distribution of matter in the Universe as reported by the Sloan Digital Sky Survey (Tegmark et al. 2006, 2004a) (we marginalize over the bias), the Baryon Acoustic Peak (Eisenstein et al. 2005), and a compilation of supernovae data (Riess et al. 2007). While the usual cosmological parameters are allowed to vary, i.e. the Hubble parameter h, the matter densities today $\Omega_m^0 h^2$ and $\Omega_b^0 h^2$, the optical depth τ, scalar spectral index n_s and the initial amplitude of fluctuations A_s via the combination $\ln(10^{10} A_s) - 2\tau$, the initial energy density of cold dark matter and the constant prefactor of the quintessence potential are adjusted such that the given energy densities today are reached. The complete set of confidence intervals for the parameters is summarized in Table 6.2.

From this set of observational data, the size of the coupling is constrained to $\beta < 0.08$ at a confidence limit of 95%. This result is in very good agreement with the findings of Bean et al. (2008), who report a constraint for the coupling strength of $\beta < 0.07$ for a cold dark matter - dark energy coupling for dark energy models with inverse power law and exponential potentials.

6.6 Newtonian Approximation

A coupling between dark matter and dark energy will also influence the physics on scales smaller than the cosmological scales considered in the previous section.

For a preliminary understanding of the physical effects that we expect on these smaller scales, we consider in this section the Newtonian limit, i.e. the limit in which $\lambda \equiv \mathcal{H}/k \ll 1$. Following e.g. Amendola (2004), (see also the discussion in Maccio et al. 2004) one can show that in this limit the perturbation of the scalar field can be expressed as

$$\delta\phi \sim 3\lambda^2 \Omega_c \beta(\phi) \delta_c, \tag{6.30}$$

Using this expression then allows to derive the approximate formula for the gravitational potential, namely

$$\Phi \sim \frac{3}{2}\frac{\lambda^2}{M^2} \sum_{\alpha \neq \phi} \Omega_\alpha \delta_\alpha \,. \tag{6.31}$$

This can be substituted in Eq. (6.20), and then yields an expression for the effective gravitational potential Φ_c felt by the dark matter in the Newtonian limit,

$$\Phi_c \equiv \Phi + \frac{\beta(\phi)}{M}\delta\phi, \tag{6.32}$$

where we can replace Φ and $\delta\phi$ using Eq. (6.31) and Eq. (6.30). With the N-body simulations in mind that will eventually study the small-scale behavior of our coupled dark energy models in detail, we can convert the resulting expression to real space, and find

$$\nabla^2 \Phi_c = -\frac{a^2}{2}\rho_c \delta_c \left(1 + 2\beta^2(\phi)\right) - \frac{a^2}{2} \sum_{\alpha \neq \phi, c} \rho_\alpha \delta_\alpha, \tag{6.33}$$

where the last term is the contribution of the uncoupled components in the universe. We can absorb the coupling factor in this equation into an effective gravitational constant, and define

$$\tilde{G}_c = G_N[1 + 2\beta^2(\phi)], \tag{6.34}$$

where G_N is the usual value of Newton's constant. It immediately follows that the coupling not only changes the value of the gravitational constant, but also that the effective gravitational interaction becomes time dependent as soon as β is a function of the scalar field ϕ. Of particular interest are the modifications to the Euler equation, which can be derived starting from Eq. (6.20), taking the Newtonian limit and inserting the expression for the effective gravitational potential Φ_c. The final result can be written as

$$\begin{aligned} &\vec{\nabla}\vec{v}_c' + \left(\mathcal{H} - \frac{\beta(\phi)}{M}\phi'\right)\vec{\nabla}\vec{v}_c + \\ &\frac{3}{2}\mathcal{H}^2 \left[\Omega_c \delta_c + 2\Omega_c \delta_c \beta^2(\phi) + \sum_{\alpha \neq \phi, c} \Omega_\alpha \delta_\alpha\right] = 0\,. \end{aligned} \tag{6.35}$$

This formula is useful because it can be used to derive the acceleration of a single cold dark matter test particle in empty space, at a distance r from the

origin, caused by a mass M_c at the origin. M_c will change, depending on the coupling as

$$\tilde{M}_c \equiv M_c e^{-\int \beta(\phi)\frac{\mathrm{d}\phi}{\mathrm{d}a}\mathrm{d}a}. \tag{6.36}$$

Then, assuming that the density of this mass is much larger than the background density, one can write the density contrast due to M_c as

$$\Omega_c \delta_c = \frac{8\pi G \tilde{M}_c \delta(0)}{3\mathcal{H}^2 a}, \tag{6.37}$$

where $\delta(\vec{r})$ is the Dirac distribution.

Inserting this in Eq. (6.35) and again converting to real space, yields the acceleration equation for the particle at position $\vec{r}$:

$$\dot{\vec{v}}_c = -\tilde{H}\vec{v}_c - \vec{\nabla}\frac{\tilde{G}_c \tilde{M}_c}{r}. \tag{6.38}$$

Here, we have defined $\tilde{H}$ by

$$\tilde{H} \equiv H\left(1 - \frac{\beta(\phi)}{M}\frac{\dot{\phi}}{H}\right) . \tag{6.39}$$

In standard cosmologies, for $\beta = 0$, this term is the well-known Hubble-drag, or friction term. In coupled dark energy models, we see that the coupling induces an extra coupling-dependent contribution to this term, effectively leading to an 'anti-friction' (in the case of a positive coupling) for the acceleration of dark matter particles. This effect is in addition to the modification of the gravitational constant that the dark matter particles feel, $\tilde{G}$ as defined in Eq. (6.34), and the varying mass of the dark matter particles.

This also summarizes the changes that need to be incorporated into any N-body code in order to study the non-linear regime of structure formation.

6.7 The Non-Linear Regime

A complete N-body code package that can simulate the non-linear structure formation in coupled dark energy models has been developed by Baldi (2009), building on the GADGET-2 code (Springel 2005). This code takes the output of the modified CMBEASY version we have described here, i.e. the evolution of the background quantities like the energy densities including the scalar field and the Hubble rate, the mass variation of cold dark matter particles, the linear growth factor and matter power spectra as computed by CMBEASY as input and then evolves a system of particles with those linear properties from a given redshift on (in the simulations considered here, from $z_i = 60$), making also the non-linear properties of coupled dark energy cosmologies accessible to quantitative study. In this section, we briefly report the results for our example models RP1 through RP5 (for the complete and detailed discussion, see Baldi 2009).

For the set of example models RP1 through RP5 (as well the reference ΛCDM model), two sets of simulation runs were carried out. The first set, a low-resolution one with a large box size of $320\,h^{-1}$Mpc and 2×128^3 particles (mass

resolutions were $M_b = 1.9 \times 10^{11} h^{-1} M_\odot$ and $M_{cdm} = 9.2 \times 10^{11} h^{-1} M_\odot$ with a smoothing length $e_s = 50\,\mathrm{kpc}$). The second set, with a much higher resolution, used a smaller box size of $80\,h^{-1}\,\mathrm{Mpc}$ with considerably more particles, 2×512^3 (here the mass resolutions were $M_b = 4.7 \times 10^7 h^{-1} M_\odot$ and $M_{cdm} = 2.3 \times 10^8 h^{-1} M_\odot$ with a smoothing length $e_s = 3.5\mathrm{kpc}$).

A first result of the simulations is that the mass function, i.e. the number of dark matter halos of a certain mass that form in our cosmologies, is well described by the fitting function given in Jenkins et al. (2001) and also the one by Sheth & Tormen (1999), which yields a a marginally better fit. Both these fitting functions use the linear power spectra and growth factor computed numerically using CMBEASY to predict the mass function. The results then are good fits for all values of the coupling and over the entire redshift range of the simulations.

A second result is the evolution of the bias between the amplitude of the density fluctuations of baryons and cold dark matter. As we have seen in the linear analysis, baryons and cold dark matter evolve differently, since only the dark matter is subjected to the additional forces due to the coupling (Mainini 2005; Mainini & Bonometto 2006). This linear bias is present on all scales, and in our coupled models substantially different from the ΛCDM prediction. In the non-linear simulations, an additional bias will develop due to the hydrodynamic pressure forces acting on the baryons, but not on the collisionless dark matter particles. The interesting result of the N-body runs now is that the effect of the dark matter - dark energy coupling is also important at smaller scales, in the mildly non-linear regime, and enhances the different clustering rates of baryons and cold dark matter. Even when artificially switching of hydrodynamic forces, and treating both baryons and dark matter as collisionless, a stronger coupling still leads to visibly higher bias due to the different effective gravitational interactions for both species.

The simulations also clearly show this effect at the center of massive collapsed structures. Indeed, halos in simulations with higher coupling contain fewer baryons than expected based on their mass and baryon fraction of the background cosmology. This difference is in principle observable, as e.g. X-ray measurements in clusters would not yield the cosmological value. The baryon fraction within the virial radius r_{200}, i.e. within the radius enclosing a mean overdensity 200 times the critical density, can be defined as

$$f_b \equiv \frac{M_b(< r_{200})}{M_{\mathrm{tot}}(< r_{200})} \tag{6.40}$$

The relative baryon fraction then has the expression

$$Y_b \equiv \frac{f_b}{\Omega_b/\Omega_m}\,, \tag{6.41}$$

for which the reference ΛCDM-simulations yield values consistent with $Y_b \sim 0.92$ found by the *Santa Barbara Cluster Comparison Project* (Frenk et al. 1999), and with the more recent results of Ettori et al. (2006) and Gottloeber & Yepes (2007). For the coupled models, however, the simulations show that the relative

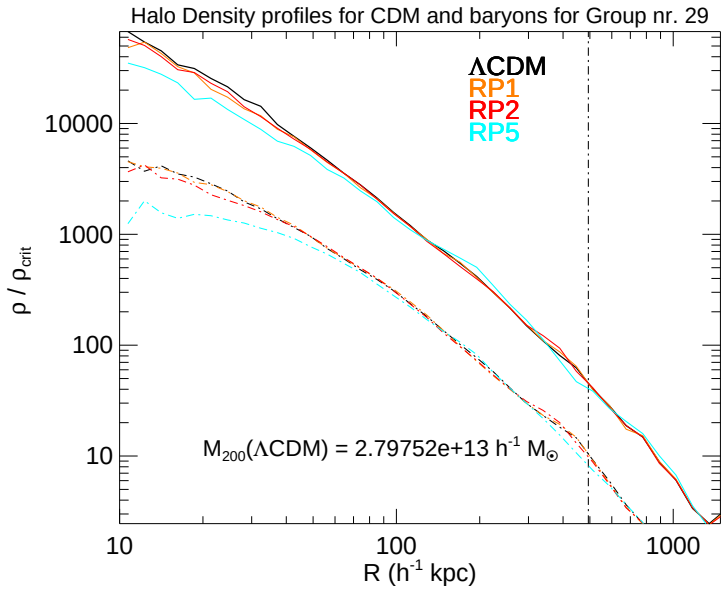

Figure 6.7: Density profile at $z = 0$ of one halo in the different example models (Baldi 2009). Solid lines show cold dark matter, dot-dashed lines baryons. The vertical line indicates the virial radius for the ΛCDM halo. Models with a higher coupling show a lower inner overdensity compared to ΛCDM.

baryon fraction decreases with increasing coupling, down to a value of $Y_b \sim 0.86-0.87$ for the RP5 case. In all cases, the fractions in clusters are smaller than the cosmological value; this could potentially alleviate tensions between the high baryon abundance estimated from CMB observations, and the somewhat lower values inferred from detailed X-ray observations of galaxy clusters (Vikhlinin et al. 2006; McCarthy et al. 2007; LaRoque et al. 2006; Afshordi et al. 2007c).

A third result of the N-body simulations is that the density profile of the halos can, even in the coupled cases, be described by an NFW (Navarro et al. 1997) profile, i.e. as

$$\frac{\rho(r)}{\rho_{\rm crit}} = \frac{\delta^*}{(r/r_s)(1+r/r_s)^2}\,. \tag{6.42}$$

The parameters in this fit are δ^*, which sets the characteristic halo density contrast relative to the critical density, and the scale radius r_s. To compare the characteristic density profiles between different simulations, one can compare corresponding structures in the different simulations. Due to the different physics involved, there obviously is no one-to-one correspondence, but since all simulations use the same random seed to produce realizations of the respective initial power spectra, it is nevertheless possible to identify objects as being the 'same' e.g. by demanding that the most bound particle lie within the virial radius of the corresponding structure in the ΛCDM simulation. The simulations now show that the scale radius for corresponding halos in the coupled models consistently increases with increasing coupling, typically by about $10\% - 35\%$

from ΛCDM to RP5, i.e. halos become less concentrated compared to ΛCDM. The density profile of on example halo chosen from the simulations is shown in Fig. 6.7, and is essentially the opposite to the results obtained by Maccio et al. (2004).

For our set of simulations, the main contribution to the lower concentration can be attributed to the 'anti-friction' term of Eq. (6.39). This term induces an extra acceleration on coupled particles in the direction of their velocity, and the system responds to this increase in kinetic energy by a small expansion and corresponding lowering of the concentration in order to maintain an equilibrium configuration. The decrease of the mass of the cold dark matter particles with time similarly causes the potential energy of the halo to decrease, also moving the system to a configuration with excess kinetic energy. However, it is indeed the 'anti-friction' term which is the dominant effect, as can be numerically verified be individually switching off either contribution, and comparing the resulting density contrasts.

The combination of these results shows that indeed coupled dark energy models are viable cosmological theories. For one specific class of these models, an inverse power law quintessence with a constant coupling, we have shown here explicitely that models with $\beta \lesssim 0.8$ are compatible with current CMB data, large scale structure observations, and SnIa survey results. Furthermore, the numerical study of the non-linear regime has shown that the properties of dark matter halos in these models could actually alleviate present tensions between observations and the ΛCDM model.

Indeed, the formalism that we have employed and the numerical implementation that we have developed allow to investigate a very large class of coupled dark energy models, since both the dark energy model and the form of the coupling can be freely specified; this provides the complete numerical framework necessary to exploit the ever increasing amount of observational data for studies of the cosmological dark sector.

7 Growing Neutrino Quintessence

In the last chapter, we have considered the ramifications of a coupling between the dark energy component and the dark matter. The coupling strength of the models we considered was generally weaker than gravity. Now, we turn to a class of models where this coupling can be considerably stronger, i.e. stronger than gravity. As we will see, these models, proposed by Amendola et al. (2008) and Wetterich (2007), then can provide a solution of the 'why now?' problem; this proposed solution is particularly compelling when instead of the mass of the dark matter it is the mass of the neutrinos that changes as a function of the scalar field. In this chapter, we will therefore extend the analytical and numerical treatment of dark energy couplings to dark energy - neutrino couplings, and then, as the main objective of this chapter, explore how linear density perturbations will behave in this kind of scenario.

The idea that cosmic acceleration might be related to neutrinos with a varying mass has been previously investigated in the literature (Fardon et al. 2004; Peccei 2005) in the 'MaVaN' scenarios; here, the slow variation of the dark energy density can be achieved without an extremely flat potential for the scalar field, but for many choices of scalar-neutrino coupling and scalar field potentials these scenarios suffer from instabilities (Afshordi et al. 2005), where the attractive force between neutrinos leads to the formation of neutrino 'nuggets', so that the combined fluid behaves like dark matter and is not a viable dark energy candidate any more; there are, however, viable regions of parameter space (Bjaelde et al. 2008). Also, the cosmology of models with neutrinos coupled to a light scalar field has been investigated in the literature (Brookfield et al. 2006b,a; Bi et al. 2005), considering scenarios where the neutrinos are heavier in the past and become lighter during the cosmological evolution, opposite from the case considered here.

7.1 The Model

The cornerstone the growing neutrino quintessence scenario is a neutrino mass that depends on the scalar field ϕ (in units of $M_{\rm P}$) responsible for the dark energy. Here, we consider the specific case of

$$m_\nu = \tilde{m}_\nu e^{-\tilde{\beta}(\phi)\phi}, \tag{7.1}$$

with a constant $\tilde{m}_\nu$. Defining $\beta(\phi) \equiv \tilde{\beta} + \partial\tilde{\beta}/\partial \ln\phi$, the change of m_ν is given by

$$\beta(\phi) = -\frac{\mathrm{d}\ln m_\nu(\phi)}{\mathrm{d}\phi}. \tag{7.2}$$

If $\beta < 0$ and ϕ, the neutrino mass will increase with time, so that with a neutrino mass today of $m_\nu(t_0) < 2.3\,\mathrm{eV}$, the mass will have been even smaller in the past. From the field equation for the field ϕ and its potential $V(\phi)$,

$$\phi'' + 2\mathcal{H}\phi' = -a^2\frac{\mathrm{d}U}{\mathrm{d}\phi} + a^2\beta(\phi)(\rho_\nu - 3p_\nu), \tag{7.3}$$

we immediately see that once the neutrinos become non-relativistic, the derivative of the potential can be balanced by the contribution from the β-dependent term. Hence, depending on the size of the coupling, the evolution of the field ϕ will effectively be stopped at a certain point in time; from then on, the scalar field potential $V(\phi)$ will contribute an (almost) constant fraction to the total energy density, just like a cosmological constant, causing the crossover to the dark energy dominated epoch. The point in time at which this crossover happens is thus given by the (particle physics) properties of neutrinos and the variation of their mass, and the crossover is triggered by the neutrinos becoming non-relativistic; together, this provides a very intriguing explanation of the 'why now' problem.

The 'force' that stops the evolution of the cosmon field can, in principle, be provided something other than neutrinos - any additional dark matter component with a mass increasing with time (with an energy density at some initial time suitably chosen). This has been discussed by Huey & Wandelt (2006); the identification of the 'growing matter' component with neutrinos, however, has the distinct advantage of not introducing any new particles, and the existence of a cosmological trigger for the transition, namely the neutrinos becoming non-relativistic.

As we had seen in Chapter 2, the background energy and pressure of the neutrinos, which follow a Fermi-Dirac distribution f_0, are given by the phase space integral, usually expressed in terms of the comoving 3-momentum $\mathbf{q} = a\mathbf{p} = q\hat{\mathbf{n}}$ as

$$\rho_\nu = a^{-4}\int q^2 dq\, d\Omega\, \epsilon(\phi) f_0(q), \tag{7.4}$$

$$p_\nu = \frac{1}{3}a^{-4}\int q^2 dq\, d\Omega\, \frac{q^2}{\epsilon(\phi)} f_0(q). \tag{7.5}$$

where $\epsilon = \epsilon(\phi) = \sqrt{q^2 + a^2 m_\nu(\phi)^2}$, which is $a(\tau)$ times the proper energy density measured by a comoving observer. In contrast to the uncoupled case, where m_ν is a constant, ϵ now depends on the cosmon field value ϕ due to the coupling between dark energy and neutrinos. Together with Eq. (7.3), these equations specify the background evolution for the coupled neutrino-dark energy system. In terms of energy densities, we can also write

$$\begin{aligned} \rho_\phi' &= -3\mathcal{H}(1+w_\phi)\rho_\phi + \beta(\phi)\phi'(1-3w_\nu)\rho_\nu, \\ \rho_\nu' &= -3\mathcal{H}(1+w_\nu)\rho_\nu - \beta(\phi)\phi'(1-3w_\nu)\rho_\nu, \end{aligned} \tag{7.6}$$

once $w_\nu = p/\rho$ is known from Eq. (7.4).

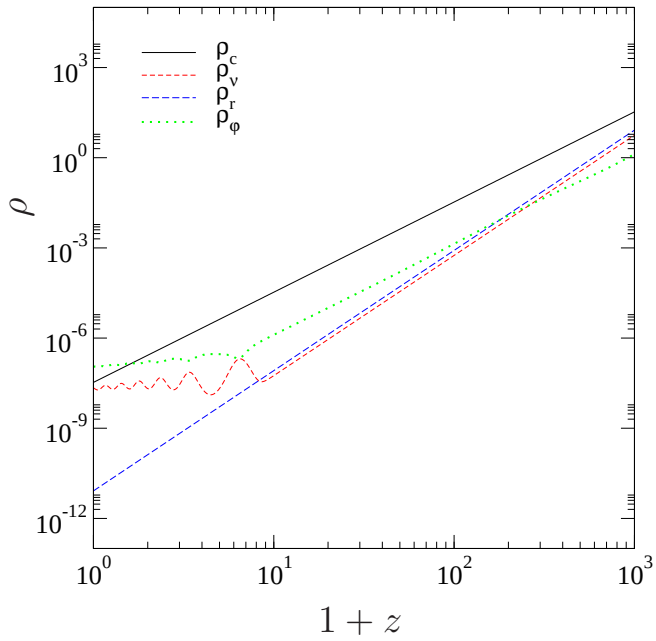

Figure 7.1: Example of the evolution of the background densities in the growing neutrino quintessence model as a function of redshift. The dashed line depicts the evolution of the neutrinos, cold dark matter is shown as a solid line, dark energy as a dotted and the energy density of photon as long dashed lines. The coupling has a value of $\beta = -52$, with $\alpha = 10$ and a neutrino mass of $m_\nu = 2.11\,eV$.

To completely describe the growing neutrino quintessence model, we assume the potential of the scalar field to be given by an exponential,

$$V(\phi) = M_{\rm P}^2 U(\phi) = M_{\rm P}^4 e^{-\alpha\phi}. \tag{7.7}$$

If we set the coupling to be constant, $\beta(\phi) = \text{const}$, then the model is described by only two parameters, the potential constant α, and the coupling strength β. In particular, at early times, while the neutrinos are still relativistic, the cosmology will be a typical early dark energy cosmology that we have discussed in Chapter 4, with the fraction of early dark energy determined by the value of α.

For concreteness, we choose example values for the constants of the theory, $\beta = -52$, $\alpha = 10$ and a rather large neutrino mass of $m_\nu = 2.11\,\text{eV}$, and compute the evolution of the background densities; the result is shown in Fig. 7.1. The effect of the neutrino coupling is evident, leading to a sudden transition from the early dark energy (tracking) behavior of the exponential potential, when neutrinos are still relativistic and almost massless, to the present phase with a dominating dark energy component, and the neutrino and dark energy components having almost constant energy densities. The time after the transition is characterized by oscillations in the coupled dark energy-neutrino fluid that decay with time. The figure does not extend into the future, which in this model is governed by an attractor solution where the scalar field and the mas-

sive neutrinos dominate; the currently observed values of the matter and dark energy densities correspond to the transition epoch from matter to scalar field domination (Amendola et al. 2008).

7.2 Linear Perturbations

Our aim in this chapter is the computation of the evolution of the linear density perturbations in this class of models. In order to obtain the first-order corrections to Eq. (7.4), one starts from the phase space distribution f, written as the zeroth-order term f_0 and the perturbation Ψ_{ps},

$$f(x^i, \tau, q, n_j) = f_0(q) \left[1 + \Psi_{ps}(x^i, \tau, q, n_j)\right]. \tag{7.8}$$

As we have done in Chapter 3, we then have to calculate how this distribution evolves in time, i.e. we have to solve the collisionless Boltzmann equation for the coupled neutrinos, which gives $\mathrm{d}f(x^i, \tau, q, n_j)/\mathrm{d}\tau$ (see e.g. Ma & Bertschinger 1995), but modified to account for the coupling and the changing neutrino mass. The full derivation of the Boltzmann equations is presented by Ichiki & Keum (2008) and Brookfield et al. (2006a); note that the equations are written in the synchronous gauge there, in contrast to the Newtonian gauge employed here. In the Newtonian gauge, the result is:

$$\begin{aligned} \frac{\partial \Psi_{ps}}{\partial \tau} &+ i\frac{q}{\epsilon}(\mathbf{k}\cdot\mathbf{n})\Psi_{ps} + \frac{d\ln f_0}{d\ln q}\left[-\mathbf{\Phi}' - i\frac{\epsilon}{q}(\mathbf{k}\cdot\mathbf{n})\mathbf{\Psi}\right] \\ &= i\frac{q}{\epsilon}(\mathbf{k}\cdot\mathbf{n})k\frac{a^2 m_\nu^2}{q^2}\frac{\partial \ln m_\nu}{\partial \phi}\frac{d\ln f_0}{d\ln q}\delta\phi. \end{aligned} \tag{7.9}$$

As usual, $\mathbf{\Psi}$ and $\mathbf{\Phi}$ are the metric perturbations - all the differences to the standard case of uncoupled neutrinos, i.e. Eq. (3.66), are contained in the right hand side of this equation (which for zero coupling vanishes, as we have seen in Section 3.3).

The perturbation Ψ_{ps} is now expanded in a Legendre series, exactly as for uncoupled neutrinos,

$$\Psi_{ps} = \sum_{l=0}^{\infty}(-i)^l(2l+1)\Psi_{ps,l}P_l(\mathbf{k}\cdot\mathbf{n}) \tag{7.10}$$

with Legendre Polynomials P_l. This then yields, in Newtonian gauge,

$$\begin{aligned} \Psi'_{ps,0} &= -\frac{qk}{\epsilon}\Psi_{ps,1} + \mathbf{\Phi}'\frac{d\ln f_0}{d\ln q}, \qquad (7.11)\\ \Psi'_{ps,1} &= \frac{qk}{3\epsilon}(\Psi_{ps,0} - 2\Psi_{ps,2}) - \frac{\epsilon k}{3q}\mathbf{\Psi}\frac{d\ln f_0}{d\ln q} + \kappa, \\ \Psi'_{ps,l} &= \frac{qk}{(2l+1)\epsilon}\left[l\Psi_{ps,l-1} - (l+1)\Psi_{ps,l+1}\right] \ , \ l \geq 2, \end{aligned}$$

where

$$\kappa = -\frac{1}{3}\frac{q}{\epsilon}k\frac{a^2 m_\nu^2}{q^2}\frac{\partial \ln m_\nu}{\partial \phi}\frac{d\ln f_0}{d\ln q}\delta\phi. \tag{7.12}$$

This term only appears in the expression for $\Psi'_{ps,1}$ which is the only one that is modified by the presence of the coupling, as can be seen from comparing with Eq. (3.73).

The quantities that we are interested in here, the perturbed energy and pressure as well as the velocity perturbation are also changed, and their expressions (and the neutrino shear) are then:

$$\begin{aligned}
\delta\rho_\nu &= 4\pi a^{-4}\int q^2 f_0(q)\left[\epsilon(\phi)\Psi_{ps,0} + \frac{\partial\epsilon}{\partial\phi}\delta\phi\right]dq \\
\delta p_\nu &= \frac{4\pi}{3}a^{-4}\int \frac{q^4}{\epsilon^2} f_0(q)\left[\epsilon\Psi_{ps,0} - \frac{\partial\epsilon}{\partial\phi}\delta\phi\right]dq \\
(\rho_\nu + p_\nu)\theta_\nu &= 4\pi k a^{-4}\int q^2 dq \frac{q^2}{\epsilon} f_0(q)\Psi_{ps,1} \qquad (7.13)\\
(\rho_\nu + p_\nu)\sigma_\nu &= \frac{8\pi}{3}a^{-4}\int q^2 dq \frac{q^2}{\epsilon} f_0(q)\Psi_{ps,2} \qquad (7.14)
\end{aligned}$$

The term $\partial\epsilon/\partial\phi$ is explicitely given by

$$\frac{\partial\epsilon}{\partial\phi} = \frac{a^2 m_\nu^2}{\epsilon}\frac{\partial \ln m_\nu}{\partial\phi} = -\beta(\phi)\frac{a^2 m_\nu^2(\phi)}{\epsilon(\phi)} \qquad (7.15)$$

With all the changes to the neutrino evolution induced by the coupling at hand, the only missing piece is the perturbed version of the Klein-Gordon equation Eq. (7.3),

$$\begin{aligned}
\delta\phi'' &+ 2\mathcal{H}\delta\phi' + \left(k^2 + a^2\frac{d^2U}{d\phi^2}\right)\delta\phi - \phi'(\mathbf{\Psi}' - 3\mathbf{\Phi}') + 2a^2\frac{dU}{d\phi}\mathbf{\Psi} \qquad (7.16)\\
&= -a^2\left[-\beta(\phi)\rho_\nu\delta_\nu(1-3c_\nu^2) - \frac{d\beta(\phi)}{d\phi}\delta\phi\rho_\nu(1-3w_\nu) - 2\beta(\phi)(\rho_\nu - 3p_\nu)\mathbf{\Psi}\right],
\end{aligned}$$

which determines the evolution of the perturbations of the scalar field. This completes the set of perturbation equations for coupled neutrinos - the perturbations for all other components are only affected through the gravitational potential, and so their equations (and their respective numerical implementations) remain identical to the uncoupled case.

7.3 Neutrino Clustering

After implementing the equations of the previous section in CMBEASY, we can now compute the perturbations of density perturbations; to demonstrate the behavior in a specific case, we compute the linear perturbations for our example model of Section 7.1, with $\beta = -52$, $\alpha = 10$ and $m_\nu = 2.11\,\mathrm{eV}$. The amplitude of the initial fluctuations is determined from the CMB anisotropies at $z_{ls} \sim 1000$.

The resulting density perturbations for two wavemodes are shown in Fig. 7.2 ($k = 0.1h/\mathrm{Mpc}$) and in Fig. 7.3 ($k = 1.1h/Mpc$). As we can see, as soon as the neutrinos become non-relativistic and their equation of state departs from the radiation value of $w_\nu = 1/3$, the neutrino perturbations start to increase, and

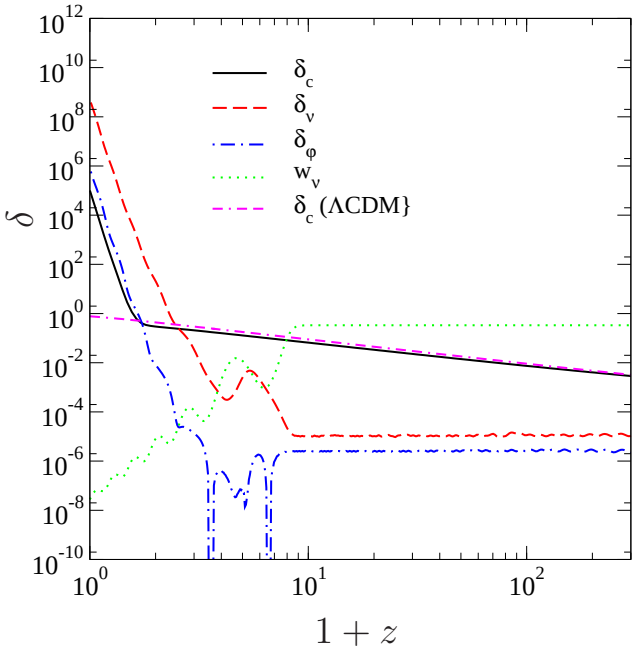

Figure 7.2: Evolution of the longitudinal density perturbations for CDM (solid), neutrinos (dashed) and the scalar field dark energy (dot-dashed) for $k = 0.1h/\mathrm{Mpc}$. The neutrino equation of state (dotted) is also shown, as well as the evolution of the cold dark matter perturbations in the reference ΛCDM model.

eventually even grow larger than the perturbations in cold dark matter. The dark energy perturbations also grow strongly - and can even overtake the dark matter perturbations in the linear approximation.

It is, however, clear, that as soon as the size of any of the perturbations reaches unity, the linear perturbation theory will no longer be able to yield reliable results, and can only give a qualitative picture of the true physics. What can be learned from the linear analysis, though, is an estimate of the time at which nonlinearities become important, and how this point in time depends on the scale. Particularly intriguing is the comparison with the standard ΛCDM-picture in Fig. 7.2. On these large scales, the scales of superclusters, the density perturbations in a ΛCDM-universe are still in the linear regime today, while in our example growing neutrino model, the perturbations quickly become nonlinear as soon as the neutrinos are no longer relativistic. Despite the relatively low fraction of neutrinos, Ω_ν, the strong neutrino clumping quickly becomes the main source of the gravitational potential, which then drags the cold dark matter fluctuations. At the same time, the large neutrino fluctuations also cause the inhomogeneities in the cosmon field to grow through their strong coupling. The corresponding growth of the gravitational potential for different scales is shown in Fig. 7.5.

In the nonlinear regime, once our linear approximation presented here is no longer valid, one would expect the neutrino structures to decouple from the expansion of the background, eventually forming stable 'neutrino lumps', like

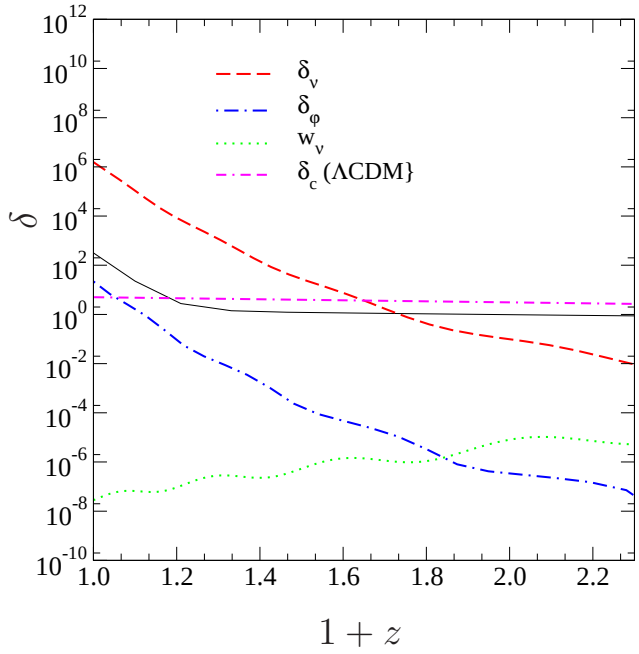

Figure 7.3: Same as Fig. 7.2 but for a scale of $k = 1.1h/Mpc$ - evolution of the longitudinal density perturbations.

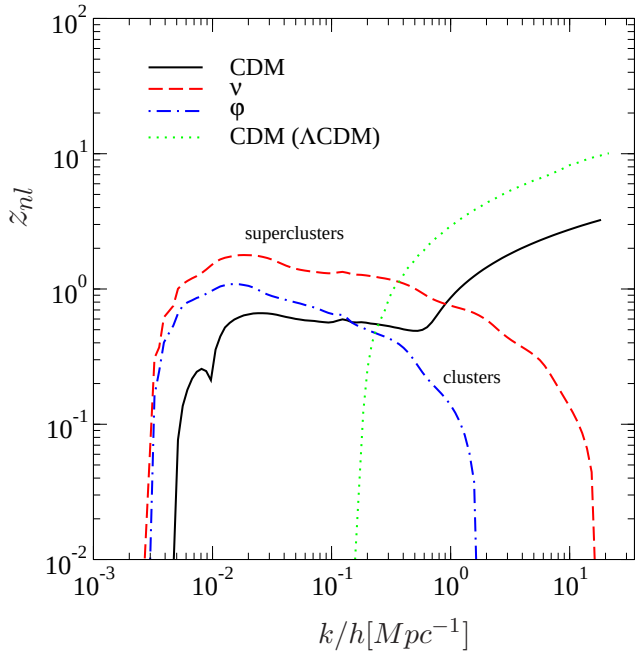

Figure 7.4: Redshift of first non-linearities as a function of the wavenumber k for cold dark matter (solid), neutrinos (dashed) and the scalar field dark energy (dot-dashed). A reference ΛCDM- model is shown as the dotted line.

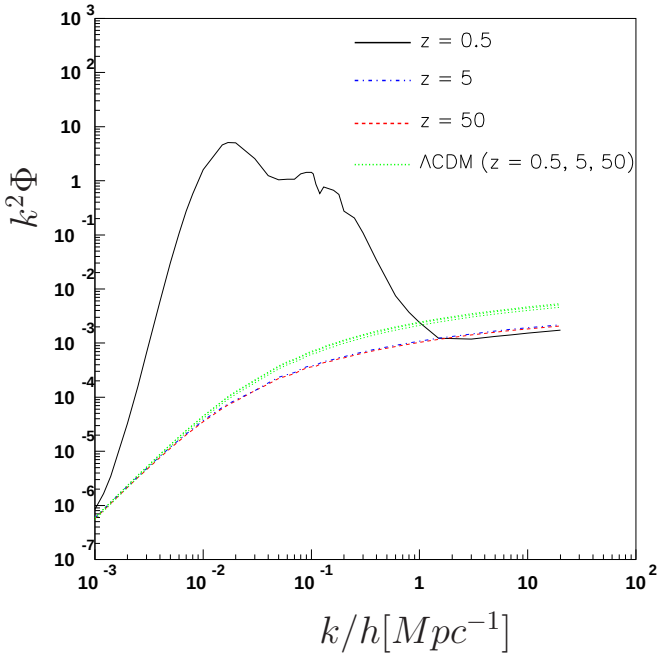

Figure 7.5: The gravitational potential in longitudinal gauge as a function of the wavenumber k for a reference ΛCDM model (dotted), and for the coupled neutrino model at redshifts $z = 0.5$ (solid), $z = 5$ (dot-dashed), $z = 50$ (dashed) (the lines for the latter two redshifts overlap). For high values of Φ, this plot does not show the true physical gravitational potential, as it is the result of a computation of only linear perturbations.

the solutions presented by Brouzakis et al. (2008). Inside these neutrino lumps, the gravitational potential would be much smaller than the huge value of the linear approximation in our example. A detailed understanding of the nonlinear regime would also allow to estimate the effect of these structures on the CMB through the integrated Sachs-Wolfe effect. Since the nonlinear regime of structure formation in this scenario is reached much earlier than in the standard ΛCDM scenario, and even on very large scales, linear perturbation theory is not any more sufficient to predict the power spectrum of the Cosmic Microwave Background, or even the matter power spectra today.

As we have seen, the linear picture is nevertheless useful for a qualitative understanding of the physical mechanisms. Fig. 7.4 shows, as a function of wavenumber k, the redshift z_{nl} at which the density perturbations of the different components become nonlinear. For comparison, the plot also shows the behavior of δ_{cdm} in a concordance ΛCDM-model, with a corresponding Ω_Λ and massless neutrinos. We define z_{nl} as the redshift at which $\delta(z_{nl}) = 1$ for the respective species. It is therefore a rough measure of the time when the first nonlinearities appear. As we are using linear perturbation theory, only the highest curve for any given k is reliable, since the lower curves are already affected by the dragging of the leading component, and in a complete nonlinear treatment, these dragging effects would be expected to be considerably lower. Fig. 7.4 shows that at the very largest scales, the universe is still almost homogeneous, and the

perturbations remain linear, even in our example growing neutrino model. On scales from about 4.4×10^3 Mpc down to 14.5 Mpc, however, we find a behavior that is very different from the concordance ΛCDM expectation, where the neutrino perturbations leave the linear regime, and possibly form large structures whose gravitational potential well will enhance the clustering of the other cosmological components, including even the scalar field. As we approach the neutrino free streaming scale, the first component leaving the linear regime is no longer the neutrinos, but the cold dark matter. It is interesting to remark that we see less clustering of cold dark matter in this regime in our growing neutrino model than in the ΛCDM case. This is in fact expected, since as we have seen in Chapter 4, the presence of early dark energy in the growing neutrino model will slow the clustering. Additionally, as we have chosen $\Omega_\Lambda = \Omega_\phi$, there is less matter in our growing neutrino model than in the reference ΛCDM model, since the massive neutrinos contribute a certain fraction to the total energy density today, unlike the massless neutrinos in the ΛCDM model - for smaller and smaller neutrino masses, this effect of course becomes correspondingly smaller, whereas the influence of the early dark energy depends on the choice of α. At small scales, finally, we find the usual pictures with the cold dark matter already in the nonlinear regime also for the ΛCDM case, and no clustering of neutrinos, as they are in the free streaming regime.

To summarize our results, we have shown that in the growing neutrino quintessence scenarios, one typically expects neutrino clustering on supercluster scales; this is a prediction of a feature that is very distinct from the concordance ΛCDM paradigm, and the observation of structures on these very large (supercluster) scales would be a strong hint in favor of the scenario outlined here. When considered together with the results that we had obtained in the last chapter, we can conclude that quintessence models with a coupling to other species can lead to vastly different cosmological evolutions, and that further investigation of this property of the dark energy continues to be a promising route towards revealing the true nature of quintessence.

8 Conclusions

In this thesis, we have studied the cosmological implications of a variety of dark energy models, in search of the fundamental properties of quintessence. Having surveyed the basics of the framework and the methodology of modern cosmology, we commenced our investigation in Chapter 4, by considering early dark energy models. In these class of models, the dark energy can contribute a substantial fraction to the total energy density even at high redshifts, before last scattering and during structure formation - unlike in the standard ΛCDM scenario, where the contribution from the cosmological constant is negligible at early times. We considered a variety of dark energy models and parameterizations, and compared the inferred values for the cosmological parameters between early dark energy models, models with a fading dark energy, and the ΛCDM cosmology.

As the central result, we found that current observational data constrain the amount of early dark energy to a few percent. We found that the inclusion of Ly-α data, or more precisely, the linear matter power spectrum inferred from observations of the Ly-α-forest in the Sloan Digital Sky Survey, yields an upper bound of $\bar{\Omega}^d_{\rm sf} \lesssim 1.7\%$ when the early dark energy is described by the $\Omega(w_0, \Omega^e_d)$ parameterization; without the Ly-α-data we found an upper bound of $\bar{\Omega}^d_{\rm sf} \lesssim 4\%$, from a combination of observational data comprising several sets of CMB data, large scale structure and SnIa surveys.

We also showed examples of early dark energy models that reproduce the spectra of fading dark energy models, showing that early dark energy cannot unambiguously be detected by measurements of the CMB temperature and E-mode polarization alone. We then pointed out that future BAO measurements, when the 'standard ruler' is calibrated off the measured CMB, have to properly account for the possibility of an early dark energy component. This can either be done by relying on a determination of the early dark energy fraction from some other, independent, source, or by introducing a calibration factor and thereby fitting for the absolute ruler scale. This will decrease the power of future BAO measurements (for a hypothetical future experiment, we found that the area of the confidence regions increased by a factor of ~ 2.3). Neglecting the possibility of early dark energy, however, would lead to a severe misinterpretation of the data, and the inferred values of the cosmological parameters would be biased.

In Chapter 5, we then considered a scalar field dark energy model with an exponential potential, which has an early dark energy component, and the *Cuscuton* model. While Cuscuton models are formulated as scalar field dark energy models, they actually reduce to a pure constraint system; Cuscuton perturbations do not introduce an additional dynamical degree of freedom, and effectively amount to a minimal modification of a cosmological constant. This motivated us to interpret both models as a modification of the law of gravity on large scales; we expressed this modification in terms of a running of the Planck Mass

at the cosmological horizon scale. Our main conclusion was that cosmological observations yield an upper bound for this kind of 'glitch' in the Planck Mass of 1.2% (at 95% confidence), severely restricting possible deviations from Einstein gravity at these scales.

We then studied coupled dark energy models. In these models, either the mass of the dark matter or e.g. of the neutrinos depends on the scalar field. In Chapter 6 we have presented the general formalism that allows to specify the form of the coupling as an arbitrary function of the field, independent of the dark energy model. We have implemented this formalism in CMBEASY, and as an example application, explored a set of coupled dark energy models with an inverse power law potential; for these models, we showed that observational data constrains the coupling strength to $\beta \lesssim 0.08$ (at 95% confidence).

We have also modified CMBEASY to produce input data for N-body simulations for coupled dark energy models. We have reviewed the results from a set of N-body simulations that were obtained using our computations in the linear regime as input. These simulations found that a larger coupling strength leads to a lower average halo concentration. Also, the baryon fraction as well as the inner overdensity of cold dark matter halos decreased with increasing coupling. These results show that coupled dark energy models are viable cosmological models, and might even alleviate present tensions between the ΛCDM model and observations.

We then extended our investigations of dark energy couplings to the growing neutrino quintessence scenario. Here, the coupling must be somewhat larger than gravitational strength, in order to effectively stop the evolution of the scalar field. We saw that these models lead to a substantial neutrino clustering on large scales, typically the scale of superclusters, a feature very distinct from the standard ΛCDM cosmology.

Since non-linear neutrino lumps in this scenario are expected to form at a redshift of about $z \approx 1$, our linear analysis does not apply to the very recent history of the universe. A full exploration of the non-linear regime is therefore necessary already to consistently compute the power spectra of the Cosmic Microwave Background; such an investigation could also reveal more intriguing features of these cosmological scenarios. Certainly, the detection of non-linear structures at these very large scales would be an important indication for a new attractive force - mediated by the cosmon.

In summary, all the dark energy scenarios that we have considered are significantly different from the 'concordance' model of cosmology, the ΛCDM universe. We have seen that these different quintessence models, with fundamentally different properties, are in agreement with observations, and that observational data is not yet precise enough to distinguish between these different alternatives. However, we have also seen that the many quintessence models do make characteristic predictions, some of which are quite surprising and intriguing; in combination with the continuing increase in the amount and precision of observational data, this variety in the phenomenology of quintessence is good reason to remain hopeful and confident that the puzzle of dark energy will be solved.

Bibliography

Acquaviva, V. & Baccigalupi, C. 2006, "Dark energy records in lensed cosmic microwave background", Phys. Rev., D74, 103510, arXiv:astro-ph/0507644

Adams, A., Arkani-Hamed, N., Dubovsky, S., Nicolis, A., & Rattazzi, R. 2006, "Causality, analyticity and an IR obstruction to UV completion", JHEP, 10, 014, arXiv:hep-th/0602178

Adelberger, E. G., Heckel, B. R., & Nelson, A. E. 2003, "Tests of the gravitational inverse-square law", Ann. Rev. Nucl. Part. Sci., 53, 77, arXiv:hep-ph/0307284

Afshordi, N., Chung, D. J. H., Doran, M., & Geshnizjani, G. 2007a, "Cuscuton Cosmology: Dark Energy meets Modified Gravity", Phys. Rev., D75, 123509, arXiv:astro-ph/0702002

Afshordi, N., Chung, D. J. H., & Geshnizjani, G. 2007b, "Cuscuton: A Causal Field Theory with an Infinite Speed of Sound", Phys. Rev., D75, 083513, arXiv:hep-th/0609150

Afshordi, N., Lin, Y.-T., Nagai, D., & Sanderson, A. J. R. 2007c, "Missing Thermal Energy of the Intracluster Medium", Mon. Not. Roy. Astron. Soc., 378, 293, arXiv:astro-ph/0612700

Afshordi, N., Zaldarriaga, M., & Kohri, K. 2005, "On the stability of dark energy with mass-varying neutrinos", Phys. Rev., D72, 065024, arXiv:astro-ph/0506663

Albrecht, A. J. & Skordis, C. 2000, "Phenomenology of a realistic accelerating universe using only Planck-scale physics", Phys. Rev. Lett., 84, 2076, arXiv:astro-ph/9908085

Aldering, G. et al. 2002, "Overview of the SuperNova / Acceleration Probe (SNAP)", arXiv:astro-ph/0209550

Amara, A. & Refregier, A. 2007, "Optimal Surveys for Weak Lensing Tomography", Mon. Not. Roy. Astron. Soc., 381, 1018, arXiv:astro-ph/0610127

Amendola, L. 2000, "Coupled quintessence", Phys. Rev., D62, 043511, arXiv:astro-ph/9908023

Amendola, L. 2001, "Dark energy and the Boomerang data", Phys. Rev. Lett., 86, 196, arXiv:astro-ph/0006300

Amendola, L. 2004, "Linear and non-linear perturbations in dark energy models", Phys. Rev., D69, 103524, arXiv:astro-ph/0311175

Amendola, L., Baldi, M., & Wetterich, C. 2008, "Growing Matter", Phys. Rev., D78, 023015, arXiv:0706.3064 [astro-ph]

Amendola, L. & Quercellini, C. 2004, "Skewness as a test of the equivalence principle", Phys. Rev. Lett., 92, 181102, arXiv:astro-ph/0403019

Amendola, L. & Tocchini-Valentini, D. 2002, "Baryon bias and structure formation in an accelerating universe", Phys. Rev., D66, 043528, arXiv:astro-ph/0111535

Anderson, G. W. & Carroll, S. M. 1997, "Dark matter with time-dependent mass", arXiv:astro-ph/9711288

Armendariz-Picon, C., Mukhanov, V. F., & Steinhardt, P. J. 2000, "A dynamical solution to the problem of a small cosmological constant and late-time cosmic acceleration", Phys. Rev. Lett., 85, 4438, arXiv:astro-ph/0004134

Armendariz-Picon, C., Mukhanov, V. F., & Steinhardt, P. J. 2001, "Essentials of k-essence", Phys. Rev., D63, 103510, arXiv:astro-ph/0006373

Astier, P. et al. 2005, "The Supernova Legacy Survey: Measurement of Omega_M, Omega_Lambda and w from the First Year Data Set", arXiv:astro-ph/0510447

Babichev, E., Mukhanov, V., & Vikman, A. 2008, "k-Essence, superluminal propagation, causality and emergent geometry", JHEP, 02, 101, arXiv:0708.0561 [hep-th]

Bahcall, N. A., Lubin, L. M., & Dorman, V. 1995, "Where is the dark matter?", Astrophys. J., 447, L81, arXiv:astro-ph/9506041

Baldi, M. 2009, "N-body simulations of coupled dark energy cosmologies", PhD thesis, Ludwig-Maximilians-Universität München

Baldi, M., Pettorino, V., Robbers, G., & Springel, V. 2008, "N-body simulations of coupled dark energy cosmologies"

Bardeen, J. M. 1980, "Gauge Invariant Cosmological Perturbations", Phys. Rev., D22, 1882

Bartelmann, M., Doran, M., & Wetterich, C. 2006, "Non-linear Structure Formation in Cosmologies with Early Dark Energy", Astron. Astrophys., 454, 27, arXiv:astro-ph/0507257

Bassett, B. A., Kunz, M., Silk, J., & Ungarelli, C. 2002, "A late-time transition in the cosmic dark energy?", Mon. Not. Roy. Astron. Soc., 336, 1217, arXiv:astro-ph/0203383

Bassett, B. A., Nichol, R. C., & Eisenstein, D. J. 2005, "WFMOS: Sounding the dark cosmos", arXiv:astro-ph/0510272

Bean, R. & Dore, O. 2004, "Probing dark energy perturbations: the dark energy equation of state and speed of sound as measured by WMAP", Phys. Rev., D69, 083503, arXiv:astro-ph/0307100

Bean, R., Flanagan, E. E., Laszlo, I., & Trodden, M. 2008, "Constraining Interactions in Cosmology's Dark Sector", arXiv:0808.1105 [astro-ph]

Bertolami, O., Gil Pedro, F., & Le Delliou, M. 2007, "Dark Energy-Dark Matter Interaction and the Violation of the Equivalence Principle from the Abell Cluster A586", Phys. Lett., B654, 165, arXiv:astro-ph/0703462

Bi, X.-J., Feng, B., Li, H., & min Zhang, X. 2005, "Cosmological evolution of interacting dark energy models with mass varying neutrinos", Phys. Rev., D72, 123523, arXiv:hep-ph/0412002

Binetruy, P. 1999, "Models of dynamical supersymmetry breaking and quintessence", Phys. Rev., D60, 063502, arXiv:hep-ph/9810553

Bjaelde, O. E. et al. 2008, "Neutrino Dark Energy – Revisiting the Stability Issue", JCAP, 0801, 026, arXiv:0705.2018 [astro-ph]

Bonvin, C., Caprini, C., & Durrer, R. 2006, "A no-go theorem for k-essence dark energy", Phys. Rev. Lett., 97, 081303, arXiv:astro-ph/0606584

Brookfield, A. W., van de Bruck, C., & Hall, L. M. H. 2008, "New interactions in the dark sector mediated by dark energy", Phys. Rev., D77, 043006, arXiv:0709.2297 [astro-ph]

Brookfield, A. W., van de Bruck, C., Mota, D. F., & Tocchini-Valentini, D. 2006a, "Cosmology of mass-varying neutrinos driven by quintessence: Theory and observations", Phys. Rev., D73, 083515, arXiv:astro-ph/0512367

Brookfield, A. W., van de Bruck, C., Mota, D. F., & Tocchini-Valentini, D. 2006b, "Cosmology with massive neutrinos coupled to dark energy", Phys. Rev. Lett., 96, 061301, arXiv:astro-ph/0503349

Brouzakis, N., Tetradis, N., & Wetterich, C. 2008, "Neutrino Lumps in Quintessence Cosmology", Phys. Lett., B665, 131, arXiv:0711.2226 [astro-ph]

Bruneton, J.-P. 2007, "On causality and superluminal behavior in classical field theories. Applications to k-essence theories and MOND-like theories of gravity", Phys. Rev., D75, 085013, arXiv:gr-qc/0607055

Caldwell, R. R., Dave, R., & Steinhardt, P. J. 1998, "Cosmological Imprint of an Energy Component with General Equation-of-State", Phys. Rev. Lett., 80, 1582, arXiv:astro-ph/9708069

Caldwell, R. R. & Doran, M. 2005, "Dark-energy evolution across the cosmological-constant boundary", Phys. Rev., D72, 043527, arXiv:astro-ph/0501104

Caldwell, R. R., Doran, M., Mueller, C. M., Schaefer, G., & Wetterich, C. 2003, "Early quintessence in light of WMAP", Astrophys. J., 591, L75, arXiv:astro-ph/0302505

Carroll, S. M. & Lim, E. A. 2004, "Lorentz-violating vector fields slow the universe down", Phys. Rev., D70, 123525, arXiv:hep-th/0407149

Carroll, S. M., Mantry, S., & Ramsey-Musolf, M. J. 2009, "Implications of a Scalar Dark Force for Terrestrial Experiments", arXiv:0902.4461 [hep-ph]

Chevallier, M. & Polarski, D. 2001, "Accelerating universes with scaling dark matter", Int. J. Mod. Phys., D10, 213, arXiv:gr-qc/0009008

Chiba, T., Okabe, T., & Yamaguchi, M. 2000, "Kinetically driven quintessence", Phys. Rev., D62, 023511, arXiv:astro-ph/9912463

Clifton, T., Mota, D. F., & Barrow, J. D. 2005, "Inhomogeneous gravity", Mon. Not. Roy. Astron. Soc., 358, 601, arXiv:gr-qc/0406001

Copeland, E. J., Liddle, A. R., & Wands, D. 1998, "Exponential potentials and cosmological scaling solutions", Phys. Rev., D57, 4686, arXiv:gr-qc/9711068

Copeland, E. J., Sami, M., & Tsujikawa, S. 2006, "Dynamics of dark energy", Int. J. Mod. Phys., D15, 1753, arXiv:hep-th/0603057

Corasaniti, P. S. & Copeland, E. J. 2003, "A model independent approach to the dark energy equation of state", Phys. Rev., D67, 063521, arXiv:astro-ph/0205544

Cyburt, R. H., Fields, B. D., Olive, K. A., & Skillman, E. 2005, "New BBN limits on physics beyond the standard model from He-4", Astropart. Phys., 23, 313, arXiv:astro-ph/0408033

Damour, T., Gibbons, G. W., & Gundlach, C. 1990, "Dark Matter, Time Varying G, and a Dilaton Field", Phys. Rev. Lett., 64, 123

Das, S. & Spergel, D. N. 2008, "Measuring Distance Ratios with CMB-Galaxy Lensing Cross-correlations", Phys. Rev. D 79, 043509 (2009)

de Bernardis, P. et al. 2000, "A Flat Universe from High-Resolution Maps of the Cosmic Microwave Background Radiation", Nature, 404, 955, arXiv:astro-ph/0004404

de Putter, R., Zahn, O., & Linder, E. V. 2009, "CMB Lensing Constraints on Neutrinos and Dark Energy", arXiv:0901.0916 [astro-ph.CO]

Dent, T., Stern, S., & Wetterich, C. 2009, "Time variation of fundamental couplings and dynamical dark energy", JCAP, 0901, 038, arXiv:0809.4628 [hep-ph]

Di Porto, C. & Amendola, L. 2008, "Observational constraints on the linear fluctuation growth rate", Phys. Rev., D77, 083508

Dickinson, C. et al. 2004, "High sensitivity measurements of the CMB power spectrum with the extended Very Small Array", Mon. Not. Roy. Astron. Soc., 353, 732, arXiv:astro-ph/0402498

Dodelson, S. 2003, Modern Cosmology (Academic Press, London)

Doran, M. 2003, "CMBEASY:: an Object Oriented Code for the Cosmic Microwave Background", arXiv:astro-ph/0302138

Doran, M. 2005, "A Primer on Cosmology and the Cosmic Microwave Background", lecture given at the Universität Heidelberg, www.thphys.uni-heidelberg.de/∼doran/cmbeasy/lecture_beta1.ps

Doran, M., Karwan, K., & Wetterich, C. 2005, "Observational constraints on the dark energy density evolution", arXiv:astro-ph/0508132

Doran, M. & Lilley, M. 2002, "The Location of CMB Peaks in a Universe with Dark Energy", Mon. Not. Roy. Astron. Soc., 330, 965, arXiv:astro-ph/0104486

Doran, M. & Müller, C. M. 2004, "Analyze This! A Cosmological Constraint Package for cmbeasy", JCAP, 0409, 003, arXiv:astro-ph/0311311

Doran, M., Muller, C. M., Schafer, G., & Wetterich, C. 2003, "Gauge-invariant initial conditions and early time perturbations in quintessence universes", Phys. Rev., D68, 063505, arXiv:astro-ph/0304212

Doran, M. & Robbers, G. 2006, "Early dark energy cosmologies", JCAP, 0606, 026, arXiv:astro-ph/0601544

Doran, M., Robbers, G., & Wetterich, C. 2007a, "Impact of three years of data from the Wilkinson Microwave Anisotropy Probe on cosmological models with dynamical dark energy", Phys. Rev., D75, 023003, arXiv:astro-ph/0609814

Doran, M., Schwindt, J.-M., & Wetterich, C. 2001, "Structure formation and the time dependence of quintessence", Phys. Rev., D64, 123520, arXiv:astro-ph/0107525

Doran, M., Stern, S., & Thommes, E. 2007b, "Baryon Acoustic Oscillations and Dynamical Dark Energy", JCAP, 0704, 015, arXiv:astro-ph/0609075

Durrer, R. 2008, The Cosmic Microwave Background (Cambridge University Press)

Einstein, A. 1916, "The foundation of the general theory of relativity", Annalen Phys., 49, 769

Eisenstein, D. J. et al. 2005, "Detection of the Baryon Acoustic Peak in the Large-Scale Correlation Function of SDSS Luminous Red Galaxies", Astrophys. J., 633, 560, arXiv:astro-ph/0501171

Erickson, J. K., Caldwell, R. R., Steinhardt, P. J., Armendariz-Picon, C., & Mukhanov, V. F. 2002, "Measuring the speed of sound of quintessence", Phys. Rev. Lett., 88, 121301, arXiv:astro-ph/0112438

Ettori, S., Dolag, K., Borgani, S., & Murante, G. 2006, "The baryon fraction in hydrodynamical simulations of galaxy clusters", Mon. Not. Roy. Astron. Soc., 365, 1021, arXiv:astro-ph/0509024

Fan, X.-H., Carilli, C. L., & Keating, B. G. 2006, "Observational constraints on Cosmic Reionization", Ann. Rev. Astron. Astrophys., 44, 415, arXiv:astro-ph/0602375

Fardon, R., Nelson, A. E., & Weiner, N. 2004, "Dark energy from mass varying neutrinos", JCAP, 0410, 005, arXiv:astro-ph/0309800

Farrar, G. R. & Peebles, P. J. E. 2004, "Interacting Dark Matter and Dark Energy", ApJ, 604, 1, arXiv:arXiv:astro-ph/0307316

Farrar, G. R. & Rosen, R. A. 2007, "A New Force in the Dark Sector?", Physical Review Letters, 98, 171302, arXiv:arXiv:astro-ph/0610298

Fedeli, C. & Bartelmann, M. 2007, "Effects of early dark energy on strong cluster lensing", Astron. Astrophys., 461, 49, arXiv:astro-ph/0607069

Fedeli, C., Moscardini, L., & Bartelmann, M. 2008, "Observing the clustering properties of galaxy clusters in dynamical-dark energy cosmologies", arXiv:0812.1097 [astro-ph]

Ferreira, P. G. & Joyce, M. 1997, "Structure formation with a self-tuning scalar field", Phys. Rev. Lett., 79, 4740, arXiv:astro-ph/9707286

Ferreira, P. G. & Joyce, M. 1998, "Cosmology with a Primordial Scaling Field", Phys. Rev., D58, 023503, arXiv:astro-ph/9711102

Fixsen, D. J. et al. 2009, "ARCADE 2 Measurement of the Extra-Galactic Sky Temperature at 3-90 GHz", arXiv:0901.0555 [astro-ph.CO]

Foster, B. Z. & Jacobson, T. 2006, "Post-Newtonian parameters and constraints on Einstein-aether theory", Phys. Rev., D73, 064015, arXiv:gr-qc/0509083

Francis, M. J., Lewis, G. F., & Linder, E. V. 2008a, "Can Early Dark Energy be Detected in Non-Linear Structure?", arXiv:0808.2840 [astro-ph]

Francis, M. J., Lewis, G. F., & Linder, E. V. 2008b, "Halo Mass Functions in Early Dark Energy Cosmologies", arXiv:0810.0039 [astro-ph]

Frenk, C. S., White, S. D. M., Bode, P., et al. 1999, "The Santa Barbara Cluster Comparison Project: A Comparison of Cosmological Hydrodynamics Solutions", ApJ, 525, 554, arXiv:arXiv:astro-ph/9906160

Frieman, J. A., Hill, C. T., Stebbins, A., & Waga, I. 1995, "Cosmology with ultralight pseudo Nambu-Goldstone bosons", Phys. Rev. Lett., 75, 2077, arXiv:astro-ph/9505060

Garcia-Bellido, J., Linde, A. D., & Linde, D. A. 1994, "Fluctuations of the gravitational constant in the inflationary Brans-Dicke cosmology", Phys. Rev., D50, 730, arXiv:astro-ph/9312039

Gottloeber, S. & Yepes, G. 2007, "Shape, spin and baryon fraction of clusters in the MareNostrum Universe", Astrophys. J., 664, 117, arXiv:astro-ph/0703164

Gromov, A., Baryshev, Y., & Teerikorpi, P. 2004, "Two-fluid matter-quintessence FLRW models: Energy transfer and the equation of state of the universe", Astron. Astrophys., 415, 813, arXiv:astro-ph/0209458

Grossi, M. & Springel, V. 2008, "The impact of Early Dark Energy on non-linear structure formation", arXiv:0809.3404 [astro-ph]

Gubser, S. S. & Peebles, P. J. E. 2004, "Cosmology with a dynamically screened scalar interaction in the dark sector", Phys. Rev. D, 70, 123511, arXiv:arXiv:hep-th/0407097

Guo, Z.-K., Ohta, N., & Tsujikawa, S. 2007, "Probing the Coupling between Dark Components of the Universe", Phys. Rev., D76, 023508, arXiv:astro-ph/0702015

Hebecker, A. & Wetterich, C. 2001, "Natural quintessence?", Phys. Lett., B497, 281, arXiv:hep-ph/0008205

Hinshaw, G. et al. 2007, "Three-year Wilkinson Microwave Anisotropy Probe (WMAP) observations: Temperature analysis", Astrophys. J. Suppl., 170, 288, arXiv:astro-ph/0603451

Hollenstein, L., Sapone, D., Crittenden, R., & Schaefer, B. M. 2009, "Constraints on early dark energy from CMB lensing and weak lensing tomography", arXiv:0902.1494 [astro-ph.CO]

Howell, D. A. et al. 2009, "Type Ia supernova science 2010-2020", arXiv:0903.1086 [astro-ph.SR]

Huey, G. & Wandelt, B. D. 2006, "Interacting quintessence, the coincidence problem and cosmic acceleration", Phys. Rev., D74, 023519, arXiv:astro-ph/0407196

Ichiki, K. & Keum, Y.-Y. 2008, "Primordial Neutrinos, Cosmological Perturbations in Interacting Dark-Energy Model: CMB and LSS", JCAP, 0806, 005, arXiv:0705.2134 [astro-ph]

Jacobson, T. & Mattingly, D. 2001, "Gravity with a dynamical preferred frame", Phys. Rev., D64, 024028, arXiv:gr-qc/0007031

Jenkins, A. et al. 2001, "Mass function of dark matter halos", Mon. Not. Roy. Astron. Soc., 321, 372, arXiv:astro-ph/0005260

Kapner, D. J. et al. 2007, "Tests of the gravitational inverse-square law below the dark-energy length scale", Phys. Rev. Lett., 98, 021101, arXiv:hep-ph/0611184

Kesden, M. & Kamionkowski, M. 2006, "Galilean Equivalence for Galactic Dark Matter", Phys. Rev. Lett., 97, 131303, arXiv:astro-ph/0606566

Kodama, H. & Sasaki, M. 1984, "Cosmological Perturbation Theory", Prog. Theor. Phys. Suppl., 78, 1

Kowalski, M. et al. 2008, "Improved Cosmological Constraints from New, Old and Combined Supernova Datasets", Astrophys. J., 686, 749, arXiv:0804.4142 [astro-ph]

Kuo, C. et al. 2004, "High Resolution Observations of the CMB Power Spectrum with ACBAR", Astrophys. J., 600, 32, arXiv:astro-ph/0212289

LaRoque, S. et al. 2006, "X-ray and Sunyaev-Zel'dovich Effect Measurements of the Gas Mass Fraction in Galaxy Clusters", Astrophys. J., 652, 917, arXiv:astro-ph/0604039

Lee, S., Liu, G.-C., & Ng, K.-W. 2006, "Constraints on the coupled quintessence from cosmic microwave background anisotropy and matter power spectrum", Phys. Rev., D73, 083516, arXiv:astro-ph/0601333

Lewis, A. & Bridle, S. 2002, "Cosmological parameters from CMB and other data: a Monte-Carlo approach", Phys. Rev., D66, 103511, arXiv:astro-ph/0205436

Lewis, A. & Challinor, A. 2006, "Weak Gravitational Lensing of the CMB", Phys. Rept., 429, 1, arXiv:astro-ph/0601594

Lewis, A., Challinor, A., & Lasenby, A. 2000, "Efficient Computation of CMB anisotropies in closed FRW models", Astrophys. J., 538, 473, arXiv:astro-ph/9911177

Linde, A. D. 1990, "Extended Chaotic Inflation and Spatial Variations of the Gravitational Constant", Phys. Lett., B238, 160

Linder, E. V. 2003, "Exploring the expansion history of the universe", Phys. Rev. Lett., 90, 091301, arXiv:astro-ph/0208512

Linder, E. V. 2007, "Theory Challenges of the Accelerating Universe", J. Phys., A40, 6697, arXiv:astro-ph/0610173

Linder, E. V. 2008, "Mapping the Cosmological Expansion", Rept. Prog. Phys., 71, 056901, arXiv:0801.2968 [astro-ph]

Linder, E. V. & Huterer, D. 2005, "How many dark energy parameters?", Phys. Rev., D72, 043509, arXiv:astro-ph/0505330

Linder, E. V. & Robbers, G. 2008, "Shifting the Universe: Early Dark Energy and Standard Rulers", JCAP 0806 (2008) 004

Ma, C.-P. & Bertschinger, E. 1995, "Cosmological perturbation theory in the synchronous and conformal Newtonian gauges", Astrophys. J., 455, 7, arXiv:astro-ph/9506072

Maccio, A. V., Quercellini, C., Mainini, R., Amendola, L., & Bonometto, S. A. 2004, "N-body simulations for coupled dark energy: halo mass function and density profiles", Phys. Rev., D69, 123516, arXiv:astro-ph/0309671

MacTavish, C. J. et al. 2005, "Cosmological parameters from the 2003 flight of BOOMERANG", arXiv:astro-ph/0507503

Mainini, R. 2005, "Dark matter - baryon segregation in the non-linear evolution of coupled dark energy model", Phys. Rev., D72, 083514, arXiv:astro-ph/0509318

Mainini, R. & Bonometto, S. 2006, "Mass functions in coupled Dark Energy models", Phys. Rev., D74, 043504, arXiv:astro-ph/0605621

Mainini, R. & Bonometto, S. 2007, "Limits on coupling between dark components", JCAP, 0706, 020, arXiv:astro-ph/0703303

Mangano, G., Miele, G., & Pettorino, V. 2003, "Coupled quintessence and the coincidence problem", Mod. Phys. Lett., A18, 831, arXiv:astro-ph/0212518

McCarthy, I. G., Bower, R. G., & Balogh, M. L. 2007, "Revisiting the Baryon Fractions of Galaxy Clusters: A Comparison with WMAP 3-year Results", Mon. Not. Roy. Astron. Soc., 377, 1457, arXiv:astro-ph/0609314

McDonald, P. et al. 2005, "The Linear Theory Power Spectrum from the Lyman-alpha Forest in the Sloan Digital Sky Survey", Astrophys. J., 635, 761, arXiv:astro-ph/0407377

Mota, D. F., Pettorino, V., Robbers, G., & Wetterich, C. 2008, "Neutrino clustering in growing neutrino quintessence", Phys.Lett.B663:160-164,2008

Müller, C. M. 2005, "Cosmological models and observation", PhD thesis, Universität Heidelberg

Nagata, R., Chiba, T., & Sugiyama, N. 2004, "WMAP constraints on scalar-tensor cosmology and the variation of the gravitational constant", Phys. Rev., D69, 083512, arXiv:astro-ph/0311274

Navarro, J. F., Frenk, C. S., & White, S. D. M. 1997, "A Universal Density Profile from Hierarchical Clustering", Astrophys. J., 490, 493, arXiv:astro-ph/9611107

Nolta, M. R. et al. 2009, "Five-Year Wilkinson Microwave Anisotropy Probe (WMAP) Observations: Angular Power Spectra", Astrophys. J. Suppl., 180, 296, arXiv:0803.0593 [astro-ph]

Peccei, R. D. 2005, "Neutrino models of dark energy", Phys. Rev., D71, 023527, arXiv:hep-ph/0411137

Peccei, R. D., Sola, J., & Wetterich, C. 1987, "Adjusting the Cosmological Constant Dynamically: Cosmons and a New Force Weaker Than Gravity", Phys. Lett., B195, 183

Peebles, P. J. E. 1980, The Large-Scale Structure of the Universe (Princeton University Press)

Peebles, P. J. E. & Ratra, B. 1988, "Cosmology with a Time Variable Cosmological 'Constant"', Astrophys. J., 325, L17

Percival, W. J. et al. 2001, "The 2dF Galaxy Redshift Survey: The power spectrum and the matter content of the universe", Mon. Not. Roy. Astron. Soc., 327, 1297, arXiv:astro-ph/0105252

Perlmutter, S. et al. 1999, "Measurements of Omega and Lambda from 42 High-Redshift Supernovae", Astrophys. J., 517, 565, arXiv:astro-ph/9812133

Pettorino, V., Baccigalupi, C., & Perrotta, F. 2005, "Scaling solutions in scalar-tensor cosmologies", JCAP, 0512, 003, arXiv:astro-ph/0508586

Pettorino, V., Mota, D. F., Robbers, G., & Wetterich, C. 2009, in Proceedings of the DSU 2008 - 4th International Workshop on the Dark Side of the Universe, Cairo

Quartin, M., Calvao, M. O., Joras, S. E., Reis, R. R. R., & Waga, I. 2008, "Dark Interactions and Cosmological Fine-Tuning", JCAP, 0805, 007, arXiv:0802.0546 [astro-ph]

Ratra, B. & Peebles, P. J. E. 1988, "Cosmological Consequences of a Rolling Homogeneous Scalar Field", Phys. Rev., D37, 3406

Readhead, A. C. S. et al. 2004, "Extended Mosaic Observations with the Cosmic Background Imager", Astrophys. J., 609, 498, arXiv:astro-ph/0402359

Riess, A. G. et al. 1998, "Observational Evidence from Supernovae for an Accelerating Universe and a Cosmological Constant", Astron. J., 116, 1009, arXiv:astro-ph/9805201

Riess, A. G. et al. 2004, "Type Ia Supernova Discoveries at z>1 From the Hubble Space Telescope: Evidence for Past Deceleration and Constraints on Dark Energy Evolution", Astrophys. J., 607, 665, arXiv:astro-ph/0402512

Riess, A. G. et al. 2007, "New Hubble Space Telescope Discoveries of Type Ia Supernovae at $z > 1$: Narrowing Constraints on the Early Behavior of Dark Energy", Astrophys. J., 659, 98, arXiv:astro-ph/0611572

Robbers, G. 2006, "Probing Dark Energy", Diploma Thesis, Universität Heidelberg

Robbers, G., Afshordi, N., & Doran, M. 2008, "Does the Planck mass run on the cosmological horizon scale?", Phys. Rev. Lett., 100, 111101, arXiv:0708.3235 [astro-ph]

Schaefer, B. E. 2007, "The Hubble Diagram to Redshift >6 from 69 Gamma-Ray Bursts", Astrophys. J., 660, 16, arXiv:astro-ph/0612285

Seager, S., Sasselov, D. D., & Scott, D. 2000, "How exactly did the Universe become neutral?", Astrophys. J. Suppl., 128, 407, arXiv:astro-ph/9912182

Sealfon, C., Verde, L., & Jimenez, R. 2005, "Limits on deviations from the inverse-square law on megaparsec scales", Phys. Rev., D71, 083004, arXiv:astro-ph/0404111

Seljak, U., Slosar, A., & McDonald, P. 2006, "Cosmological parameters from combining the Lyman-alpha forest with CMB, galaxy clustering and SN constraints", JCAP, 0610, 014, arXiv:astro-ph/0604335

Seljak, U. & Zaldarriaga, M. 1996, "A Line of Sight Approach to Cosmic Microwave Background Anisotropies", Astrophys. J., 469, 437, arXiv:astro-ph/9603033

Sheth, R. K. & Tormen, G. 1999, "Large scale bias and the peak background split", Mon. Not. Roy. Astron. Soc., 308, 119, arXiv:astro-ph/9901122

Springel, V. 2005, "The cosmological simulation code GADGET-2", Mon. Not. Roy. Astron. Soc., 364, 1105, arXiv:astro-ph/0505010

Stern, S. 2008, "Dynamical dark energy and variation of fundamental 'constants'", arXiv:0812.3377 [hep-ph]

Tauber, J. A. 2000, in IAU Symposium, Proceedings, The Planck Mission

Tegmark, M. et al. 2004a, "The 3D power spectrum of galaxies from the SDSS", Astrophys. J., 606, 702, arXiv:astro-ph/0310725

Tegmark, M. et al. 2004b, "Cosmological parameters from SDSS and WMAP", Phys. Rev., D69, 103501, arXiv:astro-ph/0310723

Tegmark, M. et al. 2006, "Cosmological Constraints from the SDSS Luminous Red Galaxies", Phys. Rev., D74, 123507, arXiv:astro-ph/0608632

The SDSS-III Collaboration. 2008, "SDSS-III: Massive Spectroscopic Surveys of the Distant Universe, the Milky Way Galaxy, and Extra-Solar Planetary Systems", Tech. rep.

Trotta, R. 2008, "Bayes in the sky: Bayesian inference and model selection in cosmology", Contemp. Phys., 49, 71, arXiv:0803.4089 [astro-ph]

Viel, M., Haehnelt, M. G., & Springel, V. 2004, "Inferring the dark matter power spectrum from the Lyman- alpha forest in high-resolution QSO absorption spectra", Mon. Not. Roy. Astron. Soc., 354, 684, arXiv:astro-ph/0404600

Vikhlinin, A. et al. 2006, "Chandra sample of nearby relaxed galaxy clusters: mass, gas fraction, and mass-temperature relation", Astrophys. J., 640, 691, arXiv:astro-ph/0507092

Vikman, A. 2007, "K-essence: cosmology, causality and emergent geometry", PhD thesis, Ludwig-Maximilians-Universität München

Waizmann, J.-C. & Bartelmann, M. 2008, "Impact of Early Dark Energy on the Planck SZ cluster sample", arXiv:0804.2815 [astro-ph]

Wang, B., Zang, J., Lin, C.-Y., Abdalla, E., & Micheletti, S. 2007, "Interacting Dark Energy and Dark Matter: observational Constraints from Cosmological Parameters", Nucl. Phys., B778, 69, arXiv:astro-ph/0607126

Wetterich, C. 1988a, "Cosmologies With Variable Newtons's 'Constant'", Nucl. Phys., B302, 645

Wetterich, C. 1988b, "Cosmology and the Fate of Dilatation Symmetry", Nucl. Phys., B302, 668

Wetterich, C. 1995, "The Cosmon model for an asymptotically vanishing time dependent cosmological 'constant'", Astron. Astrophys., 301, 321, arXiv:hep-th/9408025

Wetterich, C. 2004, "Phenomenological parameterization of quintessence", Phys. Lett., B594, 17, arXiv:astro-ph/0403289

Wetterich, C. 2007, "Growing neutrinos and cosmological selection", Phys. Lett., B655, 201, arXiv:0706.4427 [hep-ph]

Wetterich, C. 2008, "Naturalness of exponential cosmon potentials and the cosmological constant problem", Phys. Rev., D77, 103505, arXiv:0801.3208 [hep-th]

Williams, J. G., Turyshev, S. G., & Boggs, D. H. 2004, "Progress in Lunar Laser Ranging Tests of Relativistic Gravity", Phys. Rev. Lett., 93, 261101, arXiv:gr-qc/0411113

Wong, W. Y., Moss, A., & Scott, D. 2007, "How well do we understand cosmological recombination?", arXiv:0711.1357 [astro-ph]

Xia, J.-Q. & Viel, M. 2009, "Early Dark Energy at High Redshifts: Status and Perspectives", arXiv:0901.0605 [astro-ph.CO]

Zaldarriaga, M. et al. 2008, "CMBPol Mission Concept Study: Reionization Science with the Cosmic Microwave Background", arXiv:0811.3918 [astro-ph]

Zlatev, I., Wang, L.-M., & Steinhardt, P. J. 1999, "Quintessence, Cosmic Coincidence, and the Cosmological Constant", Phys. Rev. Lett., 82, 896, arXiv:astro-ph/9807002

Zuntz, J. A., Ferreira, P. G., & Zlosnik, T. G. 2008, "Constraining Lorentz violation with cosmology", Phys. Rev. Lett., 101, 261102, arXiv:0808.1824 [gr-qc]

Acknowledgments

I am very much indebted to my advisor Christof Wetterich, not only for scientific guidance and support, but also for the opportunity to enjoy science working with such a great cosmology group at a wonderful place.

I thank Michael Doran for having authored CMBEASY, showing me its secrets, and for letting me take care of it.

I thank Matthias Bartelmann for refereeing this thesis, and the entire group at ITA for many discussions about (early) dark energy and most importantly, real observations.

I have immensely enjoyed the collaboration both with Eric Linder and Niayesh Afshordi.

Valeria Pettorino, Iain Brown, David Mota, Juliane Behrend and the entire cosmology group have made it not only an interesting, but also a fun time.